

Noncovalent Interactions of Silent Agonists Binding
to the Nicotinic Acetylcholine Receptor
-and-
Investigation into Expanding the Substrate Scope
and Improving the Efficiency of
Organic Photochemical Protecting Groups

Thesis by
Catriona Emily Wilson Blunt

In Partial Fulfillment of the Requirements for
the degree of
Doctor of Philosophy

The logo for the California Institute of Technology (Caltech), featuring the word "Caltech" in a bold, orange, sans-serif font.

CALIFORNIA INSTITUTE OF TECHNOLOGY
Pasadena, California

2019
(Defended May 2, 2019)

© 2019

Catriona Emily Wilson Blunt
ORCID: [0000-0002-4663-4602]

ACKNOWLEDGEMENTS

First and foremost, I need to thank my advisor, Professor Dennis Dougherty, for welcoming into his lab and providing me with mentorship and guidance throughout my time at Caltech. I am forever grateful for the independence Dennis provided me to experiment and fail. It was grueling at times but the confidence I have gained as a scientist in my ability to design, execute, and interpret an experiment are far greater than I could ever have anticipated. Dennis is a truly great advisor who was able to adapt his mentorship style to provide the type of support I needed when I asked. I have great respect for the compassion and professionalism with which Dennis runs his Lab.

I would like to recognize the members of my thesis committee, Professor Sarah Riesman, Professor Bob Grubbs, and Professor Dave Tirrell. Despite their busy schedules, they have always been incredibly generous with their time, attention, and encouragement. I have enjoyed talking to them about my research and ideas, and have always appreciated their comments and suggestions. They provided structure and direction to my doctoral research. Additionally, Sarah Riesman has been an excellent chair, keeping me on track and our meetings focused. I would also like to recognize, Professor Henry Lester, who is practically a co-advisor for all the Dougherty Lab. This included me despite the fact I spent most of my PhD in the synthesis lab. Henry encouraged my participation in the unnaturals subgroup throughout my time at Caltech and provided his support and expertise when I eventually made the switch to the biology side of the lab.

Over the course of my PhD I have been incredibly fortunate to be surrounded by brilliant, intelligent, passionate labmates. Finding not only wonderful colleagues who have supported me in my scientific endeavors but have also become firm friends. I briefly overlapped with Dr. Ethan Van Arnem, Dr. Kristina Daeffler, Dr. Noah Duffy, Dr. Tim Miles, and Dr. Ximena da Silva at the very start of my time in the Dougherty Lab. I have been fortunate to get to know Ethan's wit and Tim's humility since they returned to Southern California. Noah stayed in town, and I have been fortunate enough to get to know Noah, through our lab's outdoors adventures and over drinks in the conference room. I have great appreciation for his openness and historical knowledge of the lab. And Kristina,

in a few short months, taught me to be brutally honest with my data: an n of two is meaningless.

I would like to recognize the members of team photochemistry/photo acid: Dr. Clint Regan, Dr. David Walton, Dr. Oliver Shafaat, Dr. Matt Davis, Kalya Busby, and Bryce Jarman. Paul and Clint showed me the ropes in the chemistry lab when I first arrived and provided me with thoughtful discussion and encouragement at every step. Paul, your work ethic and enthusiasm are next to none and inspire me. In addition, your humor and random obsession of the week have kept lab fun — I now know way more about coffee than any non-coffee drinker has a right to know. Oliver is a brilliant scientist with extensive knowledge in a wide array of subjects. Oliver got me started in BILRIC introducing me to transient spectroscopy, and also introduced me to Mammoth, or at least the little bit that was open when we went. Bryce, I am amazed by the depth of your scientific knowledge on a vast array of topics and your ability to ask insightful questions. I learn something new every time we talk. Thank you for organizing so many amazing lab activities, whether it was simply drinks around the conference room table or camping in Death Valley. Matt Davis showed me it was possible to straddle the Dougherty Lab's two very distinct subgroups and succeed in both. While I bemoaned your bad puns at the time, I now miss them. And to Kayla, — the first person I met when I arrived at Caltech — your excitement about science is infectious. Thank you for introducing me to both the formal and informal women's support networks at Caltech.

Annet Blom is one of the most dedicated organized hard working people I have met. I am forever grateful that you took the time to train me on the opus when I was in my fifth year. I would never have been able to graduate without your mentorship in lab and I would not have enjoyed my time in lab without your friendship. Richard Mosesso is a positive cheery energy in lab and is down for anything. Thank you for teaching me how to analyze my opus data and answering all of my random biology questions. Dr. Chris Marotta, your optimism made central bay the best bay. Thank you for taking the time to talk to me about working with α 7 years after you graduated and for keeping one the most organized DNA box ever — I only needed to make one construct!

Steve Grant, you are a major part of the lab even after you transferred labs, and I continue to be impressed with your focus and hard work. Also, thanks for Steve Lunch every Wednesday! Dr. Matt Rienzo, the care and thought you take in your work and in life are an inspiration. I am grateful for our friendship and I have missed your presence in lab and our pessimistic conversations ever since you graduated. Dr. Mike Post, your energy and optimism for all things are a joy to behold. Your innate ability to see the successes in others and to acknowledge it is a gift and a boon to any group you are a part of. And Dr. Betty Wong, you see value and opportunity where others do not. Thank you for telling me about all the best food in the San Gabriel Valley.

This PhD would not have been possible without the help and support of many other people in the Caltech chemistry department and across the Institute. Dr. Brian Sanders taught me how to collect the transient spectra in Chapter Four and Dr. Wesley Kramer helped me collect the cyclic voltammetry measurements in Chapter Five of this thesis. I am deeply grateful to Dr. Scott Virgil for spending hours with me trying to get the HPLC to separate my compounds and for maintaining the LCMS in the Grubbs Group, to Dr. Dave VanderVelde for maintaining the NMR instruments and for your help in taking and interpreting spectra, and to Dr. Mona Shahgholi for running the MS facility and in particular the MALDI-TOF. Thank you to Jonathan Wang and Prunima Deshpande for harvesting and preparing the oocytes needed for all the $\alpha 7$ work in this thesis. A huge thank you to Joe Drew and the rest of the chemistry stockroom staff for keeping the building running and for making sure I got all the chemicals I need.

Caltech has also provided me with lifelong friendships outside of lab. I met Dr. Belinda Wenke, Griffin Chure, Sam Ho, Bill Ireland, Dr. Renee Arias, Dr. Kelsey Boyle, Joe Redford and Emily Blythe my first semester of graduate school. Together we have celebrated each other's successes, commiserated over drinks, and had some epic game nights. Additionally, Emily was an amazing roommate for three years; her no-nonsense attitude of getting things done is something I try and emulate.

Sara Beery has been my roommate for the past three years, and the most amazing cheerleader I could have asked for as I rushed towards the end of my time at Caltech. I have truly enjoyed the discussions we shared over a good bottle of wine and an excellent

home cooked meal. I will miss living with you, Sara, and I look forward to our many future adventures.

Andrew Robbins has been my adventure buddy at Caltech since day one. I had a blast skiing and learning how to white water kayak with Andrew all over California. I would like to thank Elle Chimiak and Sujung Lim for letting me tag along on their outdoors adventures, even when I was woefully out of my depth, and for starting a community of women adventures at Caltech. I had a great time learning to set anchors in Joshua Tree and climbing a wall of ice outside of Mammoth. I also need to thank Dr. Nick Weadock, Gregg Dobrowalski, and John Kindem for all our many ski trips together.

I never would have gotten through this PhD without the ability to escape to the mountains and in particular to the snow-covered mountains of Alta, Utah. I need to thank all my Goldminer's Daughter Lodge friends for always showing me a good time when I visited; in particular, Liz Page, for letting me crash on her couch and sending me books on badass female adventurers who also happened to be scientists, and for reminding me that I could have it all, and, Brent Leyerle, for always making me laugh and pushing me to jump off cliffs. Skiing fresh snow off the Kitty with these two is a joy. Additionally, it has been amazing skiing with my longtime friends, Alta Curtis and Moni Gilmore, who both now live in Salt Lake City. More importantly I look forward to our monthly video chats. Alta and Moni are two of the best friends a person could ask for, I only wish we lived closer.

I was fortunate to make many close friends during my time at Smith College who have continued to support me from afar. Joanne Poon, thank you for letting me come cuddle with your puppy (I love you Stuart), and for all your encouragement and help networking when I was applying for jobs in consulting. Aubrey Graham, my undergrad lab partner, has been cheering me on since undergrad and now manages to do so from Thailand. And to Naomi Barshi, Dr. Julea Vlassakis, Sara Perlmutter, and Dr. Elsa Hinds: we may all be getting our PhDs from different schools in different subjects, but it has been wonderful to share this experience with you.

Lauren Young, we didn't know each other at Smith but running into you at a brunch in Los Angeles was one of the best things that has happened during the past six years. You are a true friend and have always been there for me. I would also like to thank the entire

Young/Gillman family for welcoming me into their lives and giving me a family on the West Coast. You reignited my passion for theater and showed me around this city.

This document was a long time in coming. I first started discussing graduate schools and getting my PhD back in high school. Dr. Rebecca Jackman, my high school chemistry teacher, introduced me to chemistry. It was a rocky start; after the first month of class, I told her I hated chemistry. By the end of the year it was my favorite subject and twelve years later I still love it. Your skill as a teacher and dedication to the subject is seen in the number of your students who pursue chemistry as a career, myself included. I also need to thank my undergrad thesis advisor, Professor Kevin Shea; I never would have applied to Caltech without your encouragement. Thank you for supporting me as a scientist (and as a skier!).

Finally, I need to thank my family, the ultimate support system. My brother, Rory, who has never called me but will always answer the phone and talk to me about the most mundane things: you are the taller male version of me just minus a PhD now. My mother, Mary, who will not understand a word of this thesis but will continue attempting to tell all her friends what I do because she is proud of me. My father, Jon, who is thoughtful and measured in everything he says and who asks me how far I have extended my photochemistry towards the NIR every time we see each other. The answer is still “we have some ways to go.” The three of you have encouraged and supported me at every step of this process and I am forever grateful.

ABSTRACT

This dissertation describes two very different projects. The first project focuses on the binding of a silent agonist to a ligand gated ion channel. The second project focuses on the study of development of new longer wavelength photolabile protecting groups for use in a biological setting to enable the spatially and temporally controlled release of biologically active small molecules.

Chapter I introduces ligand gated ion channels and in particular a model of agonist binding at the nicotinic acetylcholine receptor. In addition, the nonsense suppression methodology used to incorporate the non-canonical amino acids required to probe non-covalent binding interactions is detailed. The second chapter details the use of non-canonical amino acids to study the binding of silent agonist NS6740 at the nicotinic acetylcholine receptor $\alpha 7$ subunit and the discovery of a novel hydrogen bond that modulates silent agonist activity.

Chapters III, IV and V focus on efforts to expand the scope of photolabile protecting groups towards designing longer wavelength derivatives. Chapter III introduces the topic of photoremovable protecting groups and details the mechanistic background of a quinone methide based photochemical protecting group.

The fourth chapter investigates the use of quinoline and quinolinium derivatives as photochemical quinone methide precursors. Two quinoline derivatives were found to form a quinone methide transient when irradiated. Quinolinium derivatives proved photostable, most likely due to the electron withdrawing nature of the quinolinium.

The final chapter details efforts to improve the photochemical reaction efficiency of quinone photoreduction by using a radical decarboxylation strategy to trap the charge transfer state. Synthesis of two glycine containing quinone compounds is detailed and their photochemistry is evaluated. Both proved to be photostable.

PUBLISHED CONTENT AND CONTRIBUTIONS

Catriona E. W. Blunt; Dennis A. Dougherty Investigating the Binding Interactions of NS6740, a Silent Agonist of the Nicotinic Receptor. –Submitted

C.E.W.B participated in the conception of the project, conducted the electrophysiology experiments, analyzed the data, and contributed to the writing of the manuscript.

TABLE OF CONTENTS

Acknowledgements	iii
Abstract	viii
Published Content and Contributions	xi
Table of Contents	x
List of Figures	xii
List of Schemes	xiii
List of Tables	xiv
Chapter I: Introduction: Nicotinic Acetylcholine Receptor	1
1.1 Motivation	1
1.2 Nicotinic Acetylcholine Receptors: A Ligand Gated Ion Channel	1
1.3 Cation- π Binding Box	3
1.4 Structure Function Studies	5
1.5 Electrophysiology	7
1.6 Positive Allosteric Modulators	9
1.7 Thesis Summary: Part One	10
1.8 References	10
Chapter II: The Binding Interactions of NS6740, a Silent Agonist of the $\alpha 7$ Nicotinic Acetylcholine Receptor	16
2.1 Introduction	16
2.2 Results	19
2.2.1 Measuring binding interactions in the presence of a PAM	19
2.2.2 Binding interactions of TyrA with NS6740	21
2.2.3 Characterization of other potential cation- π binding interactions of NS6740 in the orthosteric binding site	26
2.2.4 Characterization of backbone hydrogen bonding to NS6740 at the orthosteric binding site	28
2.3 Discussion	28
2.4 Materials and Methods	32
2.5 References	34
Chapter III: Introduction: Photoremovable Protecting Groups	39
3.1 Motivation	39
3.2 Photoacids	39
3.3 Quinone Methide	41
3.4 Summary of Work: Part Two	46
3.5 References	46
Chapter IV: Photochemistry of Quinoline and Quinolinium <i>ortho</i>-Quinone Methide Precursors	52
4.1 Introduction	52
4.2 Quinoline <i>ortho</i> -quinone methide	54
4.2.1 Synthesis of quinoline derivatives	54

4.2.2	Photophysics.....	56
4.2.3	Photochemistry.....	59
4.3	Quinolinium <i>ortho</i> -quinone methide	63
4.3.1	Synthesis of quinolinium derivatives.....	63
4.3.2	Photochemistry.....	63
4.3.3	pH dependence of photochemistry.....	65
4.4	Conclusions	66
4.5	References	67
4.6	Experimental	71
4.6.1	General procedures.....	71
4.6.2	Synthesis.....	71
4.6.3	Quantum yield of fluorescence	81
4.6.4	Transient absorption spectroscopy.....	81
4.6.5	pH dependent relative quantum yield of reaction.....	82
4.6.6	Quantum yield of reaction.....	83
Chapter V: Attempts at Improving the Efficiency of the Quinone Trimethyl Lock Protecting Group Using a Radical Decarboxylation Strategy.....		86
5.1	Introduction	86
5.2	Results	89
5.2.1	Synthesis of a phenoxazine	89
5.2.2	Phenoxazine photochemistry	90
5.2.3	Synthesis of an acyclic quinone	91
5.2.4	Quinone photochemistry	95
5.2.5	Quinone electrochemistry	96
5.3	Discussion	97
5.4	References	98
5.5	Experimental	101
5.5.1	General procedures.....	101
5.5.2	Synthesis.....	102
5.5.3	Circular voltammetry	107
5.5.4	Additional Data	108

LIST OF FIGURES

1.1	Neuronal communication via synaptic transmission	2
1.2	The nicotinic acetylcholine receptor (nAChR).....	3
1.3	Orthosteric binding site for the $\alpha 7$ nAChR	4
1.4	Schematic of nonsense suppression during translation	6
1.5	Nonsense suppression methodology for non-canonical amino acid incorporation in ion channels in <i>Xenopus laevis</i> oocytes	8
1.6	Positive allosteric modulators (PAMs)	10
2.1	Silent agonist activity	17
2.2	Structure of side chains of non-canonical amino acids	19
2.3	Effect of pre-incubation with PAM PNU-120596 on NS6740 response	21
2.4	Cation- π plot for TyrA in the $\alpha 7$ nAChR	22
2.5	Effect of the $\alpha 7$ TyrA TyrOMe mutation on NS6740 activity	25
2.6	Cation- π plot for TyrC2 in the $\alpha 7$ nAChR	27
2.7	Purposed binding interactions of NS6740	30
2.8	Energy landscape for receptor activation	31
3.1	Förster cycle of photoacidity	40
3.2	pK_a and pK_a^* for a selection of phenol and naphthols.....	41
3.3	Quinone Methide Intermediate	42
3.4	Mechanistic steps in QM photogeneration	45
4.1	<i>ortho</i> -Quinone Methide	53
4.2	UV-Vis spectra of quinoline 10 and 13	57
4.3	Emission spectra of quinoline 10 and 13	57
4.4	Förster Analysis of quinoline 10 and 13	58
4.5	Transient absorbance spectra of quinoline 10QM	61
4.6	Quenching of quinoline 10QM Transient.....	62
4.7	Förster Analysis of quinolinium 28	65
4.8	pH dependence on the photoreactivity of quinoline 10 and 13	66
5.1	Photoremovable quinone trimethyl lock protecting group	87
5.2	Aminoquinone and aminonaphthoquinone photochemistry.....	87
5.3	Photochemistry of phenoxazine 15	15
5.4	Photochemistry of quinone qcid 30	95
5.5	Cyclic voltammetry of 28 and 35	97

LIST OF SCHEMES

4.1	Synthesis of 3-(hydroxymethyl)quinoline-4-ol (9).....	54
4.2	Synthesis of 4-(hydroxymethyl)-2-methylquinolin-3-ol (10a)	55
4.3	Synthesis of 2-(hydroxymethyl)quinoline-3-ol (13a).....	56
4.4	Photochemistry of quinoline QMPs.....	60
4.5	Synthesis of quinolinium derivatives.....	63
4.6	Photochemistry of quinolinium derivatives.....	64
5.1	Mechanism for the photoreduction of sulfide substituted quinones.....	88
5.2	Proposed quinone radical decarboxylation photoreduction	89
5.3	Synthesis of phenoxazine 15	90
5.4	Retrosynthesis for acyclic glycine substituted benzoquinone	92
5.5	Quinone cross coupling conditions.....	93
5.6	Synthesis of acyclic quinone 30	94

LIST OF TABLES

2.1	EC ₅₀ values of amomatic box residues in $\alpha 7$ for NS6740 + PNU-120596 (10 μ M).....	23
2.2	Relative Efficacy to I _{max} acetylcholine for NS6740 co-applied with type I and II PAMS at $\alpha 7$	24
2.3	EC ₅₀ values at TyrA:TyrOMe	25
2.4	EC ₅₀ values and coupling constants for genistein and ACh at TyrA	26
3.1	Photodehydration of hydroxybenzyl alcohols	43
3.2	Effect of substituents on the thermal generation of <i>ortho</i> -QMs	44
3.3	Effect of substituents on the quenching of QMs.....	44
5.1	Buchwald-Hartwig reaction conditions screened	92

Chapter 1

INTRODUCTION: NICOTINIC ACETYLCHOLINE RECEPTOR

1.1 Motivation

The brain is composed of a complex network of neurons that communicate via the propagation of electrical impulses or action potentials. An action potential travels the length of the neuron until it reaches a synapse junction where it must be converted into a chemical signal to cross the synaptic cleft (Figure 1.1). Neurotransmitters are the small molecule chemical signals that diffuse across the synaptic cleft and bind integral transmembrane receptors on the post synaptic cell. These receptors then undergo a conformational change that allows ions to flow across the membrane and initiate a new electrical signal. This process of electrical to chemical and back to electrical underlies all brain activity including sensory processing, movement, and memory. Disruptions to this process are responsible for many neurological disorders and diseases. It is therefore important to understand these processes at a chemical level. This first part of this thesis looks at a specific receptor, the nicotinic acetylcholine receptor (nAChR), binding to a new class of drugs.

1.2 Nicotinic Acetylcholine Receptors: A Ligand Gated Ion Channel

Nicotinic acetylcholine receptors (nAChRs) are part of the Cys loop superfamily of pentameric ligand gated ion channels (pLGICs). Upon neurotransmitter binding pLGICs undergo a conformational change allowing ions to flow through a channel across the membrane. This flow of ions can either initiate an excitatory response, generating an action potential such as in the cation permeable Cys-loop LGICs - nAChRs and type 3 serotonin (5-HT_{3A}) receptors or can be inhibitory, terminating an electrical signal such as in the anion permeable receptors - type A γ -aminobutyric acid (GABA_ARs), and glycine receptors (GlyRs).¹ As the name implies nAChRs bind both the native neurotransmitter acetylcholine and nicotine, the addictive component of cigarettes. nAChRs are a major pharmaceutical

target in many neurological disorders, including addiction,^{2,3} Alzheimer's disease,⁴ and schizophrenia.⁵

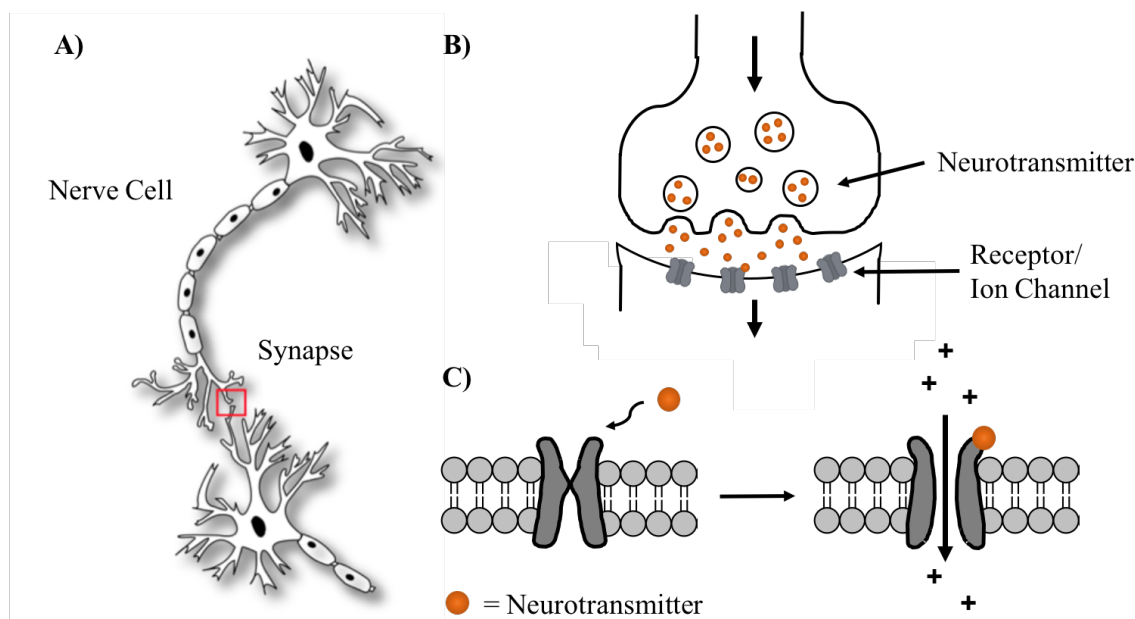


Figure 1.1: Neuronal communication via synaptic transmission: A) Cartoon of two nerve cells. Red box shows the synapse between the two cells. B) At the synapse neurotransmitters are released from the presynaptic nerve in response to an electrical signal and diffuses across the synaptic cleft to bind receptors on the postsynaptic nerve cell. C) Ligand gated ion channels (LGICs) undergo a conformational change when a neurotransmitter binds, opening a pore and allowing ions to cross the plasma membrane.

All Cys-Loop receptors, including nAChRs, have a common global architecture containing five subunits arranged in a circular configuration around a central pore (Figure 1.2).⁶ The five subunits can be either homomeric or heteromeric. Each subunit contains a large extracellular N-terminal domain composed mainly of β -sheets, a membrane spanning domain composed of four α -helices (M1-M4), and a variable intracellular domain composed mainly of the M3-M4 loop important for transport and regulation.⁷ The binding site is at a conserved location in the extracellular domain at the interface of two subunits.

There are 17 nAChR subunits $\alpha 1$ - $\alpha 10$ ($\alpha 8$ is only found in avian species) $\beta 1$ - $\beta 4$, γ , δ , and ϵ .^{8,9} The neuronal nAChR subunits, $\alpha 2$ - $\alpha 7$, $\alpha 9$, $\alpha 10$ and $\beta 2$ - $\beta 4$, combine in varying combinations and stoichiometries to form functional receptor subtypes, each with its own unique pharmacology, function, and localization. (The “muscle type” $\alpha 1_2\beta 1\gamma\delta/\epsilon$ is only found in the peripheral nervous system and at neuromuscular junctions.) The two most common neuronal subtypes found throughout the brain are $\alpha 4\beta 2$ and $\alpha 7$. This thesis will

focus on $\alpha 7$, which is a drug target for its role in neurological disorders including schizophrenia^{10,11} and Alzheimer's,^{4,12,13} as well as for its role in the cholinergic anti-inflammatory pathway.^{14,15}

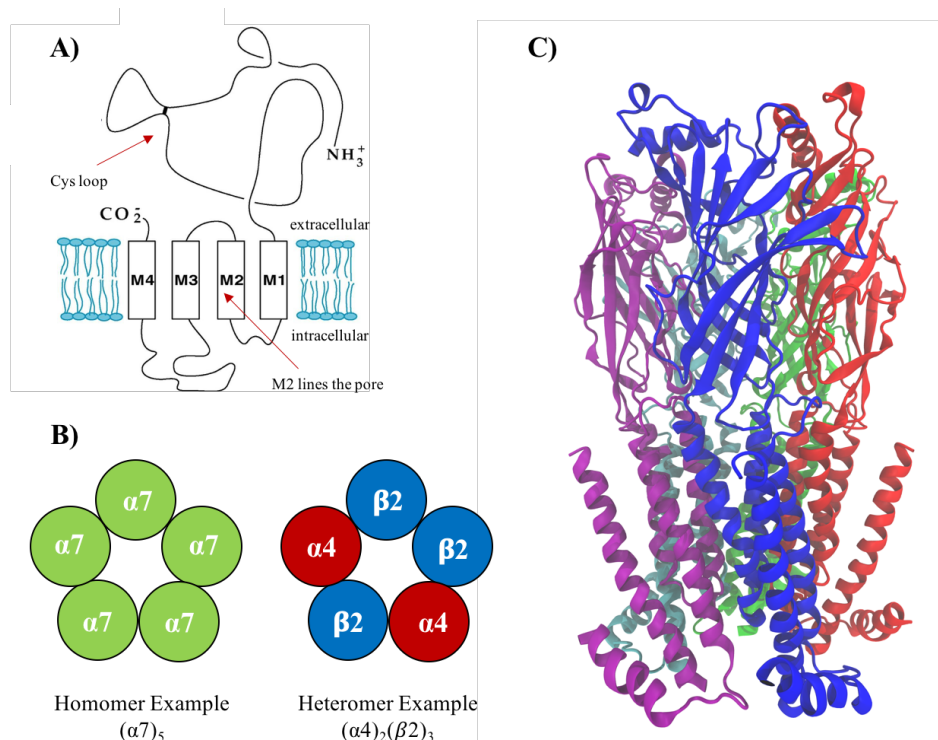


Figure 1.2: The nicotinic acetylcholine receptor (nAChR). A) Diagram of common subunit structure to all Cys-loop receptors including the nAChR: extracellular domain contains a Cys-loop formed by disulfide bond and the orthosteric ligand binding site, four α -helices from the transmembrane domain and an intracellular domain made up mostly of the M3-M4 loop. B) Examples of homomeric and heteromeric arrangements of nAChR subunits in a pentameric assembly around a central pore. C) Crystal structure of the human $\alpha 4\beta 2$ heteromeric nAChR (PDB ID: 5KXI).⁷

1.3 Cation- π Binding Box

In $\alpha 7$, as with all other nAChRs, the orthosteric agonist binding site is located at the interface of two subunits, in the extracellular domain. Each binding site is composed of six loops, three from the primary face (loops A, B and C), and three from the complementary face (loops D, E and F).^{16–18} A group of five highly conserved aromatic residues at the binding site form an “aromatic box” around the ligand — a tyrosine on loop A (TyrA Y115), a tryptophan on loop B (TrpB, W171) and loop D (TrpD, W77), and two tyrosine residues on loop C (TyrC1 and TyrC2, Y210 and Y217) (Figure 1.3).¹⁹ Despite the perfect conservation of these aromatic residues within the nAChR family, subtype

specific variations in agonist binding patterns have been noted.^{19,20} In $\alpha 7$ three noncovalent interactions have been identified as functionally relevant for agonist binding.

The first important interaction for agonist binding is a cation- π . The cation- π is a strong noncovalent electrostatic interaction between a cation and the quadrupole induced negative electrostatic potential surface on the face of an aromatic residue.^{21,22} Typical nAChR agonists contain a cationic amine, either a protonatable amine or a quaternary ammonium, that forms a noncovalent cation- π interaction with a conserved aromatic residue of the aromatic box. Unique among nAChRs, $\alpha 7$ makes a cation- π between TyrA and the ligand.²³ In all other nAChRs studied to date the primary aromatic residue involved in the cation- π is the tryptophan on loop B.^{20,23–28} For the potent $\alpha 7$ agonist, epibatidine, a second stronger cation- π interaction with TyrC2 was also identified.²³ Work by Mike Post in the group has shown that secondary amines, such as metanicoine and varenicline, form a dual cation- π with TyrC2 and TrpB at $\alpha 4\beta 2$.²⁹ Epibatidine is not a secondary amine and remains the only drug to exhibit dual functional cation- π activity at $\alpha 7$.

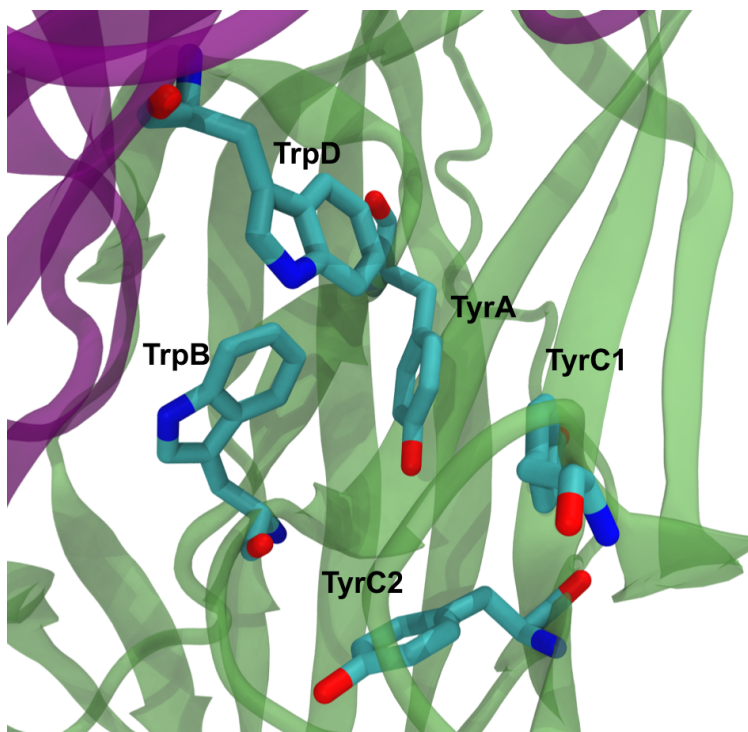


Figure 1.3: Orthosteric binding site for the $\alpha 7$ nAChR. Five aromatic residues comprise the aromatic binding box. These residues are labeled as such: TyrA (Y115), TrpB (W171), TyrC1 (Y210), and TyrC2 (Y217) come from the principal face (green) of one subunit and the final residue of the aromatic box TrpD (W77) lies on the complementary face (purple). Image based on an $\alpha 7$ - acetylcholine binding protein (AChBP) chimera bound to epibatidine (not shown) (PDB ID: 3SQ6).¹⁷

Our group has also identified two hydrogen bonds that are functionally important for agonist binding in nAChRs. The NH group of non-quaternary amines, such as nicotine, hydrogen bonds with the backbone carbonyl of TrpB.^{25,27,30} In $\alpha 7$, this interaction was observed for epibatidine, a potent agonist, and varenicline, but not for quaternary amine agonist ACh as expected.^{23,31} (Nicotine is a very weak agonist of $\alpha 7$, which prevented its study.) The other hydrogen bond occurs between the distal, from the cationic amine, end of the agonist and the backbone NH of residue Leu119 on the complementary face.^{31–33} This interaction is very important in other nAChRs such as muscle type and $\alpha 4\beta 2$,³³ but in $\alpha 7$ only the super agonist epibatidine has shown a greater than two-fold effect for mutation of this hydrogen bond.³¹ Together these three interactions are the bases of nAChR agonist binding and are the bases of the $\alpha 7$ pharmacophore.

Historically there was limited structural information about nAChRs. Initially low resolution cryo-em³⁴ structures provided information about overall globular structure, and the crystal structures of a soluble Acetylcholine binding protein (AChBP)^{17,18,35} provided information on the bind site in the extracellular domain. Subsequent prokaryotic homology models provided insights into changes between the open and closed states.^{36–39} Recently in 2016 a high-resolution structure of nAChR $\alpha 4\beta 2$ was published.^{7,40} Despite improved structural information, crystal structures don't capture protein dynamics nor are there crystal structures of every subtype. Structure function studies provide an alternative way to implicate functionally relevant interactions of ligand binding, conformational rearrangement and receptor activation.

1.4 Structure Function Studies

Sight directed mutagenesis has been extensively been used by biochemists to probe for the specific chemical interactions that are responsible for protein function. However, this methodology is limited in scope because the 20 naturally occurring amino acids do not provide the subtlety in perturbation required to identify the distinct non-covalent interactions, such as cation- π and hydrogen bonding, that are important for protein function and our lab is interested in isolating. Subtler mutations are needed to map the important interactions responsible for ligand recognition and for the development of a pharmacophore model. The Dougherty lab has developed a protocol for the *in vivo* incorporation of non-

canonical amino acids;^{41–43} this has proved a powerful tool for studying structure-function relationships in ion channels. This provides a way to study specific interactions of a protein at a chemical scale.

Nonsense suppression allows for the *in vivo* site specific incorporation of non-canonical amino acids.^{19,44} This is accomplished by interruption of normal ribosomal function by inserting a stop codon or frameshift mutation, “a nonsense mutation,” in the gene of interest (Figure 1.4). Normally a stop codon (UAG, UGA and UAA) results in termination of protein synthesis. However, in the presence of an engineered “suppressor tRNA” that recognizes the nonsense mutation – via the appropriate anti codon – and charged with the desired non-canonical amino acid, site specific incorporation of a noncanonical amino acid into the nascent protein is possible. This suppressor tRNA must be orthogonal to the host system to prevent re-charging via endogenous aminocyl tRNA synthetase. Essentially nonsense suppression allows for the “Hijacking” of the ribosome and other machinery of the cell to synthesize, fold, and post translationally modify a protein with site specific incorporation of a noncanonical amino acid.

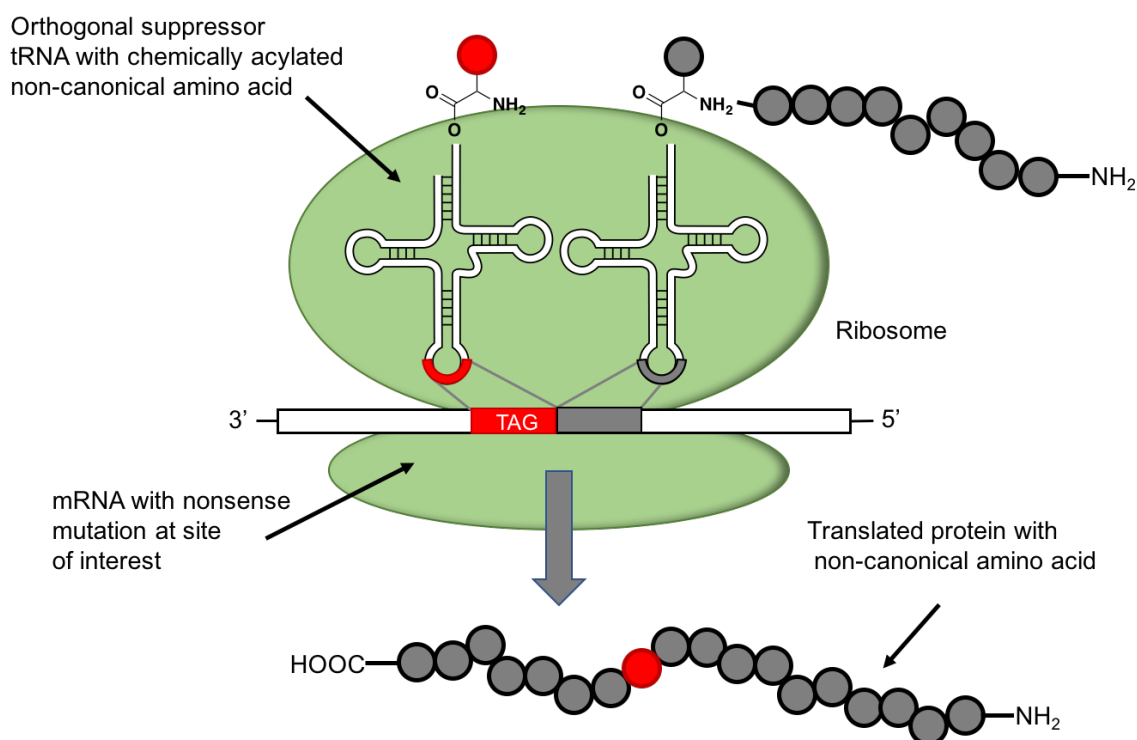


Figure 1.4: Schematic of nonsense suppression during translation. Orthogonal tRNA with correct anti-codon recognizes the stop/nonsense mRNA codon at site of interest and the ribosome incorporates the non-canonical amino acid into the nascent protein chain.

For nonsense suppression, a non-canonical amino acid must be attached to the suppressor tRNA, and in our lab this is achieved chemically. To ensure correct attachment and minimize degradation this is done in two steps.⁴³ First, the non-canonical amino acid is reacted with dCA, a dinucleotide that mimics the final uniform two bases of tRNA, and second this structure is enzymatically ligated to an orthogonal 74-mer suppressor tRNA. The advantage of this methodology is a tRNA synthetase is not required, and therefore incorporation of new non-canonical amino acids is facile and a large array of side chains with very subtle perturbations differing in as little as a single atom can be incorporated. The disadvantage of this method is the yield of protein depends stoichiometrically on the quantity of charged tRNA added to the system. Because of reagent limitation and inherent inefficiencies in the system only attomoles of protein are generated.¹⁹ Most spectroscopic techniques require much larger quantities of protein thus we use an equally sensitive technique for studying ion channels– electrophysiology.

1.5 Electrophysiology

Neuroscientists routinely use electrophysiology techniques to study ion channels by observing changes in electrical currents and potentials across lipid membranes. Electrophysiology has been used at multiple scales from individual proteins all the way up to mapping neural networks and can be used to interrogate endogenous activity in living animals and ion channels expressed in heterologous systems such as the oocytes from *Xenopus laevis*, which our lab employs.

Oocytes from *X. laevis* (the African clawed frog) are a classic model system for studying ion channel function because of their large size (1 mm in diameter), minimal expression of endogenous ion channels and ability to express eukaryotic proteins. Oocytes are large enough for direct injection of mRNA or cDNA and have the requisite cellular machinery for protein synthesis, assembly and surface trafficking of ion channels.^{45–47} Expressed ion channels have almost identical physiology to receptors expressed in other cell systems or those found in native neuronal environments. They are also amenable to nonsense suppression as acylated tRNA can also be directly injected into the cell alongside mRNA containing the correct nonsense mutation in the gene of interest (Figure 1.5).¹⁹

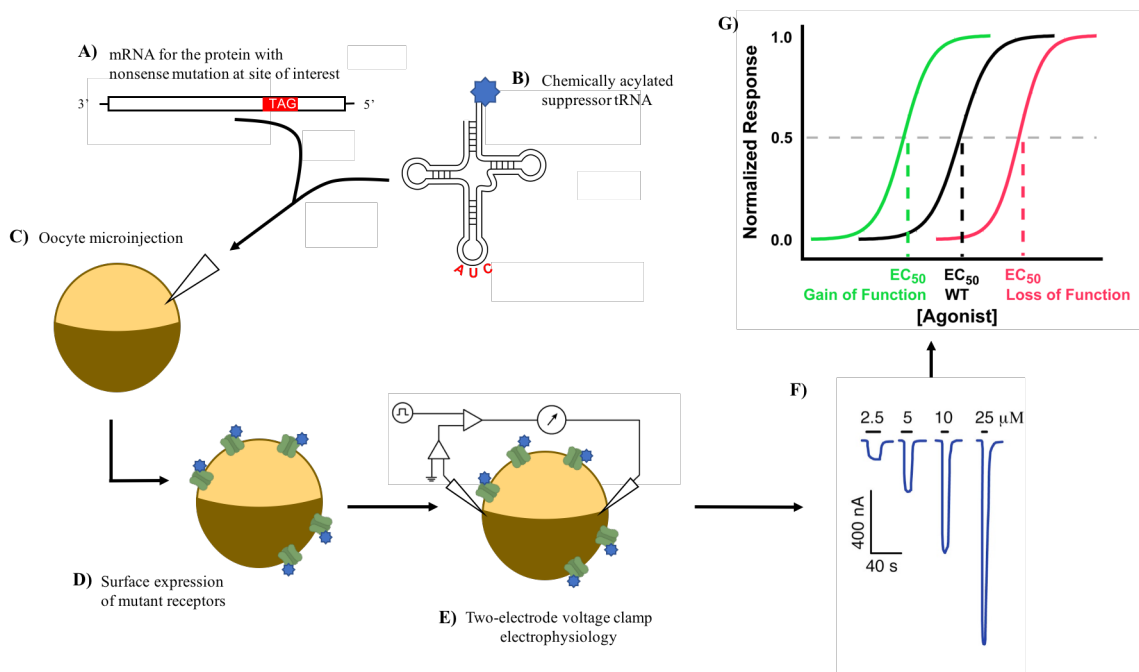


Figure 1.5: Nonsense suppression methodology for non-canonical amino acid incorporation into ion channels in *Xenopus laevis* oocytes. A) mRNA with a stop codon, “nonsense mutation,” at site of interest. B) orthogonal tRNA with correct anticodon chemically acylated to a non-canonical amino acid of interest. C) Injection of both mRNA and tRNA into the oocyte. D) Oocyte machinery translates, post translationally modifies and traffics to the surface the ion channel of interest with the non-canonical amino acid incorporated at the desired position. E) Two electrode voltage clamped (TEVC) electrophysiology readout of ion channel function. F) Application of increasing concentrations of agonist result in more channels opening and an increase of observed current during TECV experiments. G) After normalization, responses are plotted and fit to the Hill Equation. The concentration that results in a half maximal response, EC_{50} , provides a functional comparison between mutations. A gain of function results in a leftward shift and decreases the EC_{50} while a loss of function results in a rightward shift and an increase on the EC_{50} .

Agonist binding to a LGIC results in the channel opening and ions flowing through the pore to generate a current. This current can be measured easily using a whole cell two-electrode voltage clamp (TEVC) setup (Figure 1.5). In TEVC, the oocyte is impaled with two glass electrodes. The first electrode measures the internal potential relative to an external reference electrode in the oocyte bath media and the second electrode responds to variations in voltage by applying an appropriate current to maintain a constant “clamped” membrane potential. The variation in current required to maintain a clamped membrane potential provides a measure for the net charge flowing through ion channels in the open state. This system is very sensitive, enabling currents of tens of nA to μ A to be measured during whole cell recording and requires only a very small amount of protein for measurable signal response. This means that nonsense suppression can be used to study ion channels. An eight-channel recoding rig — the OpusXpress 6000A — in our lab makes

TEVC experiments much more efficient because it is capable of simultaneous multi-channel voltage clamping, buffer perfusion, and drug application.

The major electrophysiology functional assay used in this dissertation is the dose response. In a typical dose response experiment an oocyte expressing the LGIC of interest is subjected to increasing doses of agonist and the resulting whole-cell currents are measured. After normalization to max observed current and plotting, the data are fit to the Hill equation, a simplified model of cooperative binding:

$$I([A]) = \frac{I_{max}}{1 + \left(\frac{[A]}{EC_{50}}\right)^{n_H}} \quad (Eq. 1. 1)$$

where I is the observed whole cell current, $[A]$ is the agonist concentration, I_{max} is the current at saturating concentrations of agonist, EC_{50} is the concentration of agonist required to elicit a half maximal response and n_H is the Hill coefficient. EC_{50} provides a readout for the magnitude of the energetic perturbation caused by a given mutation; The log(fold-change in EC_{50}) is roughly proportional to the $\Delta\Delta G$ value. An increase in EC_{50} corresponds to a loss of function (more agonist is required to open the same number of channels) and a decrease in EC_{50} corresponds to a gain in function (less agonist is needed to open the same number of channels).

1.6 Positive Allosteric Modulators

In addition to agonists that bind at the orthosteric binding site, compounds have been developed that can modulate $\alpha 7$ function from binding sites distant from the agonist binding site, a process known as allosteric modulation. These compounds can either act as positive allosteric modulators (PAMs) that in the presence of an agonist can increase currents, or as negative allosteric modulators (NAMs) which inhibit agonist activation or block the channel suppressing currents. PAMs can potentiate agonist currents in two ways, either by reducing the EC_{50} , a “gain of function,” and/or by increasing current response for all doses (Figure 1.6). There are two major classes of PAMs, Type I and Type II, which are identified by their macroscopic effects on channel conductance.⁴⁸ Type I PAMs, such as 5-methoxyindole (5-HI) and genistein, increase peak current most likely through decreasing the energetic barrier to opening.^{49,50} Type II PAMs, such as PNU-120596, slow desensitization and can reactivate desensitized receptors in addition to increasing peak current (Figure 1.6).^{49,51} PAMs have received attention as therapeutic agents^{14,52–54} because

they allow for the modulation of receptor activity without interrupting endogenous activation. In addition, they show higher selectivity because the allosteric binding site is less conserved than the orthosteric binding site potentially reducing side effects.⁵⁵ Finally, they have proven useful tools in probing receptor function.

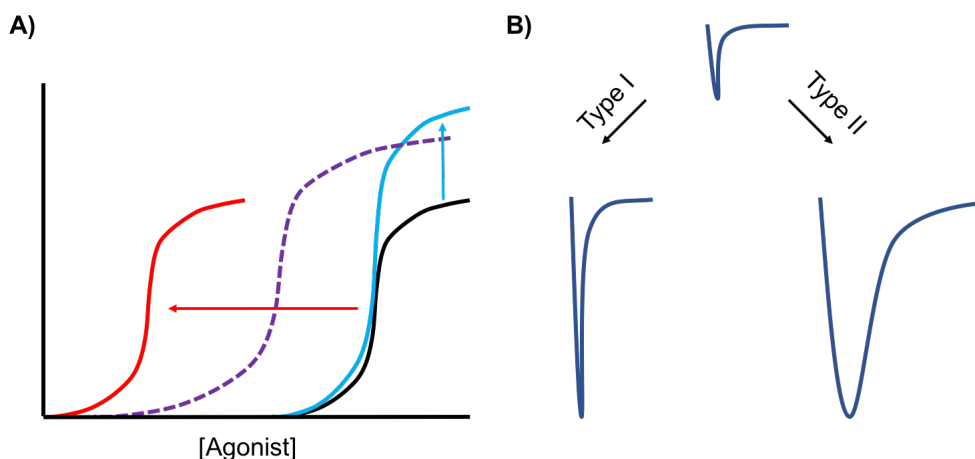


Figure 1.6: Positive Allosteric Modulators (PAMs). A) Possible Effects of a PAM on EC₅₀ curves: A gain of function (red), an increase in signal (blue) or most commonly a combination of both (purple) relative to agonist alone (black). B) Two classes of PAMs for α7 nAChRs: type I elicit a change in peak height and type II affect peak height as well as closure rate and can also reactivate the desensitized state.

1.7 Summary of Part One of Dissertation Work

In part one of this dissertation non-canonical amino acids were incorporated into the α7 nAChR using nonsense suppression, and binding of the silent agonist, NS6740, to the receptor was characterized using electrophysiology. Non-canonical mutagenesis of α7 aromatic box residues revealed a hydrogen bond to the TyrA OH that was detrimental to channel opening. Its removal resulted in a gain of function and converted the silent agonist NS6740 into a partial agonist. Both type I and II PAMs were used to understand the nature of this activity. These results suggest a mechanism by which silent agonist, NS6740, functions.

1.8 References

- (1) Lemoine, D.; Jiang, R.; Taly, A.; Chataigneau, T.; Specht, A.; Grutter, T. Ligand-Gated Ion Channels: New Insights into Neurological Disorders and Ligand Recognition. *Chem. Rev.* **2012**, *112* (12), 6285–6318. <https://doi.org/10.1021/cr3000829>.

- (2) Leslie, F. M.; Mojica, C. Y.; Reynaga, D. D. Nicotinic Receptors in Addiction Pathways. *Mol. Pharmacol.* **2013**, *83* (4), 753–758. <https://doi.org/10.1124/mol.112.083659>.
- (3) Feduccia, A. A.; Chatterjee, S.; Bartlett, S. E. Neuronal Nicotinic Acetylcholine Receptors: Neuroplastic Changes Underlying Alcohol and Nicotine Addictions. *Front. Mol. Neurosci.* **2012**, *5*. <https://doi.org/10.3389/fnmol.2012.00083>.
- (4) Lombardo, S.; Maskos, U. Role of the Nicotinic Acetylcholine Receptor in Alzheimer's Disease Pathology and Treatment. *Neuropharmacology* **2015**, *96*, Part B, 255–262. <https://doi.org/10.1016/j.neuropharm.2014.11.018>.
- (5) Martin, L. F.; Freedman, R. Schizophrenia and the Alpha7 Nicotinic Acetylcholine Receptor. *Int. Rev. Neurobiol.* **2007**, *78*, 225–246. [https://doi.org/10.1016/S0074-7742\(06\)78008-4](https://doi.org/10.1016/S0074-7742(06)78008-4).
- (6) Thompson, A. J.; Lester, H. A.; Lummis, S. C. R. The Structural Basis of Function in Cys-Loop Receptors. *Q. Rev. Biophys.* **2010**, *43* (4), 449–499. <https://doi.org/10.1017/S0033583510000168>.
- (7) Morales-Perez, C. L.; Noviello, C. M.; Hibbs, R. E. X-Ray Structure of the Human A4 β 2 Nicotinic Receptor. *Nature* **2016**, *538* (7625), 411–415. <https://doi.org/10.1038/nature19785>.
- (8) Zoli, M.; Pistillo, F.; Gotti, C. Diversity of Native Nicotinic Receptor Subtypes in Mammalian Brain. *Neuropharmacology* **2015**, *96*, Part B, 302–311. <https://doi.org/10.1016/j.neuropharm.2014.11.003>.
- (9) Giastas, P.; Zouridakis, M.; Tzartos, S. J. Understanding Structure-Function Relationships of the Human Neuronal Acetylcholine Receptor: Insights from the First Crystal Structures of Neuronal Subunits. *Br. J. Pharmacol.* **2017**, n/a-n/a. <https://doi.org/10.1111/bph.13838>.
- (10) Wang, Y.; Xiao, C.; Indersmitten, T.; Freedman, R.; Leonard, S.; Lester, H. A. The Duplicated A7 Subunits Assemble and Form Functional Nicotinic Receptors with the Full-Length A7. *J. Biol. Chem.* **2014**, *289* (38), 26451–26463. <https://doi.org/10.1074/jbc.M114.582858>.
- (11) Lasala, M.; Corradi, J.; Bruzzone, A.; Esandi, M. del C.; Bouzat, C. A Human-Specific, Truncated A7 Nicotinic Receptor Subunit Assembles with Full-Length A7 and Forms Functional Receptors with Different Stoichiometries. *J. Biol. Chem.* **2018**, *293* (27), 10707–10717. <https://doi.org/10.1074/jbc.RA117.001698>.
- (12) Moretti, M.; Zoli, M.; George, A. A.; Lukas, R. J.; Pistillo, F.; Maskos, U.; Whiteaker, P.; Gotti, C. The Novel A7 β 2-Nicotinic Acetylcholine Receptor Subtype Is Expressed in Mouse and Human Basal Forebrain: Biochemical and Pharmacological Characterization. *Mol. Pharmacol.* **2014**, *86* (3), 306–317. <https://doi.org/10.1124/mol.114.093377>.
- (13) Tong, M.; Arora, K.; White, M. M.; Nichols, R. A. Role of Key Aromatic Residues in the Ligand-Binding Domain of A7 Nicotinic Receptors in the Agonist Action of β -Amyloid. *J. Biol. Chem.* **2011**, *286* (39), 34373–34381. <https://doi.org/10.1074/jbc.M111.241299>.
- (14) Dineley, K. T.; Pandya, A. A.; Yakel, J. L. Nicotinic ACh Receptors as Therapeutic Targets in CNS Disorders. *Trends Pharmacol. Sci.* **2015**, *36* (2), 96–108. <https://doi.org/10.1016/j.tips.2014.12.002>.

- (15) Egea, J.; Buendia, I.; Parada, E.; Navarro, E.; León, R.; Lopez, M. G. Anti-Inflammatory Role of Microglial $\alpha 7$ nAChRs and Its Role in Neuroprotection. *Biochem. Pharmacol.* **2015**, *97* (4), 463–472. <https://doi.org/10.1016/j.bcp.2015.07.032>.
- (16) Brejc, K.; van Dijk, W. J.; Klaassen, R. V.; Schuurmans, M.; van Der Oost, J.; Smit, A. B.; Sixma, T. K. Crystal Structure of an ACh-Binding Protein Reveals the Ligand-Binding Domain of Nicotinic Receptors. *Nature* **2001**, *411* (6835), 269–276. <https://doi.org/10.1038/35077011>.
- (17) Li, S.-X.; Huang, S.; Bren, N.; Noridomi, K.; Dellisanti, C. D.; Sine, S. M.; Chen, L. Ligand-Binding Domain of an $\alpha 7$ -Nicotinic Receptor Chimera and Its Complex with Agonist. *Nat. Neurosci.* **2011**, *14* (10), 1253–1259. <https://doi.org/10.1038/nn.2908>.
- (18) Nemecek, A.; Taylor, P. Creating an $\alpha 7$ Nicotinic Acetylcholine Recognition Domain from the Acetylcholine-Binding Protein: Crystallographic and Ligand Selectivity Analyses. *J. Biol. Chem.* **2011**, *286* (49), 42555–42565. <https://doi.org/10.1074/jbc.M111.286583>.
- (19) Dougherty, D. A. Cys-Loop Neuroreceptors: Structure to the Rescue? *Chem. Rev.* **2008**, *108* (5), 1642–1653. <https://doi.org/10.1021/cr078207z>.
- (20) Van Arnam, E. B.; Dougherty, D. A. Functional Probes of Drug-Receptor Interactions Implicated by Structural Studies: Cys-Loop Receptors Provide a Fertile Testing Ground. *J. Med. Chem.* **2014**, *57* (15), 6289–6300. <https://doi.org/10.1021/jm500023m>.
- (21) Dougherty, D. A. Cation- π Interactions in Chemistry and Biology: A New View of Benzene, Phe, Tyr, and Trp. *Science* **1996**, *271* (5246), 163–168. <https://doi.org/10.1126/science.271.5246.163>.
- (22) Dougherty, D. A. The Cation- π Interaction. *Acc. Chem. Res.* **2013**, *46* (4), 885–893. <https://doi.org/10.1021/ar300265y>.
- (23) Puskar, N. L.; Xiu, X.; Lester, H. A.; Dougherty, D. A. Two Neuronal Nicotinic Acetylcholine Receptors, $\alpha 4\beta 4$ and $\alpha 7$, Show Differential Agonist Binding Modes. *J. Biol. Chem.* **2011**, *286* (16), 14618–14627. <https://doi.org/10.1074/jbc.M110.206565>.
- (24) Beene, D. L.; Brandt, G. S.; Zhong, W.; Zacharias, N. M.; Lester, H. A.; Dougherty, D. A. Cation- π Interactions in Ligand Recognition by Serotonergic (5-HT_{3A}) and Nicotinic Acetylcholine Receptors: The Anomalous Binding Properties of Nicotine. *Biochemistry* **2002**, *41* (32), 10262–10269.
- (25) Da Silva Tavares, X.; Blum, A. P.; Nakamura, D. T.; Puskar, N. L.; Shanata, J. A. P.; Lester, H. A.; Dougherty, D. A. Variations in Binding Among Several Agonists at Two Stoichiometries of the Neuronal, $\alpha 4\beta 2$ Nicotinic Receptor. *J. Am. Chem. Soc.* **2012**, *134* (28), 11474–11480. <https://doi.org/10.1021/ja3011379>.
- (26) Post, M. R.; Limapichat, W.; Lester, H. A.; Dougherty, D. A. Heterologous Expression and Nonsense Suppression Provide Insights into Agonist Behavior at $\alpha 6\beta 2$ Nicotinic Acetylcholine Receptors. *Neuropharmacology* **2015**, *97*, 376–382. <https://doi.org/10.1016/j.neuropharm.2015.04.009>.
- (27) Xiu, X.; Puskar, N. L.; Shanata, J. A. P.; Lester, H. A.; Dougherty, D. A. Nicotine Binding to Brain Receptors Requires a Strong Cation- π Interaction. *Nature* **2009**, *458* (7237), 534. <https://doi.org/10.1038/nature07768>.

- (28) Zhong, W.; Gallivan, J. P.; Zhang, Y.; Li, L.; Lester, H. A.; Dougherty, D. A. From Ab Initio Quantum Mechanics to Molecular Neurobiology: A Cation- π Binding Site in the Nicotinic Receptor. *Proc. Natl. Acad. Sci. U. S. A.* **1998**, *95* (21), 12088–12093.
- (29) Post, M. R.; Tender, G. S.; Lester, H. A.; Dougherty, D. A. Secondary Ammonium Agonists Make Dual Cation- π Interactions in A4 β 2 Nicotinic Receptors. *eNeuro* **2017**, *4* (2), ENEURO.0032-17.2017. <https://doi.org/10.1523/ENEURO.0032-17.2017>.
- (30) Cashin, A. L.; Petersson, E. J.; Lester, H. A.; Dougherty, D. A. Using Physical Chemistry To Differentiate Nicotinic from Cholinergic Agonists at the Nicotinic Acetylcholine Receptor. *J. Am. Chem. Soc.* **2005**, *127* (1), 350–356. <https://doi.org/10.1021/ja0461771>.
- (31) Van Arnem, E. B.; Blythe, E. E.; Lester, H. A.; Dougherty, D. A. An Unusual Pattern of Ligand-Receptor Interactions for the A7 Nicotinic Acetylcholine Receptor, with Implications for the Binding of Varenicline. *Mol. Pharmacol.* **2013**, *84* (2), 201–207. <https://doi.org/10.1124/mol.113.085795>.
- (32) Blum, A. P.; Lester, H. A.; Dougherty, D. A. Nicotinic Pharmacophore: The Pyridine N of Nicotine and Carbonyl of Acetylcholine Hydrogen Bond across a Subunit Interface to a Backbone NH. *Proc. Natl. Acad. Sci. U. S. A.* **2010**, *107* (30), 13206–13211. <https://doi.org/10.1073/pnas.1007140107>.
- (33) Blum, A. P.; Van Arnem, E. B.; German, L. A.; Lester, H. A.; Dougherty, D. A. Binding Interactions with the Complementary Subunit of Nicotinic Receptors. *J. Biol. Chem.* **2013**, *288* (10), 6991–6997. <https://doi.org/10.1074/jbc.M112.439968>.
- (34) Unwin, N. Refined Structure of the Nicotinic Acetylcholine Receptor at 4Å Resolution. *J. Mol. Biol.* **2005**, *346* (4), 967–989. <https://doi.org/10.1016/j.jmb.2004.12.031>.
- (35) Celie, P. H. N.; van Rossum-Fikkert, S. E.; van Dijk, W. J.; Brejc, K.; Smit, A. B.; Sixma, T. K. Nicotine and Carbamylcholine Binding to Nicotinic Acetylcholine Receptors as Studied in AChBP Crystal Structures. *Neuron* **2004**, *41* (6), 907–914. [https://doi.org/10.1016/S0896-6273\(04\)00115-1](https://doi.org/10.1016/S0896-6273(04)00115-1).
- (36) Hilf, R. J. C.; Dutzler, R. X-Ray Structure of a Prokaryotic Pentameric Ligand-Gated Ion Channel. *Nature* **2008**, *452* (7185), 375–379. <https://doi.org/10.1038/nature06717>.
- (37) Hilf, R. J. C.; Dutzler, R. Structure of a Potentially Open State of a Proton-Activated Pentameric Ligand-Gated Ion Channel. *Nature* **2009**, *457* (7225), 115–118. <https://doi.org/10.1038/nature07461>.
- (38) Prevost, M. S.; Sauguet, L.; Nury, H.; Van Renterghem, C.; Huon, C.; Poitevin, F.; Baaden, M.; Delarue, M.; Corringer, P.-J. A Locally Closed Conformation of a Bacterial Pentameric Proton-Gated Ion Channel. *Nat. Struct. Mol. Biol.* **2012**, *19* (6), 642–649. <https://doi.org/10.1038/nsmb.2307>.
- (39) Sauguet, L.; Shahsavari, A.; Poitevin, F.; Huon, C.; Menny, A.; Nemecek, A.; Haouz, A.; Changeux, J.-P.; Corringer, P.-J.; Delarue, M. Crystal Structures of a Pentameric Ligand-Gated Ion Channel Provide a Mechanism for Activation. *Proc. Natl. Acad. Sci.* **2013**, 201314997. <https://doi.org/10.1073/pnas.1314997111>.
- (40) Walsh, R. M.; Roh, S.-H.; Gharpure, A.; Morales-Perez, C. L.; Teng, J.; Hibbs, R. E. Structural Principles of Distinct Assemblies of the Human A4 β 2 Nicotinic

- Receptor. *Nature* **2018**, 557 (7704), 261–265. <https://doi.org/10.1038/s41586-018-0081-7>.
- (41) Dougherty, D. A.; Van Arnem, E. B. In Vivo Incorporation of Non-Canonical Amino Acids by Using the Chemical Aminoacylation Strategy: A Broadly Applicable Mechanistic Tool. *ChemBioChem* **2014**, n/a-n/a. <https://doi.org/10.1002/cbic.201402080>.
 - (42) Nowak, M. W.; Kearney, P. C.; Sampson, J. R.; Saks, M. E.; Labarca, C. G.; Silverman, S. K.; Zhong, W.; Thorson, J.; Abelson, J. N.; Davidson, N. Nicotinic Receptor Binding Site Probed with Unnatural Amino Acid Incorporation in Intact Cells. *Science* **1995**, 268 (5209), 439–442.
 - (43) Nowak, M. W.; Gallivan, J. P.; Silverman, S. K.; Labarca, C. G.; Dougherty, D. A.; Lester, H. A. In Vivo Incorporation of Unnatural Amino Acids into Ion Channels in *Xenopus* Oocyte Expression System. *Methods Enzymol.* **1998**, 293, 504–529.
 - (44) Leisle, L.; Valiyaveetil, F.; Mehl, R. A.; Ahern, C. A. Incorporation of Non-Canonical Amino Acids. *Adv. Exp. Med. Biol.* **2015**, 869, 119–151. https://doi.org/10.1007/978-1-4939-2845-3_7.
 - (45) Papke, R. L.; Smith-Maxwell, C. High Throughput Electrophysiology with *Xenopus* Oocytes. *Comb. Chem. High Throughput Screen.* **2009**, 12 (1), 38–50.
 - (46) Peng, H. B. *Xenopus* Laevis: Practical Uses in Cell and Molecular Biology. Solutions and Protocols. *Methods Cell Biol.* **1991**, 36, 657–662.
 - (47) Wagner, C. A.; Friedrich, B.; Setiawan, I.; Lang, F.; Bröer, S. The Use of *Xenopus* Laevis Oocytes for the Functional Characterization of Heterologously Expressed Membrane Proteins. *Cell. Physiol. Biochem. Int. J. Exp. Cell. Physiol. Biochem. Pharmacol.* **2000**, 10 (1–2), 1–12. <https://doi.org/10.1159/000016341>.
 - (48) Grønlien, J. H.; Håkerud, M.; Ween, H.; Thorin-Hagene, K.; Briggs, C. A.; Gopalakrishnan, M.; Malysz, J. Distinct Profiles of A7 NACHR Positive Allosteric Modulation Revealed by Structurally Diverse Chemotypes. *Mol. Pharmacol.* **2007**, 72 (3), 715–724. <https://doi.org/10.1124/mol.107.035410>.
 - (49) Williams, D. K.; Wang, J.; Papke, R. L. Investigation of the Molecular Mechanism of the A7 Nicotinic Acetylcholine Receptor Positive Allosteric Modulator PNU-120596 Provides Evidence for Two Distinct Desensitized States. *Mol. Pharmacol.* **2011**, 80 (6), 1013–1032. <https://doi.org/10.1124/mol.111.074302>.
 - (50) Hurst, R.; Rollema, H.; Bertrand, D. Nicotinic Acetylcholine Receptors: From Basic Science to Therapeutics. *Pharmacol. Ther.* **2013**, 137 (1), 22–54. <https://doi.org/10.1016/j.pharmthera.2012.08.012>.
 - (51) daCosta, C. J. B.; Free, C. R.; Corradi, J.; Bouzat, C.; Sine, S. M. Single-Channel and Structural Foundations of Neuronal A7 Acetylcholine Receptor Potentiation. *J. Neurosci. Off. J. Soc. Neurosci.* **2011**, 31 (39), 13870–13879. <https://doi.org/10.1523/JNEUROSCI.2652-11.2011>.
 - (52) Wallace, T. L.; Porter, R. H. P. Targeting the Nicotinic Alpha7 Acetylcholine Receptor to Enhance Cognition in Disease. *Biochem. Pharmacol.* **2011**, 82 (8), 891–903. <https://doi.org/10.1016/j.bcp.2011.06.034>.
 - (53) Thomsen, M. S.; Mikkelsen, J. D. Type I and II Positive Allosteric Modulators Differentially Modulate Agonist-Induced up-Regulation of A7 Nicotinic

- Acetylcholine Receptors. *J. Neurochem.* **2012**, *123* (1), 73–83.
<https://doi.org/10.1111/j.1471-4159.2012.07876.x>.
- (54) Lendvai, B.; Kassai, F.; Szájli, A.; Némethy, Z. A7 Nicotinic Acetylcholine Receptors and Their Role in Cognition. *Brain Res. Bull.* **2013**, *93*, 86–96.
<https://doi.org/10.1016/j.brainresbull.2012.11.003>.
- (55) Yang, J.-S.; Seo, S. W.; Jang, S.; Jung, G. Y.; Kim, S. Rational Engineering of Enzyme Allosteric Regulation through Sequence Evolution Analysis. *PLoS Comput. Biol.* **2012**, *8* (7), e1002612.
<https://doi.org/10.1371/journal.pcbi.1002612>.

Chapter 2

THE BINDING INTERACTIONS OF NS6740, A SILENT AGONIST OF $\alpha 7$ THE NICOTINIC ACETYLCHOLINE RECEPTOR

Abstract

The $\alpha 7$ nicotinic acetylcholine receptor (nAChR) is an important drug target for a number of neurological and inflammatory disorders. Silent agonists are an emerging class of drugs that bind to the receptor but do not open the channel. Instead they shift the receptor to a desensitized state. Silent agonists have shown promise at targeting a subset of $\alpha 7$ nAChR mediated signaling processes. We use non-canonical amino acid mutagenesis to characterize the binding to $\alpha 7$ by the silent agonist NS6740. We find that like $\alpha 7$ agonists, NS6740 forms a cation- π interaction with TyrA. We also showed that NS6740 makes a novel hydrogen bond to TyrA and that this interaction is necessary for the silent agonist activity of NS6740.

2.1 Introduction

The nicotinic acetylcholine receptor (nAChR) $\alpha 7$ subtype^{1,2} is the second most abundant neuronal nAChR subtype, and is found throughout the brain both presynaptically, where it facilitates neurotransmitter release, and postsynaptically, where it modulates synaptic transmission. While $\alpha 7$ subunits predominantly form homomeric receptors, heteromeric $\alpha 7\beta 2$ receptors have been reported.³⁻⁵ The homomeric $\alpha 7$ nAChR is involved in cognitive function and memory has been linked to many neurological disorders including Alzheimer's and schizophrenia.⁶ $\alpha 7$ is also expressed on non-excitabile cells including astrocytes, microglia and endothelial cells where it plays a functional role in immunity, inflammation and neuroprotection.^{1,7} The $\alpha 7$ nAChR is currently a drug target.

Despite being one of the most abundant nAChRs in the brain the $\alpha 7$ subtype is not optimized for synaptic transmission. Unlike other neuronal nAChRs, it is characterized by very short very low probability channel opening.⁸ This is due to agonist concentration-dependent desensitization; channel opening occurs when only one or two of the five orthosteric binding sites are occupied and binding to additional sites results in

desensitization.^{9–12} Choline, the ubiquitous biological precursor for ACh, is an agonist of $\alpha 7$.¹³ It is also highly permeable to calcium (PCa:PNa of ≥ 10).^{14,15} None of these features are ideal for synaptic transmission. Taken together with the fact that $\alpha 7$ is expressed outside the synapse of neurons and in non-excitabile cells it has been hypothesized that $\alpha 7$ may participate in metabotropic signaling as well as ionotropic signaling.¹⁶

Silent agonists are an emerging class of drugs developed to target $\alpha 7$. Upon binding, they do not open the channel but rather induce a conformational change which stabilizes a desensitized state (Figure 2.1). This can be confirmed by the co-application of a type II positive allosteric modulator (PAM) such as PNU-120596, which shifts the equilibrium toward a conducting open state, presumably by destabilizing the desensitized state and/or stabilizing the open state. It has been proposed that the desensitized and open states associated with a silent agonist are different from those associated with a conventional agonist.^{17,18} Silent agonists should not be thought of as competitive antagonists. Competitive antagonists simply block agonist binding and do not induce a conformational change that is sensitive to binding of a type II PAM.

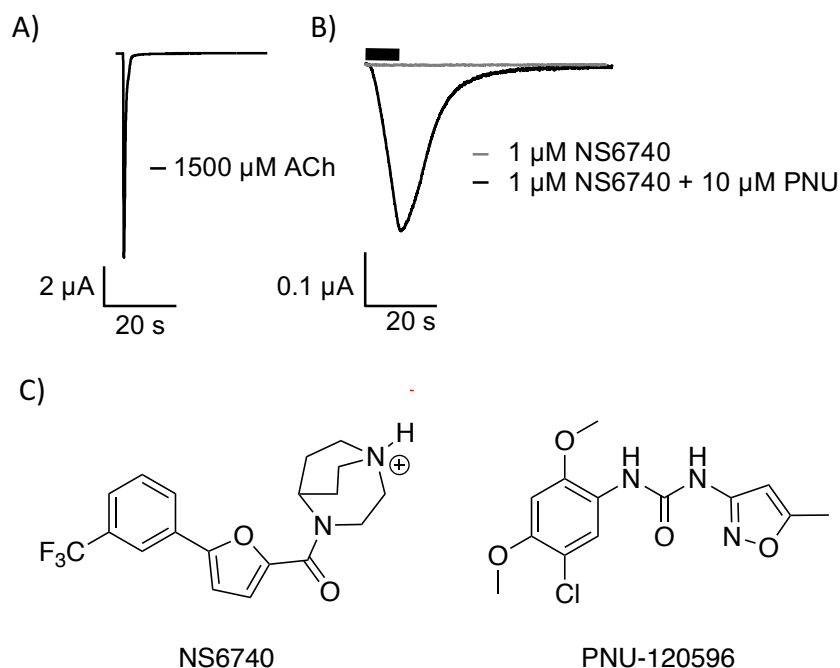


Figure 2.1: Silent agonist activity. A) Representative current trace for application of acetylcholine (ACh) on $\alpha 7$. B) Representative current trace for the silent agonist, NS6740, on $\alpha 7$ and the co-application of NS6740 and the Type II positive allosteric modulator (PAM) PNU-120596. C) Structure of NS6740 and PNU-120596.

The first silent agonist to be characterized, NS6740,¹⁹ has been shown *in vitro* to modulate the inflammatory response of microglia cells as part of the cholinergic anti-inflammatory pathway²⁰ and in mouse models treated neuropathic pain.²¹ Another silent agonist, PMP-072, was shown in mouse models to have anti-arthritic effects.²² The exact signaling mechanism behind these physiological effects is unclear, but it has been hypothesized that silent agonist may activate a metabotropic signaling pathway in $\alpha 7$.¹⁶ If true, silent agonists represent novel therapeutic agents for the selective targeting of a specific subset of $\alpha 7$ -mediated signaling pathways, such as those related to chronic inflammation and neuropathic pain.

Little is known about the core pharmacophore of silent agonists, and a better understanding of the binding of silent agonists at the orthosteric site could guide the design of new silent agonists. So far all characterized silent agonists have a cationic nitrogen, either a protonatable amine or a quaternary ammonium, and are believed to bind at the orthosteric site.²¹ Initial studies on alkylammonium ligands showed that increasing bulk around the cation reduced agonist activity while maintaining desensitization activity.^{17,23} NS6740 has a bulky bicyclo [3.2.2] ring system, but derivatives of NS6740 lacking the bulky bicyclic ring system still exhibit silent agonist activity.²⁴

Electrophysiology can be used to gain vital structure-function information on ion channels. However, silent agonists require a PAM to generate an electrophysiological signal, complicating matters. This chapter uses non-canonical amino acid mutagenesis (Figure 2.2) to probe the binding of the silent agonist NS6740 at the orthosteric site and compares the results to previous work from our lab looking at the binding of typical agonists such as acetylcholine (ACh) and nicotine. We find that the silent agonist NS6740 makes a cation- π interaction to TyrA and a never before characterized, functionally significant hydrogen bond to TyrA.

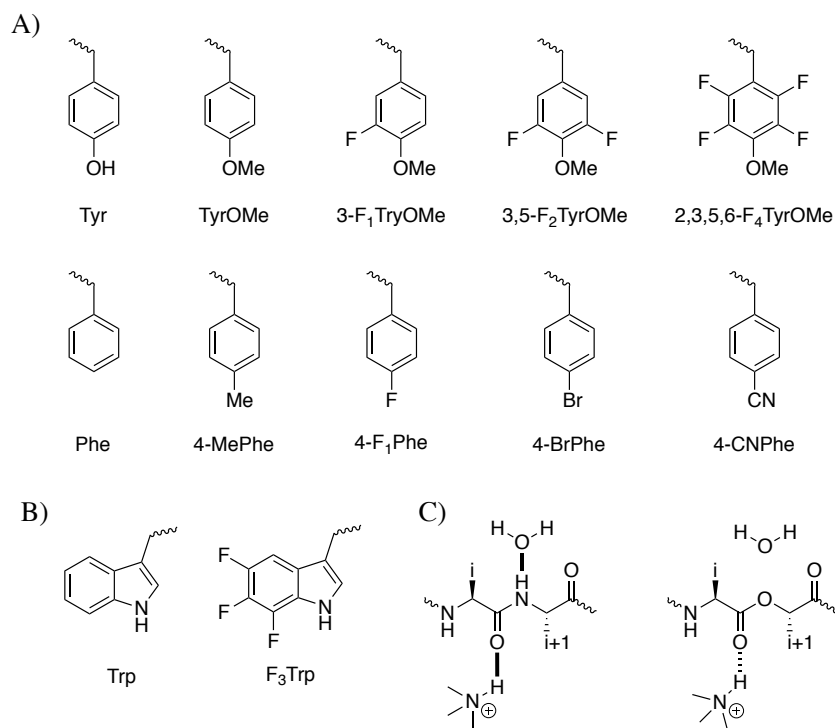


Figure 2.2: Structures of the side chains of noncanonical amino acids. A) Tyrosine derivatives. B) Tryptophan derivatives. C) Backbone amide to ester mutation strategy for perturbing a hydrogen bond.

2.2 Results

2.2.1 Measuring binding interactions in the presence of a PAM:

The metric for measuring the effect of noncanonical amino acid incorporation, EC_{50} , is a composite measure of several equilibria, including agonist binding and channel gating events. Therefore, there is ambiguity in how a specific mutation shifts EC_{50} , because a mutation can affect gating, binding or both. Single channel measurements can provide more detailed kinetic analysis on which equilibrium is being perturbed. However, single channel studies are labor intensive and are not suitable to this project given the number of mutations probed and protein expression limitations for $\alpha 7$.

Noncanonical amino acid mutagenesis allows for very subtle and precise modifications of the protein. This coupled with our knowledge of the structure of the binding site, allows us to probe interactions within the binding site, and conclude that observed shifts in EC_{50} are a result of attenuated binding interactions. However, a complicating factor in this project is the need to co-apply a PAM with the silent agonist of

interest for a signal to be observed. In ion channels, allosteric modulators can induce a long-range conformational change to the orthosteric binding site, altering the binding affinity of the agonist, or they can modulate the gating transition of the receptor. If the former mechanism were operative, it would complicate analysis of silent agonist binding. Fortunately, our lab have previously shown that in $\alpha 7$ the type II PAM PNU-120596 does not alter the orthosteric binding site, as determined by detailed interactions with the native agonist ACh.²⁵ This was done by comparing the impact of a mutation on receptor function with or without the co-application of the PAM. Given that PNU-120596 does not alter the agonist binding site, we can assume that any change from mutations made to the binding site are from an interaction with NS6740 not PNU-120596. As such, studies of NS6740 were performed in the presence of 10 μ M PNU-120596, producing robust signals.

Previous work in our lab using PNU-120596 was done by pre-application of the PAM to cells before the agonist was applied. This was done to ensure the PAM had come to binding equilibrium. At the start of this study the OPUS, our electrophysiology rig, only had one working perfusion pump making pre-application impossible without manually replacing pipet tips between every does. Only a slight increase to EC_{50} and minimal changes to trace shape were observed when oocytes were not pre-incubated with 10 μ M PNU-120596 compared to cells that were pre-incubated for 30 seconds (Figure 2.3). Preincubation can also serve as a control to ensure mutations do not convert PNU-120596 from a PAM to an allosteric agonist. This was not a concern since all mutations had previously been screened by Marotta et al..²⁵ All subsequent experiments were carried out without any pre-incubation.

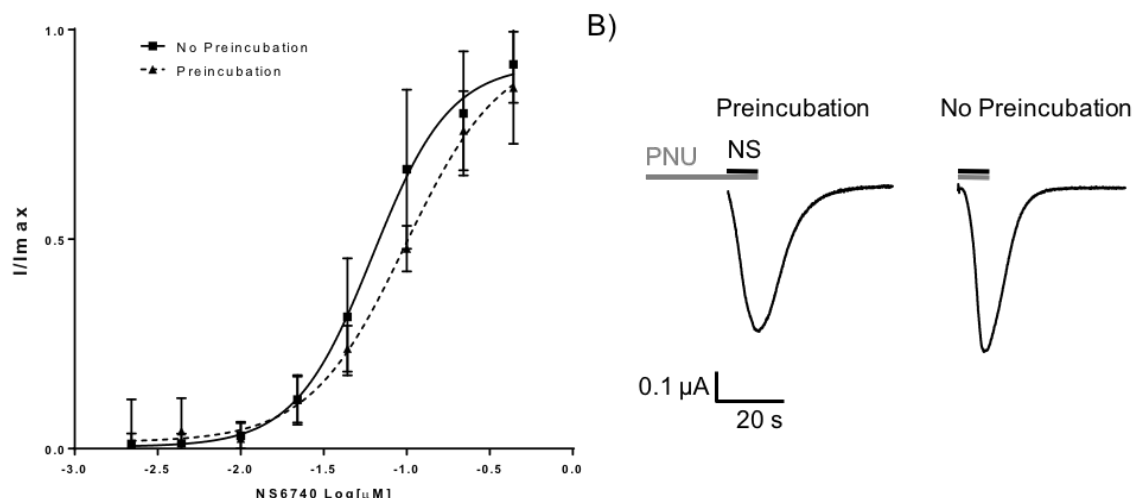


Figure 2.3: Effect of pre-incubation with PAM PNU-120596 on NS6740 response. A) Shows EC_{50} curves with (98 ± 11 nM) and without pre-incubation (62 ± 4.5 nM). B) Shows representative traces with and without pre-incubation.

2.2.2 Binding interaction of TyrA with NS6740:

First we looked at whether the silent agonist, NS6740, still forms a cation- π interaction with TyrA (Y115) like traditional $\alpha 7$ agonists.^{26,27} It is possible to identify a cation- π interaction by progressively fluorinating the aromatic group, reducing the π electron density of the aromatic ring surface, and thus weakening the interaction. When plotted against calculated cation- π binding energies, this results in a “fluorination” plot. This approach also applies to other deactivating substituents on the aromatic side chain, including cyano and bromo functional groups. However, fluorination affects the pK_a of the hydroxyl functional group of tyrosine as well as the strength of the cation- π interaction. Therefore, to study tyrosine residues, such as TyrA, it is necessary to either methylate the hydroxyl group, producing TyrOMe, or remove the hydroxyl group entirely and use Phe derivatives.

NS6740 does form a cation- π interaction with TyrA (Table 2.1, Figure 2.4). The fluorination plot shows a linear relationship. The slope of the fluorination plot (-0.16 ± 0.03) is similar to that of acetylcholine (-0.15 ± 0.02) at TyrA for $\alpha 7$.²⁵ This suggests a similar strength of interaction, despite the increased bulkiness of the ligand. Using acetylcholine, we have previously shown that a sterically significant substituent is needed

at the 4-position of the A-site residue.^{25,27} This effect is less pronounced for NS6740 but still noticeable, with Phe and 4-F-Phe not falling on the line.

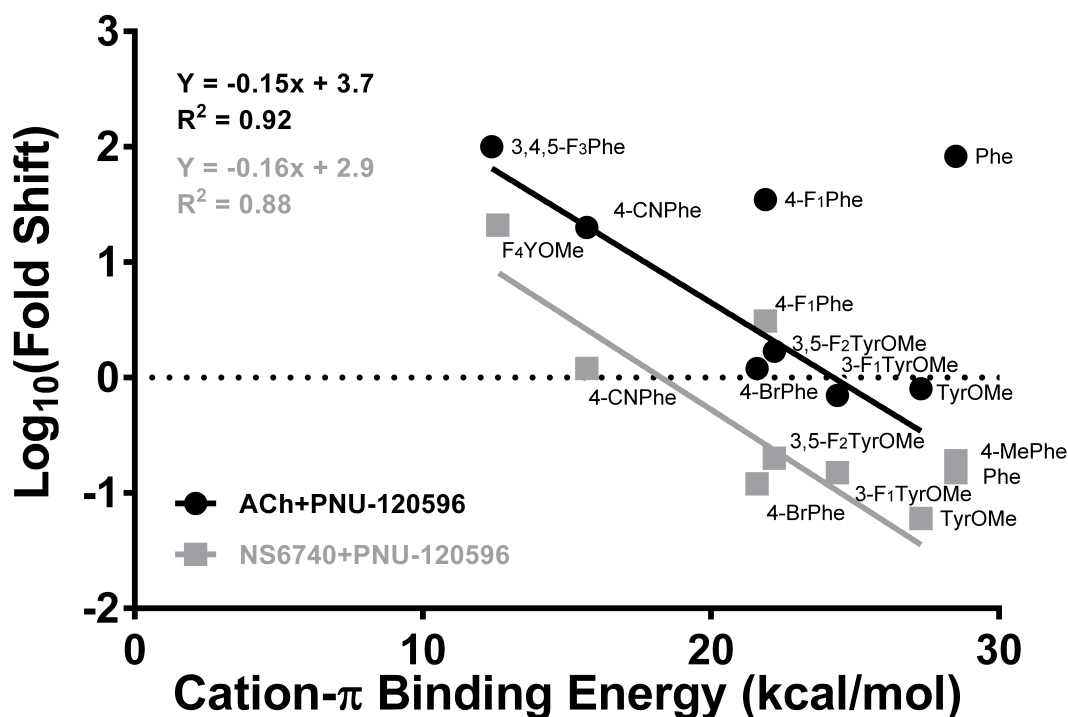


Figure 2.4: Cation- π plot for TyrA in the $\alpha 7$ nAChR. TyrA shows a cation- π interaction with silent agonist NS6740 in the presence PAM PNU-120596. The similar slope of the linear regression analysis of the $\text{Log}_{10}[\text{Fold Shift}]$ to ACh indicates a similar strength interaction (NS6740, -0.16 ± 0.03 and ACh -0.15 ± 0.02). The downward shift is because of the removal of the TyrA hydrogen bond resulting in an across the board gain of function for TyrA mutations in the presence of NS6740 nor the agonist ACh. ACh data is adapted from Marotta et al..²⁵

A novel observation is that TyrA forms a functionally relevant hydrogen bond for activation of NS6740. A large *gain of function* was observed when Tyr was replaced by TyrOMe (Table 2.1). The hydroxyl group of TyrA can act as both a hydrogen bond donor and acceptor. Methylation of the hydroxyl group removes the hydrogen bond donating ability of the residue but not its hydrogen bond accepting ability. Note that activation by ACh is unaffected by the Tyr-to-TyrOMe mutation, both in the presence or absence of PNU-120596.²⁵ While our lab has observed a *loss* of function for this mutation before,^{28–30} most notably in muscle type nAChR, this is the first time we have ever seen gain of function for TyrOMe.

Table 2.1: EC₅₀ Values of Aromatic Box Residues in $\alpha 7$ for NS6740 + PNU-120596 (10 μ M)

Mutation	EC ₅₀ (nM \pm SEM)	Hill (\pm SEM)	I _{max} (μ A)	Fold Shift From WT	n
WT	62 \pm 4.5	1.9 \pm 0.21	0.24-2.4	-	13
TyrA					
TyrOMe	3.6 \pm 0.19	3 \pm 0.41	0.33-34	0.06	10
3-F ₁ TyrOMe	9.2 \pm 1.1	2 \pm 0.41	0.19-25	0.15	11
3,5-F ₂ TyrOMe	12 \pm 1.4	2 \pm 0.41	0.43-39	0.20	12
4-BrPhe	7.2 \pm 0.41	2.7 \pm 0.31	0.13-25	0.12	13
4-CNPh	71 \pm 2.8	3.1 \pm 0.27	2.9-32	1.20	13
2,3,5,6-F ₄ TyrOMe	1300 \pm 110	3.4 \pm 0.74	0.01-1.6	21	10
Phe	9.1 \pm 0.4	2.9 \pm 0.34	1.2-16	0.15	14
4-MePhe	12 \pm 0.56	2.5 \pm 0.28	0.01-0.29	0.19	13
4-F ₁ Phe	190 \pm 7.7	2.1 \pm 0.15	0.13-2.7	3.10	13
TrpB					
Trp	66 \pm 3.5	2.4 \pm 0.25	0.06-0.46	1.10	13
Wah	13 \pm 0.67	2.6 \pm 0.33	7.9-43	0.20	12
F ₃ -Trp	340 \pm 10	2.3 \pm 0.12	0.02-6.8	5.50	14
TyrC2					
Phe	60 \pm 9.1	2 \pm 0.33	0.01-0.41	0.96	13
TyrOMe	46 \pm 2.8	2.2 \pm 0.26	0.01-0.08	0.74	10
4-F ₁ Phe	85 \pm 9.5	1.9 \pm 0.32	0.01-0.02	1.40	11
3-F ₁ TyrOMe	160 \pm 8.5	2.3 \pm 0.17	0.01-0.27	2.70	13
3,5-F ₂ TyrOMe	160 \pm 12	2.7 \pm 0.43	0.01-0.12	2.50	11
4-BrPhe	38 \pm 7.1	1.6 \pm 0.26	0.02-0.13	0.60	10
TrpD					
Trp	90 \pm 6.8	1.8 \pm 0.22	0.01-0.15	1.40	13
F ₃ -Trp	9.2 \pm 0.37	3.1 \pm 0.39	0.53-9.5	0.15	12
Leu 114					
Leu	78 \pm 7.4	2.9 \pm 0.2	0.04-12	1.3	18
Lah	88 \pm 5.5	1.6 \pm 0.024	0.01-0.60	1.4	8
Ser172					
Thr	57 \pm 4	1.8 \pm 0.21	1.2-44	1	11
Tah	500 \pm 33	2.6 \pm 0.31	0.66-41	7.6	16

The shift in EC_{50} was accompanied by an increase in relative efficacy for the NS6740/PNU-120596 combination, being 1.9 ± 0.32 for the TyrOMe mutant vs. 0.027 ± 0.004 for the wild type, relative to activation by ACh (Table 2.2). A comparable effect was not seen when judging the impact of PNU-120596 on ACh activation – wild type and the TyrOMe mutant show only a small difference.

Table 2.2: Relative Efficacy to I_{max} Acetylcholine for NS6740 Co-Applied with Type 1 and 2 PAMs at $\alpha 7$ (SEM)

Method	Drug	WT	n	TyrA	TyrOMe	n
PEAK Height	NS6740	NR		0.13	± 0.1	15
	ACh	1.00 ± 0.039	19	0.325	± 0.056	16
	NS6740+PNU-120596	0.027 ± 0.004	19	1.9	± 0.32	16
	ACh	1.25 ± 0.10	19	0.60	± 0.071	16
	NS6740+Genistein	NR		0.13	± 0.4	15
Area	NS6740	NR		0.34	± 0.053	16
	NS6740+PNU-120596	0.49 ± 0.093	18	21	± 6.9	17
	NS6740+Genistein	NR		1.33	± 0.3	15

The increase in efficacy for the TyrOMe mutant was so great, we hypothesized that the PAM PNU-120596 may no longer be needed for NS6740 to open the channel (Table 2.3, Figure 2.5). This proved to be true, as NS6740 acts as partial agonist on the mutant channel with an EC_{50} of 150 ± 22 nM. The shape of the signal changed in the absence of PNU-120596 to resemble a much more traditional $\alpha 7$ agonist trace, which is characterized by its sharp peak and fast desensitization (Figure 2.5). This is understandable, given that PNU-120596 acts by disrupting the desensitized state, resulting in broader signals when co-applied with an agonist.

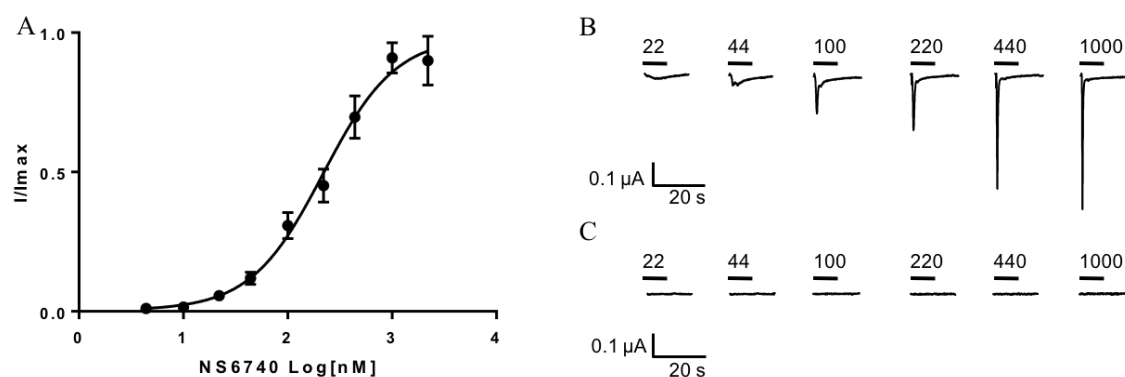


Figure 2.5: Effect of the $\alpha 7$ TyrA TyrOMe mutation on NS6740 activity. A) EC_{50} curve for application of NS6740 on $\alpha 7$ TyrA TyrOMe without any type 2 PAM. B) Representative current traces for NS6740 on $\alpha 7$ TyrA TyrOMe. C) Representative current traces for NS6740 on $\alpha 7$ wild type receptors.

During efficacy experiments, no suppression of signal for applications of ACh after application of NS6740 were observed for wild type receptors in contrast to previous work, which indicated NS6740 had a slow binding off rate.¹⁸ This is most likely due to variations in experimental set-up. However, for the TyrOMe mutation a significant decrease in the efficacy of ACh after application of NS6740 was observed (Table 2.2). This indicates that TyrOMe may lower the binding off rate for NS6740.

Table 2.3: EC_{50} Values at TyrA:TyrOMe

Drug	EC_{50} (nM \pm SEM)		Hill (\pm SEM)		I_{max} (μ A)	n
NS6740	150	\pm 22	1.7	\pm 0.37	0.052-1.8	10
NS6740+PNU-120596	3.6	\pm 0.19	3	\pm 0.41	0.33-35	10
NS6740+Genistein	8.4	\pm 0.75	1.6	\pm 0.16	0.22-7.2	12

To further explore the effect of the TyrA TyrOMe mutation on the partial agonist activity of NS6740 we investigated the co-application of NS6740 with genistein, a type I PAM for $\alpha 7$. Type 1 PAMs, like genistein, are believed to bind in the same transmembrane region as PNU-120596 but do not destabilize the desensitized state and instead only increase peak current. Double mutant cycle analysis using acetylcholine established that like PNU-120596, genistein doesn't alter the binding site, at least for the TyrA TyrOMe mutation (Table 2.4). Co-application of NS6740 and genistein at wild type receptors did not produce an appreciable current. For the TyrA TyrOMe mutant, genistein shifted the

EC₅₀ curve and generated a broader signal both effects similar to what is seen with PNU-120596 (Table 2.3). No increase in efficacy was observed using standard peak height analysis but efficacy did increase as a measure of the area under the curve an alternative measure sometimes used for $\alpha 7$ because of its fast desensitization (Table 2.2). Efficacy experiments were hampered by low currents of NS6740 at TyrA TyrOMe which necessitated testing efficacy at EC₁₀₀; normally type I PAMs are screened at concentrations lower than EC₅₀ to allow for observation of full potentiation.

Table 2.4: EC₅₀ Values and Coupling Constants for Genistein and ACh at TyrA

Mutation	EC ₅₀ (μ M \pm SEM)	Hill (\pm SEM)	Imax (μ A)	Fold Shift From WT	n
WT	120 \pm 8	1.8 \pm 0.2	1.1-23	-	20
TyrA: TyrOMe	130 \pm 8	2.3 \pm 0.23	2.9-48	1.1	10

2.2.3 Characterization of other potential cation- π binding interactions of NS6740 in the orthosteric binding site

Previous work has shown that the high affinity agonist epibatidine makes a cation- π interaction with TyrC2 (Y217) at $\alpha 7$ in addition to the cation- π interaction at TyrA.²⁷ Low currents (Table 2.1) prevented a complete study of TyrC2; no signal was detected for more strongly perturbing residues such as 4-CNPhe or 2,3,5,6-F₄TyrOMe. However, it is still clear that NS6740 does not make a strong cation- π interaction (Figure 2.6); the most perturbing residue measured, 4-BrPhe, was essentially wild type.

Acetylcholine also does not form a cation- π interaction at TyrC2, but two trends were noted. First, bulk is required at the 4 position for ACh binding.²⁵ This is not true for NS6740 - Phe and TyrOMe have similar fold shifts, 0.96 and 0.74 respectively. This may be because NS6740 is bulkier and compensates for the loss of bulk at the 4 position. Secondly, TyrC2 is sensitive to 3- or 5- substitutions on the ring system for ACh binding.²⁵ This is also true for NS6740; the largest losses of function at TyrC2 were for 3-F₁TyrOMe and 3,5-F₂TyrOMe. However, the magnitude of the effect was much smaller (approximately 2.5-fold for NS6740 compared to greater than 10-fold for ACh). Again, the bulk of the silent agonist may explain this. Overall, interaction of NS6740 with TyrC2 does not appear to play an important functional role.

The remaining members of the aromatic box were also probed and NS6740 was found not to make meaningful interactions with any of the other residues screened. Insertion of the highly perturbing residue F₃-Trp at TrpB (W171) resulted in a modest 5.5-fold shift (Table 2.1) indicating, at best, a very weak interaction. Substitution by F₃-Trp at TrpD (W77) showed a slight gain of function, consistent with observations for acetylcholine binding to $\alpha 7$ (Table 2.1).²⁵ TrpD has never been implicated in a cation- π interaction with an agonist in any nAChR.²⁶ TyrC1 (Y210), the final aromatic residue that composes the classical binding box, was not probed, because historically any perturbation at this site in $\alpha 7$ has resulted in very large losses of function,²⁷ and it has never been implicated in a cation- π interaction in any Cys-loop receptor.²⁶

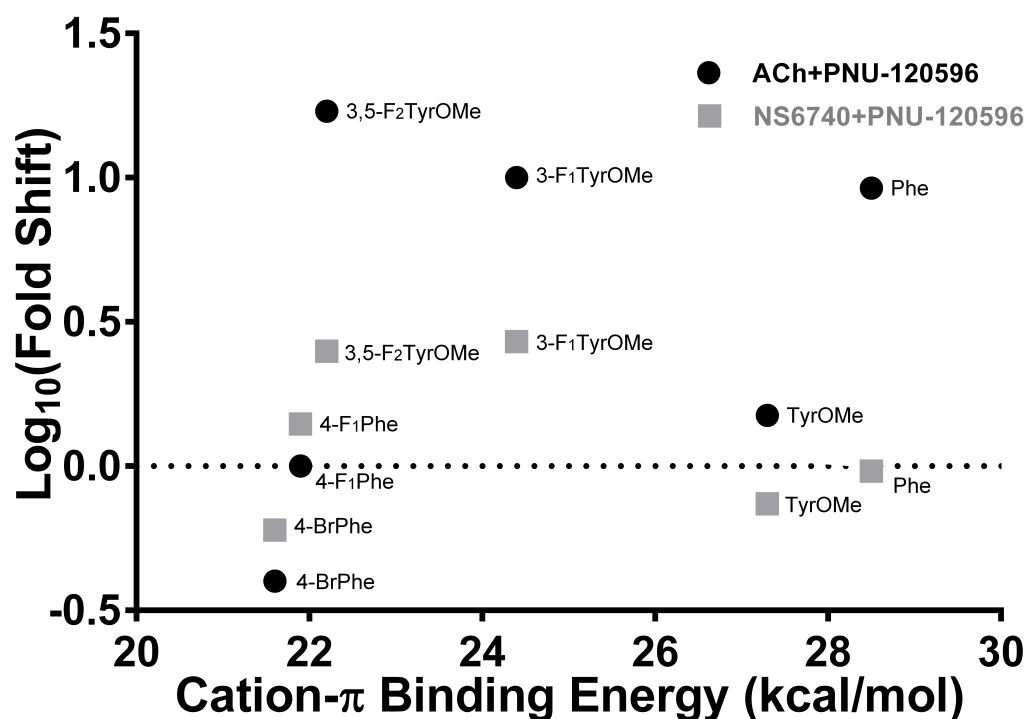


Figure 2.6: Cation- π plot for TyrC2 in the $\alpha 7$ nAChR. TyrC2 shows no cation- π interaction with silent agonist NS6740 nor the agonist ACh. ACh data is taken from Marotta et al.²⁵

2.2.4 Characterization of backbone hydrogen bonding to NS6740 at the orthosteric binding site

Next we looked at important backbone hydrogen bonding interactions within the orthosteric binding site. Incorporation of α -hydroxy analogs at appropriate locations eliminates the hydrogen bond donating backbone NH and weakens the hydrogen bonding ability of the carbonyl (i-1) by converting it to an ester (Figure 2.2). This assay allows for the study of functionally relevant hydrogen bonds only: crystal structures may show the presence of a hydrogen bond but EC₅₀ will only shift if the hydrogen bond is functionally relevant.

Like with other non-quaternary amine cation agonists a hydrogen bond between NS6740 and the carbonyl of TrpB was observed. (Table 2.1, S172). Second, L141 has been shown to act as a hydrogen bond donor for epibatidine but not acetylcholine or varenicline.³¹ NS6740 does not make a functionally relevant hydrogen bond at this site (Table 2.1). Finally, the carbonyl of S170 was shown to act as a hydrogen bond acceptor. A significant gain of function was observed when the residue (i+1) was mutated to the corresponding hydroxy acid (Table 2.1, TrpB Wah). This is consistent with previous work on $\alpha 7$.²⁵

2.3 Discussion

This work focuses on the binding interactions of the silent agonist NS6740 at the $\alpha 7$ nAChR. Noncanonical amino acids were used to probe the orthosteric site, and the results for NS6740 — in the presence of the Type 2 PAM PNU-120596 — were compared to the endogenous agonist ACh. This resulted in three major findings: first, we confirmed that NS6740 binds at the orthosteric site; second, TyrA forms a hydrogen bond that discourages activation in the presence of NS6740, and this hydrogen bond is a requirement for silent agonist activity; and third, NS6740 forms a cation- π interaction with TyrA, consistent with several agonists of $\alpha 7$.

It was predicted that NS6740 binds at least partially in the orthosteric binding site, given that NS6740 contains a cationic nitrogen at physiological pH and is a competitive inhibition of the native agonist.²¹ Using noncanonical amino acids to probe binding interactions of the orthosteric binding site, we showed that NS6740 does indeed bind at the

orthosteric binding site. This is evidenced by the cation- π interaction to TyrA and hydrogen bonds to TyrA and to the backbone carbonyl of TrpB. This is the most direct evidence so far concerning the binding site of NS6740. Furthermore, we observe subtle differences in those interactions that give insight into the nature of silent agonist binding.

An intriguing finding of the present work is the key role of a hydrogen bond involving the OH of TyrA as the donor. This was revealed by the strong gain of function for the TyrOMe mutation, an effect not seen with this substitution in any other study. This relatively subtle mutation profoundly impacts receptor response to NS6740, turning the silent agonist – which produces no signal on its own – to a conventional partial agonist. Additionally, removal of the Tyr OH appears to lower the binding off rate for NS6740 which further indicates an altered binding site. In principle, the hydrogen bond acceptor could be another residue side chain, the protein backbone, or the silent agonist itself. We propose that the most likely hydrogen bonding partner is the amide carbonyl of NS6740. Related compounds lacking the amide carbonyl, but maintaining a similar overall structure, have been reported in the literature as partial agonists of $\alpha 7$,¹⁹ supporting the importance of the carbonyl of NS6740 to its silent agonist activity. Secondly, the distance between the cationic nitrogen and carbonyl of NS6740 is $\sim 5.9\text{\AA}$. While there is some variability, a typical distance observed in x-ray crystal structures between the backbone carbonyl of TrpB, which also makes a hydrogen bond to ligand, and the TyrA OH is 5.8\AA , as seen in the antagonist MLA bound and *apo* crystal structures of the $\alpha 7$ -AChBP chimera.^{32,33} This suggests that the receptor could easily adapt to an arrangement such as shown in Figure 2.7. It is probable that the hydrogen bond between the carbonyl of NS6740 and the OH of TyrA locks the receptor in a closed or an alternative desensitized state (**D***). Removal of the TyrA OH, as in the case of TyrOMe, removes this interaction and turns NS6740 into a partial agonist possible by allowing the binding box to shift or contract. X-ray crystal structures of $\alpha 7$ -AChBP chimera with full agonists bound have a shorter TyrA OH to TrpB distance (5.0\AA).^{32,34}

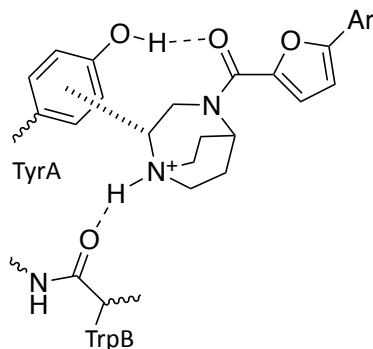


Figure 2.7: Scheme of purposed binding interactions of NS6740 at the orthosteric binding site of $\alpha 7$ nAChR. Showing a hydrogen bond and a cation- π interaction to TyrA and a hydrogen bond to TrpB

Figure 2.8 presents a simplified model to describe the energy landscape of receptor activation based on the observed binding of NS6740 to mutated receptors. ACh stabilizes the open state (**O**), enabling channel activation. In the $\alpha 7$ nAChR, the desensitized state **D** is readily reached via either the open or the closed ACh-bound state (the latter path is not shown in Figure 2.8). A silent agonist such as NS6740 is thought to stabilize an alternative desensitized state, **D***, which cannot gate.¹⁸ Addition of a type II PAM such as PNU-120596 destabilizes **D*** and/or stabilizes an alternative open state, **O***, allowing channel gating. The TyrA to TyrOMe mutation results in a sharp peak (Figure 2.8), typical of normal agonist activity and fast desensitization, indicating that removal of the hydrogen bond results in NS6740 stabilizing a more typical open state and acting on its own as a partial agonist. Figure 2.8 shows the mutation acting in a manner similar to that of ACh, but other mechanisms are possible.

Attempts to further characterization the effect of the TyrOMe mutation on the nature of observed open state using the type I PAM genistein proved inconclusive. Type I PAMs, such as genistein, do not affect the **D*** state and instead increase peak conductance through other mechanisms possibly lowering the barrier to the traditional **O** state.^{10,35} When co-applied with NS6740, genistein did not open wild type receptors confirming that type I PAMs do not affect the **D*** state. Genistein did acted as a PAM shifting the EC_{50} dramatically for TyrA TyrOMe receptors however efficacy as measured by peak height did not alter. If Genistein had resulted in significant increase in peak conductance it would have supported the theory that NS6740 bound to the TyrA TyrOMe mutated receptor access the traditional **O** state. However, it is impossible to rule out the theory because,

given the experimental need to use a saturating dose, any increase in peak conductance would have been small and may have been lost to noise. Genistein did significantly broaden the peak and this was reflected by an increase in efficacy as measured by area. Peak broadening is $\alpha 7$ is a sign of an altered desensitized state typically associated with type II PAMs such as PNU-120596. Genistein may have some type II PAM like macroscopic qualities: a review of the literature showed that the distinction between type I and II PAMs is not clear cut and PAMs have been identified that exhibit intermediate type I/II macroscopic properties.^{36–39}

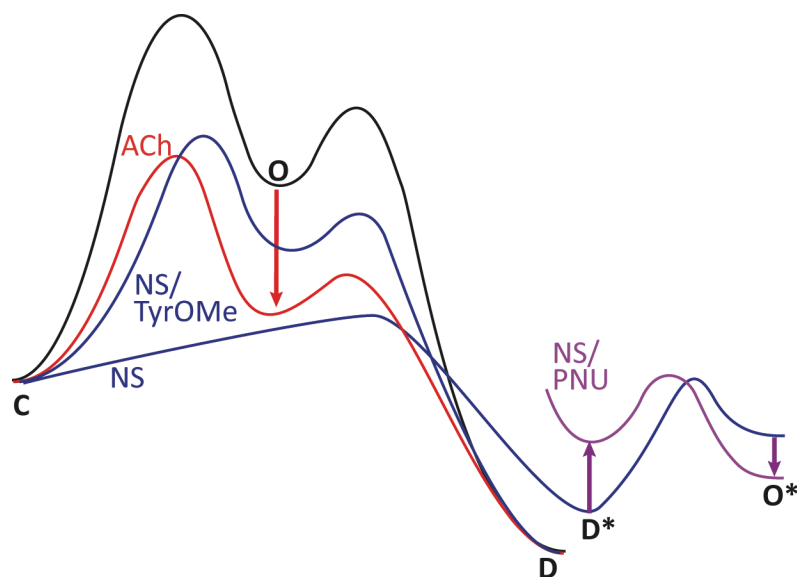


Figure 2.8. Schematic summarizing the energy landscape for receptor activation based on the results described here. The scheme is based in part on previously published models of Papke.¹⁸ Shown are the conventional closed (C), open (O), and desensitized (D) states, as well as alternative desensitized and open states (D* and O*) that are accessed by a silent agonist.

The final major finding is that, like all agonists tested at $\alpha 7$, NS6740 forms a cation- π interaction to TyrA. A typical dependence of EC_{50} on the cation- π binding ability of the residue at the TyrA position is seen (Figure 2.4). A caveat is that, when probing for a cation- π interaction at TyrA, we have altered the OH of the Tyr so that the hydrogen bond of Figure 2.7 does not form. It is conceivable that this change turns on a cation- π interaction that is absent in the wild type receptor. We consider this unlikely, since no other aromatic residue shows a cation- π interaction, and a cation- π interaction to TyrA is a universal feature of compounds that activate the $\alpha 7$ nAChR.

We have used noncanonical amino acids and nonsense suppression to probe the binding of NS6740, a silent agonist. This was the first structure-function study of a silent agonist, and we showed that a specific hydrogen bond inhibits agonist activity and is important for suppressing channel opening for silent agonists. Given these results, in the future it may be possible to probe the desensitized state using nonsense suppression and silent agonists.

Acknowledgements:

We thank Chris Marotta for making almost all the constructs needed for this project, providing thoughtful insights into expressing and working with $\alpha 7$ and the Moore Foundation for funding.

2.4 Materials and Methods

Molecular Biology. The rat nAChR $\alpha 7$ subunit (pAMV vector), Ric3 (pAMV vector), and NACHO (pAMV vector), were used as the bases for all constructs. Residue numbering was based on the full-length protein containing the signaling sequence as found on the UniProt database (Q05941). Site directed mutagenesis was performed by PCR using the Stratagene QuikChange protocol with primers from Integrated DNA Technologies. The circular cDNA plasmids were linearized with *NotI-HF* (New England BioLabs) and purified (Qiagen). DNA was then transcribed *in vitro* using the T7 mMessage Machine kit (Ambion) and the mRNA was isolated using the RNeasy purification kit (Qiagen). The Amber (UAG) stop codon was used for incorporating noncanonical amino acids in the $\alpha 7$ subunit. The 74-nucleotide THG73 tRNA and 76-nucleotide THG73 tRNA were *in vitro* transcribed using the MEGAscript T7 (Ambion) kit and isolated using CHROMA SPIN DEPC-H₂O columns (Clontech). Final concentrations were determined by UV-Vis.

Oocyte Preparation and Injection. *Xenopus laevis* oocytes (stage IV and V) were retrieved as described previously.⁴⁰ For conventional mutagenesis experiments, $\alpha 7$ and Ric3 mRNA were mixed 1:1 by weight and oocytes were injected with 50 nL solution containing 20 ng mRNA. Cells were incubated at 18 °C for 24 hrs in ND96 solution (96 mM NaCl, 1.8mM CaCl₂, 2 mM KCl, 1mM MgCl₂, 5 mM HEPES at pH 7.5) enriched

with theophylline (6.7 mM), sodium pyruvate (2.5 mM) and kanamycin (0.1 mg/ml). Kanamycin was used because other antibiotics have been shown to reduce $\alpha 7$ expression levels.⁴¹

Noncanonical amino acid incorporation. The NVOC protected, cyanomethylester form of the noncanonical amino acid was coupled to the dinucleotide dCA and enzymatically ligated to the UAG-suppressor 74-mer THG73 tRNA_{CUA}. The product was verified via matrix assisted laser desorption/ionization (MALDI) time of flight mass spectrometry using a 3-hydroxypicolinic acid matrix.⁴⁰ The noncanonical amino acid-coupled tRNA was deprotected with a M365LP1 365 nm 1150 mW LED lamp (Thor Labs) immediately before co-injection with mRNA containing a UAG mutation at the site of interest. mRNA and tRNA were injected in a 1:1 or 2:1 volume ratio in a total volume of 50 or 75 nL respectively so that cells were injected with a 40 ng 1:1 mixture of $\alpha 7$ -UAG and Ric3 mRNA. For noncanonical amino acids that showed little or no response after 24 hr incubation, oocytes were subjected to a second round of injection and incubation as before. If this procedure was not effective, oocytes were double injected with a 75nL solution containing 40 ng mRNA of $\alpha 7$ -UAG, Ric3 and NACHO 1:1:1 mixture. A read-through/reaminoacylation test served as a negative control. Full length unacylated 76-mer tRNA was co-injected with mRNA. Lack of current showed no detectable reaminoacylation at the suppression site.

Drug Preparation. Acetylcholine chloride (Sigma-Aldrich) was dissolved in ND96 Buffer to make a 1M stock solution. NS6740 was synthesized as described previously²¹ and dissolved in DMSO to form a 20 mM stock solution. PNU-120596 (Selleckchem) was dissolved in DMSO to 150 mM stock. Further dilutions were made for experimentation using ND96 Buffer.

Electrophysiology. Agonist-induced currents were recorded using an OpusXpress 6000A (Axon Instruments/ Molecular Devices) in TEVC mode at a voltage clamped holding potential of -60 mV. Voltage and current electrodes were filled with 3M KCl. Oocytes were perfused with ND96 media at a rate of 3 ml/minute. Drug applications consisted of co-application of 1 mL dose of drug solution over 8 seconds followed by a 15 second pause to allow response to reach maximum before being washed out for 300 seconds at a rate of

3 ml/min. Concentrations of NS6740 were varied over several orders of magnitude to generate a dose-response curve. For efficacy experiments 1 mL of EC₁₀₀ dose of drug was applied over 8 seconds followed by a 1 minute incubation followed by 10 minute washout.

Data Analysis. Data were sampled at 50 Hz and then low pass filtered at 5Hz. For NS6740 co-applied with PNU-120596 EC₅₀ measurements were recorded as peak height. Data for dose response curves were baselined, and normalized on a per cell basis, and then averaged on a per-concentration basis and fit to the Hill equation using Prism 6 (GraphPad Software). For relative efficacy experiments ACh doses were normalized to an initial ACh does and all other drug applications were normalized to an immediately preceding acetylcholine dose and reported as $R_{\max} = I_{\max}(\text{drug})/I_{\max}(\text{ACh})$. In data tables N refers to the total number of oocytes analyzed. Cells from different frogs on at least two different days were used for each point. EC₅₀ and Hill coefficient errors are presented as SEM.

2.5 References

- (1) Corradi, J.; Bouzat, C. Understanding the Bases of Function and Modulation of A7 Nicotinic Receptors: Implications for Drug Discovery. *Mol. Pharmacol.* **2016**, *90* (3), 288–299. <https://doi.org/10.1124/mol.116.104240>.
- (2) Papke, R. L. Merging Old and New Perspectives on Nicotinic Acetylcholine Receptors. *Biochem. Pharmacol.* **2014**, *89* (1), 1–11. <https://doi.org/10.1016/j.bcp.2014.01.029>.
- (3) Liu, Q.; Huang, Y.; Xue, F.; Simard, A.; DeChon, J.; Li, G.; Zhang, J.; Lucero, L.; Wang, M.; Sierks, M.; et al. A Novel Nicotinic Acetylcholine Receptor Subtype in Basal Forebrain Cholinergic Neurons with High Sensitivity to Amyloid Peptides. *J. Neurosci. Off. J. Soc. Neurosci.* **2009**, *29* (4), 918–929. <https://doi.org/10.1523/JNEUROSCI.3952-08.2009>.
- (4) Liu, Q.; Huang, Y.; Shen, J.; Steffensen, S.; Wu, J. Functional A7β2 Nicotinic Acetylcholine Receptors Expressed in Hippocampal Interneurons Exhibit High Sensitivity to Pathological Level of Amyloid β Peptides. *BMC Neurosci.* **2012**, *13*, 155. <https://doi.org/10.1186/1471-2202-13-155>.
- (5) Moretti, M.; Zoli, M.; George, A. A.; Lukas, R. J.; Pistillo, F.; Maskos, U.; Whiteaker, P.; Gotti, C. The Novel A7β2-Nicotinic Acetylcholine Receptor Subtype Is Expressed in Mouse and Human Basal Forebrain: Biochemical and Pharmacological Characterization. *Mol. Pharmacol.* **2014**, *86* (3), 306–317. <https://doi.org/10.1124/mol.114.093377>.
- (6) Dineley, K. T.; Pandya, A. A.; Yakel, J. L. Nicotinic ACh Receptors as Therapeutic Targets in CNS Disorders. *Trends Pharmacol. Sci.* **2015**, *36* (2), 96–108. <https://doi.org/10.1016/j.tips.2014.12.002>.
- (7) Egea, J.; Buendia, I.; Parada, E.; Navarro, E.; León, R.; Lopez, M. G. Anti-Inflammatory Role of Microglial Alpha7 NACHRs and Its Role in

- Neuroprotection. *Biochem. Pharmacol.* **2015**, *97* (4), 463–472. <https://doi.org/10.1016/j.bcp.2015.07.032>.
- (8) Pesti, K.; Szabo, A. K.; Mike, A.; Vizi, E. S. Kinetic Properties and Open Probability of A7 Nicotinic Acetylcholine Receptors. *Neuropharmacology* **2014**, *81*, 101–115. <https://doi.org/10.1016/j.neuropharm.2014.01.034>.
 - (9) Andersen, N.; Corradi, J.; Sine, S. M.; Bouzat, C. Stoichiometry for Activation of Neuronal A7 Nicotinic Receptors. *Proc. Natl. Acad. Sci.* **2013**, *110* (51), 20819–20824. <https://doi.org/10.1073/pnas.1315775110>.
 - (10) Williams, D. K.; Wang, J.; Papke, R. L. Investigation of the Molecular Mechanism of the A7 Nicotinic Acetylcholine Receptor Positive Allosteric Modulator PNU-120596 Provides Evidence for Two Distinct Desensitized States. *Mol. Pharmacol.* **2011**, *80* (6), 1013–1032. <https://doi.org/10.1124/mol.111.074302>.
 - (11) Williams, D. K.; Stokes, C.; Horenstein, N. A.; Papke, R. L. The Effective Opening of Nicotinic Acetylcholine Receptors with Single Agonist Binding Sites. *J. Gen. Physiol.* **2011**, *137* (4), 369–384. <https://doi.org/10.1085/jgp.201010587>.
 - (12) Williams, D. K.; Peng, C.; Kimbrell, M. R.; Papke, R. L. Intrinsically Low Open Probability of A7 Nicotinic Acetylcholine Receptors Can Be Overcome by Positive Allosteric Modulation and Serum Factors Leading to the Generation of Excitotoxic Currents at Physiological Temperatures. *Mol. Pharmacol.* **2012**, *82* (4), 746–759. <https://doi.org/10.1124/mol.112.080317>.
 - (13) Papke, R. L.; Bencherif, M.; Lippiello, P. An Evaluation of Neuronal Nicotinic Acetylcholine Receptor Activation by Quaternary Nitrogen Compounds Indicates That Choline Is Selective for the A7 Subtype. *Neurosci. Lett.* **1996**, *213* (3), 201–204. [https://doi.org/10.1016/0304-3940\(96\)12889-5](https://doi.org/10.1016/0304-3940(96)12889-5).
 - (14) Albuquerque, E. X.; Alkondon, M.; Pereira, E. F.; Castro, N. G.; Schrattenholz, A.; Barbosa, C. T.; Bonfante-Cabarcas, R.; Aracava, Y.; Eisenberg, H. M.; Maelicke, A. Properties of Neuronal Nicotinic Acetylcholine Receptors: Pharmacological Characterization and Modulation of Synaptic Function. *J. Pharmacol. Exp. Ther.* **1997**, *280* (3), 1117–1136.
 - (15) Seguela, P.; Wadiche, J.; Dineley-Miller, K.; Dani, J. A.; Patrick, J. W. Molecular Cloning, Functional Properties, and Distribution of Rat Brain Alpha 7: A Nicotinic Cation Channel Highly Permeable to Calcium. *J. Neurosci.* **1993**, *13* (2), 596–604. <https://doi.org/10.1523/JNEUROSCI.13-02-00596.1993>.
 - (16) Kabbani, N.; Nichols, R. A. Beyond the Channel: Metabotropic Signaling by Nicotinic Receptors. *Trends Pharmacol. Sci.* **2018**, *39* (4), 354–366. <https://doi.org/10.1016/j.tips.2018.01.002>.
 - (17) Papke, R. L.; Chojnacka, K.; Horenstein, N. A. The Minimal Pharmacophore for Silent Agonism of the A7 Nicotinic Acetylcholine Receptor. *J. Pharmacol. Exp. Ther.* **2014**, *350* (3), 665–680. <https://doi.org/10.1124/jpet.114.215236>.
 - (18) Papke, R. L.; Stokes, C.; Damaj, M. I.; Thakur, G. A.; Manther, K.; Treinin, M.; Bagdas, D.; Kulkarni, A. R.; Horenstein, N. A. Persistent Activation of A7 Nicotinic ACh Receptors Associated with Stable Induction of Different Desensitized States. *Br. J. Pharmacol.* **2018**, *175* (11), 1838–1854. <https://doi.org/10.1111/bph.13851>.
 - (19) Briggs, C. A.; Grønlien, J. H.; Curzon, P.; Timmermann, D. B.; Ween, H.; Thorin-Hagene, K.; Kerr, P.; Anderson, D. J.; Malysz, J.; Dyhring, T.; et al. Role of

- Channel Activation in Cognitive Enhancement Mediated by A7 Nicotinic Acetylcholine Receptors. *Br. J. Pharmacol.* **2009**, *158* (6), 1486–1494. <https://doi.org/10.1111/j.1476-5381.2009.00426.x>.
- (20) Thomsen, M. S.; Mikkelsen, J. D. The A7 Nicotinic Acetylcholine Receptor Ligands Methyllycaconitine, NS6740 and GTS-21 Reduce Lipopolysaccharide-Induced TNF- α Release from Microglia. *J. Neuroimmunol.* **2012**, *251* (1–2), 65–72. <https://doi.org/10.1016/j.jneuroim.2012.07.006>.
- (21) Papke, R. L.; Bagdas, D.; Kulkarni, A. R.; Gould, T.; AlSharari, S. D.; Thakur, G. A.; Damaj, M. I. The Analgesic-like Properties of the Alpha7 NACHR Silent Agonist NS6740 Is Associated with Non-Conducting Conformations of the Receptor. *Neuropharmacology* **2015**, *91*, 34–42. <https://doi.org/10.1016/j.neuropharm.2014.12.002>.
- (22) Van Maanen, M. A.; Papke, R. L.; Koopman, F. A.; Koepke, J.; Bevaart, L.; Clark, R.; Lamppu, D.; Elbaum, D.; LaRosa, G. J.; Tak, P. P.; et al. Two Novel A7 Nicotinic Acetylcholine Receptor Ligands: In Vitro Properties and Their Efficacy in Collagen-Induced Arthritis in Mice. *PloS One* **2015**, *10* (1), e0116227. <https://doi.org/10.1371/journal.pone.0116227>.
- (23) Quadri, M.; Papke, R. L.; Horenstein, N. A. Dissection of N,N-Diethyl-N'-Phenylpiperazines as A7 Nicotinic Receptor Silent Agonists. *Bioorg. Med. Chem.* **2016**, *24* (2), 286–293. <https://doi.org/10.1016/j.bmc.2015.12.017>.
- (24) Chojnacka, K.; Papke, R. L.; Horenstein, N. A. Synthesis and Evaluation of a Conditionally-Silent Agonist for the A7 Nicotinic Acetylcholine Receptor. *Bioorg. Med. Chem. Lett.* **2013**, *23* (14), 4145–4149. <https://doi.org/10.1016/j.bmcl.2013.05.039>.
- (25) Marotta, C. B.; Lester, H. A.; Dougherty, D. A. An Unaltered Orthosteric Site and a Network of Long-Range Allosteric Interactions for PNU-120596 in A7 Nicotinic Acetylcholine Receptors. *Chem. Biol.* **2015**, *22* (8), 1063–1073. <https://doi.org/10.1016/j.chembiol.2015.06.018>.
- (26) Van Arnam, E. B.; Dougherty, D. A. Functional Probes of Drug-Receptor Interactions Implicated by Structural Studies: Cys-Loop Receptors Provide a Fertile Testing Ground. *J. Med. Chem.* **2014**, *57* (15), 6289–6300. <https://doi.org/10.1021/jm500023m>.
- (27) Puskar, N. L.; Xiu, X.; Lester, H. A.; Dougherty, D. A. Two Neuronal Nicotinic Acetylcholine Receptors, A4 β 4 and A7, Show Differential Agonist Binding Modes. *J. Biol. Chem.* **2011**, *286* (16), 14618–14627. <https://doi.org/10.1074/jbc.M110.206565>.
- (28) Nowak, M. W.; Kearney, P. C.; Sampson, J. R.; Saks, M. E.; Labarca, C. G.; Silverman, S. K.; Zhong, W.; Thorson, J.; Abelson, J. N.; Davidson, N. Nicotinic Receptor Binding Site Probed with Unnatural Amino Acid Incorporation in Intact Cells. *Science* **1995**, *268* (5209), 439–442.
- (29) Lummis, S. C. R.; L Beene, D.; Harrison, N. J.; Lester, H. A.; Dougherty, D. A. A Cation-Pi Binding Interaction with a Tyrosine in the Binding Site of the GABAC Receptor. *Chem. Biol.* **2005**, *12* (9), 993–997. <https://doi.org/10.1016/j.chembiol.2005.06.012>.

- (30) Daeffler, K. N.-M.; Lester, H. A.; Dougherty, D. A. Functional Evaluation of Key Interactions Evident in the Structure of the Eukaryotic Cys-Loop Receptor GluCl. *ACS Chem. Biol.* **2014**, *9* (10), 2283–2290. <https://doi.org/10.1021/cb500323d>.
- (31) Van Arnem, E. B.; Blythe, E. E.; Lester, H. A.; Dougherty, D. A. An Unusual Pattern of Ligand-Receptor Interactions for the A7 Nicotinic Acetylcholine Receptor, with Implications for the Binding of Varenicline. *Mol. Pharmacol.* **2013**, *84* (2), 201–207. <https://doi.org/10.1124/mol.113.085795>.
- (32) Li, S.-X.; Huang, S.; Bren, N.; Noridomi, K.; Dellisanti, C. D.; Sine, S. M.; Chen, L. Ligand-Binding Domain of an A7-Nicotinic Receptor Chimera and Its Complex with Agonist. *Nat. Neurosci.* **2011**, *14* (10), 1253–1259. <https://doi.org/10.1038/nn.2908>.
- (33) Nemezc, A.; Taylor, P. Creating an A7 Nicotinic Acetylcholine Recognition Domain from the Acetylcholine-Binding Protein: Crystallographic and Ligand Selectivity Analyses. *J. Biol. Chem.* **2011**, *286* (49), 42555–42565. <https://doi.org/10.1074/jbc.M111.286583>.
- (34) Celie, P. H. N.; van Rossum-Fikkert, S. E.; van Dijk, W. J.; Brejc, K.; Smit, A. B.; Sixma, T. K. Nicotine and Carbamylcholine Binding to Nicotinic Acetylcholine Receptors as Studied in AChBP Crystal Structures. *Neuron* **2004**, *41* (6), 907–914. [https://doi.org/10.1016/S0896-6273\(04\)00115-1](https://doi.org/10.1016/S0896-6273(04)00115-1).
- (35) Hurst, R.; Rollema, H.; Bertrand, D. Nicotinic Acetylcholine Receptors: From Basic Science to Therapeutics. *Pharmacol. Ther.* **2013**, *137* (1), 22–54. <https://doi.org/10.1016/j.pharmthera.2012.08.012>.
- (36) Dinklo, T.; Shaban, H.; Thuring, J. W.; Lavreysen, H.; Stevens, K. E.; Zheng, L.; Mackie, C.; Grantham, C.; Vandenberg, I.; Meulders, G.; et al. Characterization of 2-[[4-Fluoro-3-(Trifluoromethyl)Phenyl]Amino]-4-(4-Pyridinyl)-5-Thiazolemethanol (JNJ-1930942), a Novel Positive Allosteric Modulator of the A7 Nicotinic Acetylcholine Receptor. *J. Pharmacol. Exp. Ther.* **2011**, *336* (2), 560–574. <https://doi.org/10.1124/jpet.110.173245>.
- (37) Dunlop, J.; Lock, T.; Jow, B.; Sitzia, F.; Grauer, S.; Jow, F.; Kramer, A.; Bowlby, M. R.; Randall, A.; Kowal, D.; et al. Old and New Pharmacology: Positive Allosteric Modulation of the A7 Nicotinic Acetylcholine Receptor by the 5-Hydroxytryptamine_{2B/C} Receptor Antagonist SB-206553 (3,5-Dihydro-5-Methyl-N-3-Pyridinylbenzo[1,2-b:4,5-B']Di Pyrrole-1(2H)-Carboxamide). *J. Pharmacol. Exp. Ther.* **2009**, *328* (3), 766–776. <https://doi.org/10.1124/jpet.108.146514>.
- (38) Malysz, J.; Grønlien, J. H.; Anderson, D. J.; Håkerud, M.; Thorin-Hagene, K.; Ween, H.; Wetterstrand, C.; Briggs, C. A.; Faghih, R.; Bunnelle, W. H.; et al. In Vitro Pharmacological Characterization of a Novel Allosteric Modulator of A7 Neuronal Acetylcholine Receptor, 4-(5-(4-Chlorophenyl)-2-Methyl-3-Propionyl-1H-Pyrrol-1-Yl)Benzenesulfonamide (A-867744), Exhibiting Unique Pharmacological Profile. *J. Pharmacol. Exp. Ther.* **2009**, *330* (1), 257–267. <https://doi.org/10.1124/jpet.109.151886>.
- (39) Sahdeo, S.; Wallace, T.; Hirakawa, R.; Knoflach, F.; Bertrand, D.; Maag, H.; Misner, D.; Tombaugh, G. C.; Santarelli, L.; Brameld, K.; et al. Characterization of RO5126946, a Novel A7 Nicotinic Acetylcholine Receptor–Positive Allosteric Modulator. *J. Pharmacol. Exp. Ther.* **2014**, *350* (2), 455–468. <https://doi.org/10.1124/jpet.113.210963>.

- (40) Nowak, M. W.; Gallivan, J. P.; Silverman, S. K.; Labarca, C. G.; Dougherty, D. A.; Lester, H. A. In Vivo Incorporation of Unnatural Amino Acids into Ion Channels in *Xenopus* Oocyte Expression System. *Methods Enzymol.* **1998**, *293*, 504–529.
- (41) Amici, M.; Eusebi, F.; Miledi, R. Effects of the Antibiotic Gentamicin on Nicotinic Acetylcholine Receptors. *Neuropharmacology* **2005**, *49* (5), 627–637.
<https://doi.org/10.1016/j.neuropharm.2005.04.015>.

Chapter 3

INTRODUCTION: PHOTOREMOVABLE PROTECTING GROUPS

3.1 Motivation

Photoremovable protecting groups (PPGs), or photocages, allow, with high spatiotemporal control, for the non-invasive modulation of a system and have many applications in chemistry, chemical biology, and medicine.¹⁻³ Standard PPGs require UV light to effectively uncage. However, UV light is absorbed by tissue, causing DNA damage and limiting penetration depths to millimeters. Longer wavelength light penetrates much further into tissue without damage in what is known as the optical window between 650 and 900 nm; 810 nm light can penetrate a human skull.⁴ The development of PPGs that function with near infrared (NIR) light has great promise in medicine as a generalizable method for noninvasive targeted drug delivery and with the potential to reduce off target side effects. Coumarin,⁵⁻⁷ BODIPY,⁸⁻¹⁴ quinone,^{15,16} and cyanine¹⁷⁻¹⁹ based PPGs have shown promise towards this end; however, there are still very few PPGs that function at visible or NIR wavelengths.

The challenge in designing new visible and NIR PPGs is multifold. The organic PPG must be soluble in aqueous solution, biocompatible, absorb light at long wavelength and the reaction must occur with the available energy in high quantum yield. The energy of activation required fundamentally limits how far a photochemical reaction can be pushed into the visible spectrum. In the most common PPG, 6-nitroveratryloxycarbonyl (NVOC), the key photochemical step is radical bond homolysis, which has an activation energy of 80 - 120 kcal/mol.²⁰ NIR light (650 - 900 nm) has an available excitation energy of 44 - 32 kcal/mol. There has been little success extending NVOC protecting groups into the visible spectrum.²¹ Alternative photochemical reactions, such as photoacids, that have smaller activation energies will be required to develop NIR PPGs.

3.2 Photoacids

Photoacids undergo excited state proton transfer (ESPT), typically from S_1 , and are characterized by a bathochromic shift in the absorbance and fluorescence spectra of the

conjugate base relative to the acid.²²⁻²⁴ For photoacids, photoexcitation results in the molecules becoming stronger acids. Hydroxyarenes, the most commonly studied class of photoacids, can exhibit a drop of 5-12 pK_a units in the electronically excited state, which corresponds, at room temperature, to an energy difference of 7-14 kcal/mol a relatively small energetic perturbation.²⁵ ESPT is a reversible adiabatic process, which is fundamentally different from photoacid generators (PAGs) which when photolyzed produce an irreversible ground-state acid.

The Förster cycle model of photoacidity is used to approximate the excited state acidity constant (pK_a^{*}).²² Thermodynamically, photoacidity is defined as the change in relative free energies of the acid and conjugate base in the excited state. The Förster cycle considers only the S₀-S₁ electronic transition energies (E_{0,0}); in Figure 3.1 $h\nu_1$ is the E_{0,0} for the acid and $h\nu_2$ is the E_{0,0} for the conjugate base. Photoacidity is in competition with fluorescence (k_f), non-radiative decay (k_{nr}) as well as other quenching processes. Typically, E_{0,0} values are estimated by averaging S₀-S₁ and S₁-S₀ energy bands from the absorbance and fluorescence spectra of both the acid and conjugate base. The excited state pK_a^{*} is then derived using the Förster equation (eq. 3.1) and the relationship between the electronic transition energies and the change in free energy between the acid and conjugate base in the ground and excited states in the system ($h\nu_1 - h\nu_2$) = ΔE_{0,0} = ΔG_a - ΔG_a^{*}. Estimates of pK_a^{*} derived from the Förster cycle model are typically within 1 pK_a unit of the true pK_a^{*} when compared to more accurate but time consuming methods that measure rates directly.²⁵

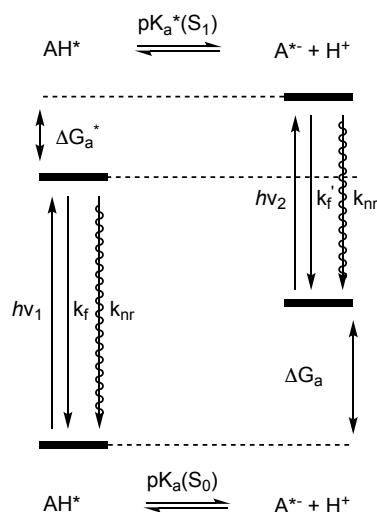


Figure 3.1: Förster Cycle of Photoacidity.

$$pK_a^* = pK_a - \frac{(hv_1 - hv_2)}{2.3RT} = pK_a - \frac{\Delta E_{0,0}}{2.3RT} \quad (\text{Eq. 3.1})$$

Mechanistically, excitation results in the intramolecular charge transfer (ICT) of electron density from the oxygen to the aromatic core. For this reason, 1-naphthol (**2**) ($pK_a^* = -0.2$) exhibits greater photoacidity than 2-naphthol (**3**) ($pK_a^* = -2.8$) (Figure 3.2) because substitution breaks degeneracy of naphthalene's two singlet excited states L_a and L_b and 1-naphthol stabilizes the more polar state L_a .^{22,26} Similarly, addition of electron withdrawing groups, such as cyano groups, at C₅ and C₈ where negative charge localizes in the excited state results in “super” photoacids ($pK_a^* < 0$).²⁷ Computation and further experimentation has shown that photoacidity derives from the excess stabilization of the conjugate base relative to the acid in the excited state following ICT.^{28,29}

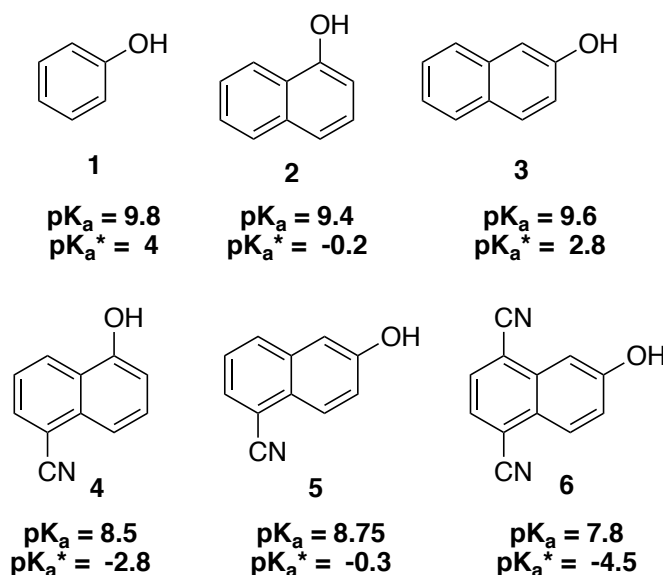


Figure 3.2: Ground state pK_a and first excited state pK_a^* for a selection of phenol and naphthols.²⁵

3.3 *Ortho*-Quinone Methide

An emerging class of photoacid dependent PPGs is based on the photogeneration of a quinone methide (QMs) intermediate.^{1,30,31} QMs are a reactive intermediate in chemistry and have significant biology activity.^{32–34} QMs react with nucleotides resulting in alkylation and cross linking of DNA and are implicated in the biological activity of the anticancer agents mitomycin,^{35–38} anthracyclins,^{39,40} and tamoxifen.⁴¹ QMs are structurally related to benzoquinones with one of the carbonyls replaced with a methylene making them much more polarized (Figure 3.3a). The polarized nature of the QM makes them very

reactive to nucleophilic attack at the methylene carbon, which results in rearomatization of the phenol (Figure 3.3b). Additionally, *ortho*-QMs, react with electron rich alkenes in an inverse electron demand Diels-Alder reaction to generate chroman derivatives (Figure 3.3b). The reactive nature of QMs prohibits isolation and instead QMs are identified through transient spectroscopy such as laser flash photolysis (LFP) and by analysis of reaction products with nucleophiles and electron rich dienophiles.

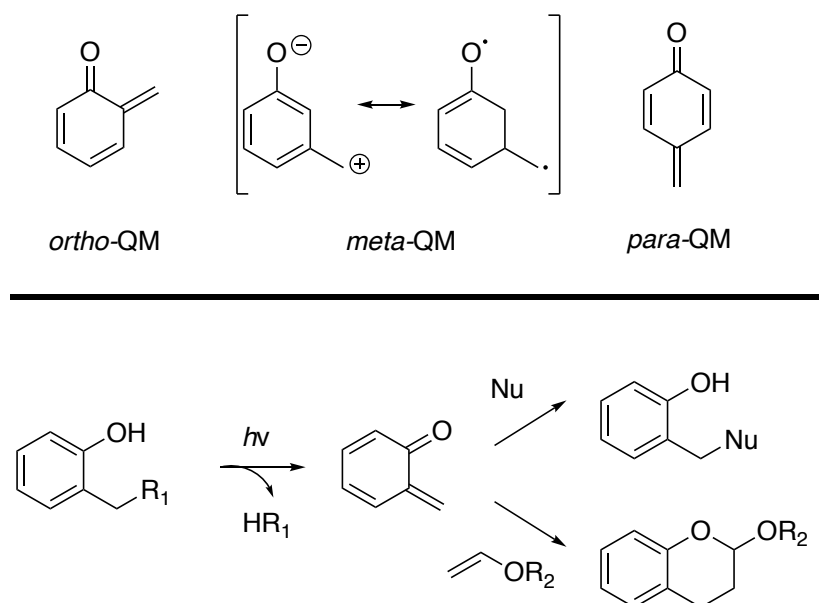


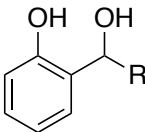
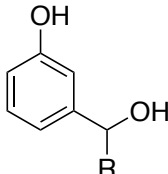
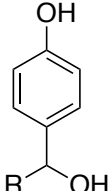
Figure 3.3: Quinone methide (QM) intermediate. a) Structure of the *ortho*-, *meta*- and *para*-QM b) formation of QM with light and reaction with nucleophiles and for *ortho*-QM with electron rich dienophiles in an inverse demand Diels-Alder.

Wan investigated a series of benzophenol quinone methide precursors (QMP)s and showed that the quantum yield of reaction for the photochemical generation of the QM was inversely correlated to the distance between the carbonyl and the methylene.⁴² This is consistent with the Zimmerman *ortho*-*meta* effect^{43,44} and the fact that *ortho*-QMPs undergo a more efficient excited state intramolecular proton transfer (ESIPT) event. Transient spectroscopy showed that the lifetime of the *ortho*- and *para*-QMs were similar at 5-10 seconds in aqueous solution.⁴² The lifetime of *meta*-QMs is significantly shorter and is reminiscent of a benzylic cation emphasizing the non-Kekulé nature of the *meta*-QM.⁴² Phenyl substitution of the methylene stabilizes the positive charge of the zwitterionic resonance structure of QMs increasing the lifetime of the QM. QM formation is accelerated in aqueous solvents relative to aprotic solvents,⁴⁵ further supporting the zwitterionic nature of the transition state, and Hammett plots additionally indicate a degree

of aromaticity and charge delocalization in the transition state.⁴⁶ The photodehydration of hydroxybenzyl alcohol derivatives to generate QMs is quite generalizable, with many bis aryl systems proving to be good QMPs.^{47–54}

Leaving group, substitution, and solvent all influence the efficiency of QM photogeneration. Ammonium salts are the best leaving group with reported quantum yields (Φ_{rxn}) near one,⁵⁵ ($\text{HNR}_3^+ > \text{HNR}_2 > \text{HOR} > \text{H}_2\text{O}$).⁴⁵ Consistent with the electron deficient nature of the QM intermediate electron donating groups greatly improve QM formation while electron withdrawing groups suppress formation of the QM intermediate (Table 3.2).⁴⁶ The effects are stronger for substitution at the 5- than the 4- position presumably because substituents at the 5- position are linked through resonance to the formation of the exocyclic methylene. Additionally, electron donating groups decrease QM reactivity to nucleophilic attack relative to electron withdrawing groups (Table 3.3).⁴⁶

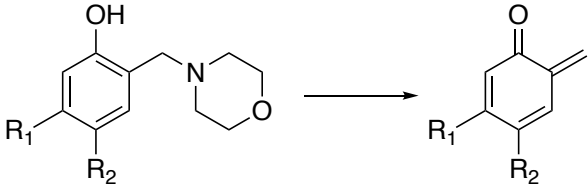
Table 3.1: Photodehydration of hydroxybenzyl alcohols in 1:1 MeOH:H₂O showing the quantum yield of reaction for the methyl ether at low conversion (<20%) and the lifetime of the QM intermediate in 1:1 MeCN:H₂O.⁴²

				
7 R = H 8 R = Ph	9 R = H 10 R = Ph	11 R = H 12 R = Ph		
Compound	Isomer	R	Φ_{rxn}	τ
7	<i>ortho</i>	H	0.23	
8	<i>ortho</i>	Ph	0.46	5-10 sec
9	<i>meta</i>	H	0.12	
10	<i>meta</i>	Ph	0.23	30 ns
11	<i>para</i>	H	0.007	
12	<i>para</i>	Ph	0.1	5 sec

Popik has developed photoelimination of naphthol QMPs (NQMPs) as a class of PPGs and shown that they efficiently and cleanly release alcohols, amines, including tertiary amines, carboxylic acids, and phenols.^{30,31,56} Notable NQMPs were able to

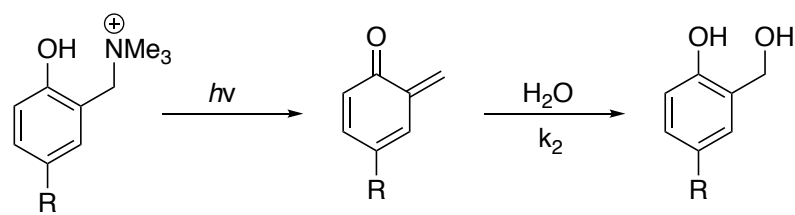
efficiently and rapidly directly release alcohols, something that has proven problematic with other PPGs.³¹ NQMPs have also shown their utility in photolithography.⁵⁷ One major drawback to QMPs as a photolabile protecting group is that the chromophore is preserved, reducing efficiency of photolysis due to internal filtering effects. Popik solved this problem by developing a 2,5-dihydroxybenzyl QMP that tautomerizes to a methylquinone from the QM.^{58,59}

Table 3.2: Effect of substituents on the thermal generation of *ortho*-QMs.⁴⁶



Compound	R ₁	R ₂	T °C	t _{1/2} (min)
13	COOMe	H	100	Stable
14	H	COOMe	100	149
15	H	H	50	115
16	H	OMe	22	11
17	OMe	H	22	4

Table 3.3: Effect of substituents on the quenching of QM with the nucleophile H₂O.⁴⁶



Compound	R	k ₂ (H ₂ O) M ⁻¹ s ⁻¹
18	OMe	1.9
19	H	7.8
20	Cl	22.8
21	COOMe	363.0
22	CN	1999.0
23	NO ₂	25400.0

Mechanistic work on hydroxybenzyl alcohols illustrates that photodehydration to generate a QM is a photoacid dependent process. Deprotonation of the phenol in the excited state is required for reactivity of a QMP: no QM intermediate is observed at pHs lower than the pK_a^* of the phenol^{30,42} and methoxy QMP derivatives show no reactivity.⁴² Conflicting reports suggest that photogeneration of QMs under alkaline conditions from the conjugate base may be possible.^{45,60} Finally the process is insensitive to oxygen, indicating the reaction is from the singlet state (S_1).⁴² After ESPT formation of the QM intermediate proceeds rapidly; distribution of negative charge into aromatic system of the excited state phenolate drives the heterolytic cleavage of the benzylic C-OH bond. The exact mechanism of benzylic C-OH bond cleavage is not fully established and may be substrate and solvent dependent (Figure 3.4). Cleavage may be concerted with ESPT in the excited state or dehydration may occur in the ground state after proton transfer.^{48,61,62} An oxetane intermediate forms before ring opening to the QM for naphthalol *ortho*-QMPs with poor leaving groups.³⁰ This is also true for thio-*o*-quinone methides,^{63,64} but computation³⁰ and experimental studies⁴² suggest that the oxetane intermediate is not on the reaction path for *ortho*-hydroxybenzyl alcohol despite being identified at cryogenic temperatures.^{65,66} More recently an alternative mechanism has been proposed for some anthracene QMPs; photoionization and deprotonation result in a phenoxyl radical, and subsequent homolytic cleavage of the OH leaving group generates the QM.⁶⁷

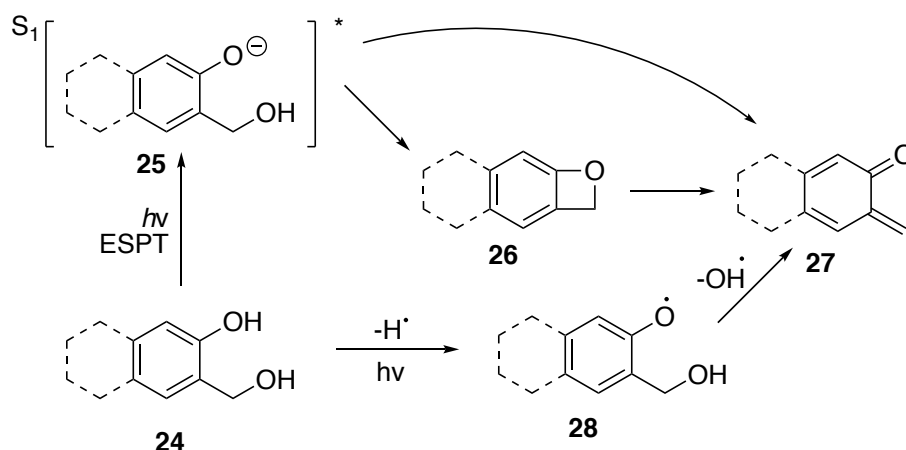


Figure 3.4: Mechanistic steps in QM photogeneration.

We were excited that about the possibility of extending the wavelength of QM formation into the visible and possibly the NIR because of the proposed two-step nature of the photochemical process; ESPT followed by ground state dehydration is more energetically favorable at long wavelengths than a concerted mechanism. Previous efforts to extend the wavelength of irradiation have focused on extending the cyclic aromatic core; irradiation of an anthracene QMP at 420 nm resulted in photodehydration to yield the *ortho*-QM ($\Phi_{\text{rxn}} = 0.023 \pm 0.001$).⁶⁸ One possible concern with increasing electronic conjugation is it also lowers the energy of first triplet state (T_1) and increases the efficiency of intersystem crossing (ISC) reducing QM generation.^{68,69} However, Freccero showed that with the right geometry and leaving group QM formation could be favored over ISC and singlet oxygen sensitization.⁶⁹ Continued extension of the aromatic polycyclic framework is not practical, and therefore this thesis investigates photogeneration of QMs from model heteroaromatic QMPs to better design longer wavelength QMPs.

3.4 Summary of Work: Part Two

In the second part of this dissertation two classes of photochemical reactions were investigated in efforts towards rationally design longer wavelength PPGs. Chapter IV investigates a series of quinoline and quinolinium QMPs for photochemical reactivity: 3-(hydroxymethyl)quinolin-4-ol was found to be photostable, however both 4-(hydroxymethyl)quinolin-3-ol and 2-(hydroxymethyl)quinolin-3-ol were found to form QM intermediates when irradiated under neutral aqueous conditions. The reactivity was pH dependent and under acidic conditions photogeneration of QM intermediates was quenched; positively charged quinolinium derivatives also did not show any photochemical reactivity. Chapter V describes efforts towards improving the efficiency of quinone photoreduction through a radical decarboxylation. A glycine moiety was installed on two different quinones; both proved to be photostable.

3.5 References

- (1) Klán, P.; Šolomek, T.; Bochet, C. G.; Blanc, A.; Givens, R.; Rubina, M.; Popik, V.; Kostikov, A.; Wirz, J. Photoremovable Protecting Groups in Chemistry and Biology: Reaction Mechanisms and Efficacy. *Chem. Rev.* **2013**, *113* (1), 119–191. <https://doi.org/10.1021/cr300177k>.

- (2) Ellis-Davies, G. C. R. Caged Compounds: Photorelease Technology for Control of Cellular Chemistry and Physiology. *Nat. Methods* **2007**, *4* (8), 619–628. <https://doi.org/10.1038/nmeth1072>.
- (3) Yu, H.; Li, J.; Wu, D.; Qiu, Z.; Zhang, Y. Chemistry and Biological Applications of Photo-Labile Organic Molecules. *Chem. Soc. Rev.* **2010**, *39* (2), 464–473. <https://doi.org/10.1039/b901255a>.
- (4) Henderson, T. A. Multi-Watt near-Infrared Light Therapy as a Neuroregenerative Treatment for Traumatic Brain Injury. *Neural Regen. Res.* **2016**, *11* (4), 563–565. <https://doi.org/10.4103/1673-5374.180737>.
- (5) Fournier, L.; Gauron, C.; Xu, L.; Aujard, I.; Le Saux, T.; Gagey-Eilstein, N.; Maurin, S.; Dubruille, S.; Baudin, J.-B.; Bensimon, D.; et al. A Blue-Absorbing Photolabile Protecting Group for in Vivo Chromatically Orthogonal Photoactivation. *ACS Chem. Biol.* **2013**, *8* (7), 1528–1536. <https://doi.org/10.1021/cb400178m>.
- (6) Fournier, L.; Aujard, I.; Le Saux, T.; Maurin, S.; Beaupierre, S.; Baudin, J.-B.; Jullien, L. Coumarinylmethyl Caging Groups with Redshifted Absorption. *Chem. – Eur. J.* **2013**, *19* (51), 17494–17507. <https://doi.org/10.1002/chem.201302630>.
- (7) Lin, Q.; Yang, L.; Wang, Z.; Hua, Y.; Zhang, D.; Bao, B.; Bao, C.; Gong, X.; Zhu, L. Coumarin Photocaging Groups Modified with an Electron-Rich Styryl Moiety at the 3-Position: Long-Wavelength Excitation, Rapid Photolysis, and Photobleaching. *Angew. Chem. Int. Ed.* **2018**, *57* (14), 3722–3726. <https://doi.org/10.1002/anie.201800713>.
- (8) Umeda, N.; Takahashi, H.; Kamiya, M.; Ueno, T.; Komatsu, T.; Terai, T.; Hanaoka, K.; Nagano, T.; Urano, Y. Boron Dipyrromethene As a Fluorescent Caging Group for Single-Photon Uncaging with Long-Wavelength Visible Light. *ACS Chem. Biol.* **2014**, *9* (10), 2242–2246. <https://doi.org/10.1021/cb500525p>.
- (9) Goswami, P. P.; Syed, A.; Beck, C. L.; Albright, T. R.; Mahoney, K. M.; Unash, R.; Smith, E. A.; Winter, A. H. BODIPY-Derived Photoremovable Protecting Groups Unmasked with Green Light. *J. Am. Chem. Soc.* **2015**, *137* (11), 3783–3786. <https://doi.org/10.1021/jacs.5b01297>.
- (10) Rubinstein, N.; Liu, P.; Miller, E. W.; Weinstein, R. Meso-Methylhydroxy BODIPY: A Scaffold for Photo-Labile Protecting Groups. *Chem. Commun.* **2015**, *51* (29), 6369–6372. <https://doi.org/10.1039/C5CC00550G>.
- (11) Takeda, A.; Komatsu, T.; Nomura, H.; Naka, M.; Matsuki, N.; Ikegaya, Y.; Terai, T.; Ueno, T.; Hanaoka, K.; Nagano, T.; et al. Unexpected Photo-Instability of 2,6-Sulfonamide-Substituted BODIPYs and Its Application to Caged GABA. *ChemBioChem* **2016**, *17* (13), 1233–1240. <https://doi.org/10.1002/cbic.201600097>.
- (12) Palao, E.; Slanina, T.; Muchová, L.; Šolomek, T.; Vítek, L.; Klán, P. Transition-Metal-Free CO-Releasing BODIPY Derivatives Activatable by Visible to NIR Light as Promising Bioactive Molecules. *J. Am. Chem. Soc.* **2016**, *138* (1), 126–133. <https://doi.org/10.1021/jacs.5b10800>.
- (13) Štacko, P.; Muchová, L.; Vítek, L.; Klán, P. Visible to NIR Light Photoactivation of Hydrogen Sulfide for Biological Targeting. *Org. Lett.* **2018**, *20* (16), 4907–4911. <https://doi.org/10.1021/acs.orglett.8b02043>.
- (14) Peterson, J. A.; Wijesooriya, C.; Gehrmann, E. J.; Mahoney, K. M.; Goswami, P. P.; Albright, T. R.; Syed, A.; Dutton, A. S.; Smith, E. A.; Winter, A. H. Family of

- BODIPY Photocages Cleaved by Single Photons of Visible/Near-Infrared Light. *J. Am. Chem. Soc.* **2018**, *140* (23), 7343–7346. <https://doi.org/10.1021/jacs.8b04040>.
- (15) Walton, D. P.; Dougherty, D. A. A General Strategy for Visible-Light Decaging Based on the Quinone Trimethyl Lock. *J. Am. Chem. Soc.* **2017**, *139* (13), 4655–4658. <https://doi.org/10.1021/jacs.7b01548>.
 - (16) Regan, C. J.; Walton, D. P.; Shafaat, O. S.; Dougherty, D. A. Mechanistic Studies of the Photoinduced Quinone Trimethyl Lock Decaging Process. *J. Am. Chem. Soc.* **2017**, *139* (13), 4729–4736. <https://doi.org/10.1021/jacs.6b12007>.
 - (17) Gorka, A. P.; Nani, R. R.; Zhu, J.; Mackem, S.; Schnermann, M. J. A Near-IR Uncaging Strategy Based on Cyanine Photochemistry. *J. Am. Chem. Soc.* **2014**, *136* (40), 14153–14159. <https://doi.org/10.1021/ja5065203>.
 - (18) Nani, R. R.; Gorka, A. P.; Nagaya, T.; Kobayashi, H.; Schnermann, M. J. Near-IR Light-Mediated Cleavage of Antibody–Drug Conjugates Using Cyanine Photocages. *Angew. Chem. Int. Ed.* **2015**, *54* (46), 13635–13638. <https://doi.org/10.1002/anie.201507391>.
 - (19) Nani, R. R.; Gorka, A. P.; Nagaya, T.; Yamamoto, T.; Ivanic, J.; Kobayashi, H.; Schnermann, M. J. In Vivo Activation of Duocarmycin–Antibody Conjugates by Near-Infrared Light. *ACS Cent. Sci.* **2017**, *3* (4), 329–337. <https://doi.org/10.1021/acscentsci.7b00026>.
 - (20) Blanksby, S. J.; Ellison, G. B. Bond Dissociation Energies of Organic Molecules. *Acc. Chem. Res.* **2003**, *36* (4), 255–263. <https://doi.org/10.1021/ar020230d>.
 - (21) Aujard, I.; Benbrahim, C.; Gouget, M.; Ruel, O.; Baudin, J.-B.; Neveu, P.; Jullien, L. O-Nitrobenzyl Photolabile Protecting Groups with Red-Shifted Absorption: Syntheses and Uncaging Cross-Sections for One- and Two-Photon Excitation. *Chem. Eur. J.* **2006**, *12* (26), 6865–6879. <https://doi.org/10.1002/chem.200501393>.
 - (22) Tolbert, L. M.; Solntsev, K. M. Excited-State Proton Transfer: From Constrained Systems to “Super” Photoacids to Superfast Proton Transfer†. *Acc. Chem. Res.* **2002**, *35* (1), 19–27. <https://doi.org/10.1021/ar990109f>.
 - (23) Wan, P.; Shukla, D. Utility of Acid-Base Behavior of Excited States of Organic Molecules. *Chem. Rev.* **1993**, *93* (1), 571–584. <https://doi.org/10.1021/cr00017a024>.
 - (24) Tomin, V. I.; Demchenko, A. P.; Chou, P.-T. Thermodynamic vs. Kinetic Control of Excited-State Proton Transfer Reactions. *J. Photochem. Photobiol. C Photochem. Rev.* **2015**, *22*, 1–18. <https://doi.org/10.1016/j.jphotochemrev.2014.09.005>.
 - (25) Pines, E. UV-Visible Spectra and Photoacidity of Phenols, Naphthols and Pyrenols. In *The Chemistry of Phenols: Part 1*; Rappoport, Z., Ed.; Wiley: Chichester, West Sussex, 2003; pp 491–527.
 - (26) Tolbert, L. M.; Haubrich, J. E. Enhanced Photoacidities of Cyanonaphthols. *J. Am. Chem. Soc.* **1990**, *112* (22), 8163–8165. <https://doi.org/10.1021/ja00178a049>.
 - (27) Tolbert, L. M.; Haubrich, J. E. Photoexcited Proton Transfer from Enhanced Photoacids. *J. Am. Chem. Soc.* **1994**, *116* (23), 10593–10600. <https://doi.org/10.1021/ja00102a028>.
 - (28) Granucci, G.; Hynes, J. T.; Millié, P.; Tran-Thi, T.-H. A Theoretical Investigation of Excited-State Acidity of Phenol and Cyanophenols. *J. Am. Chem. Soc.* **2000**, *122* (49), 12243–12253. <https://doi.org/10.1021/ja993730j>.

- (29) Agmon, N.; Rettig, W.; Groth, C. Electronic Determinants of Photoacidity in Cyanonaphthols. *J. Am. Chem. Soc.* **2002**, *124* (6), 1089–1096. <https://doi.org/10.1021/ja003875m>.
- (30) Arumugam, S.; Popik, V. V. Photochemical Generation and the Reactivity of O-Naphthoquinone Methides in Aqueous Solutions. *J. Am. Chem. Soc.* **2009**, *131* (33), 11892–11899. <https://doi.org/10.1021/ja9031924>.
- (31) Kulikov, A.; Arumugam, S.; Popik, V. V. Photolabile Protection of Alcohols, Phenols, and Carboxylic Acids with 3-Hydroxy-2-Naphthalenemethanol. *J. Org. Chem.* **2008**, *73* (19), 7611–7615. <https://doi.org/10.1021/jo801302m>.
- (32) Lukeman, M. Photochemical Generation and Characterization of Quinone Methides. In *Quinone Methides*; Rokita, S., Ed.; Reactive Intermediates in Chemistry and Biology; John Wiley & Sons: Hoboken, NJ, 2009; Vol. 1, pp 1–32.
- (33) Toteva, M. M.; Richard, J. P. The Generation and Reactions of Quinone Methides. *Adv. Phys. Org. Chem.* **2011**, *45*, 39–91. <https://doi.org/10.1016/B978-0-12-386047-7.00002-3>.
- (34) Singh, M. S.; Nagaraju, A.; Anand, N.; Chowdhury, S. Ortho-Quinone Methide (o-QM): A Highly Reactive, Ephemeral and Versatile Intermediate in Organic Synthesis. *RSC Adv.* **2014**, *4* (99), 55924–55959. <https://doi.org/10.1039/C4RA11444B>.
- (35) Tomasz, M. Mitomycin C: Small, Fast and Deadly (but Very Selective). *Chem. Biol.* **1995**, *2* (9), 575–579.
- (36) Han, I.; Russell, D. J.; Kohn, H. Studies on the Mechanism of Mitomycin C(1) Electrophilic Transformations: Structure-Reactivity Relationships. *J. Org. Chem.* **1992**, *57* (6), 1799–1807. <https://doi.org/10.1021/jo00032a037>.
- (37) Li, V. S.; Kohn, H. Studies on the Bonding Specificity for Mitomycin C-DNA Monoalkylation Processes. *J. Am. Chem. Soc.* **1991**, *113* (1), 275–283. <https://doi.org/10.1021/ja00001a040>.
- (38) Tomasz, M.; Das, A.; Tang, K. S.; Ford, M. G. J.; Minnock, A.; Musser, S. M.; Waring, M. J. The Purine 2-Amino Group as the Critical Recognition Element for Sequence-Specific Alkylation and Cross-Linking of DNA by Mitomycin C. *J. Am. Chem. Soc.* **1998**, *120* (45), 11581–11593. <https://doi.org/10.1021/ja9824019>.
- (39) Taatjes, D. J.; Gaudiano, G.; Resing, K.; Koch, T. H. Alkylation of DNA by the Anthracycline, Antitumor Drugs Adriamycin and Daunomycin. *J. Med. Chem.* **1996**, *39* (21), 4135–4138. <https://doi.org/10.1021/jm960519z>.
- (40) Angle, S. R.; Rainier, J. D.; Woytowicz, C. Synthesis and Chemistry of Quinone Methide Models for the Anthracycline Antitumor Antibiotics. *J. Org. Chem.* **1997**, *62* (17), 5884–5892. <https://doi.org/10.1021/jo970539o>.
- (41) Fan, P. W.; Zhang, F.; Bolton, J. L. 4-Hydroxylated Metabolites of the Antiestrogens Tamoxifen and Toremifene Are Metabolized to Unusually Stable Quinone Methides. *Chem. Res. Toxicol.* **2000**, *13* (1), 45–52. <https://doi.org/10.1021/tx990144v>.
- (42) Diao, L.; Yang, C.; Wan, P. Quinone Methide Intermediates from the Photolysis of Hydroxybenzyl Alcohols in Aqueous Solution. *J. Am. Chem. Soc.* **1995**, *117* (19), 5369–5370. <https://doi.org/10.1021/ja00124a024>.

- (43) Zimmerman, H. E. The Meta Effect in Organic Photochemistry: Mechanistic and Exploratory Organic Photochemistry. *J. Am. Chem. Soc.* **1995**, *117* (35), 8988–8991. <https://doi.org/10.1021/ja00140a014>.
- (44) Zimmerman, H. E. Meta–Ortho Effect in Organic Photochemistry: Mechanistic and Exploratory Organic Photochemistry. *J. Phys. Chem. A* **1998**, *102* (28), 5616–5621. <https://doi.org/10.1021/jp9803182>.
- (45) Nakatani, K.; Higashida, N.; Saito, I. Highly Efficient Photochemical Generation of O-Quinone Methide from Mannich Bases of Phenol Derivatives. *Tetrahedron Lett.* **1997**, *38* (28), 5005–5008. [https://doi.org/10.1016/S0040-4039\(97\)01071-X](https://doi.org/10.1016/S0040-4039(97)01071-X).
- (46) Weinert, E. E.; Dondi, R.; Colloredo-Melz, S.; Frankenfield, K. N.; Mitchell, C. H.; Freccero, M.; Rokita, S. E. Substituents on Quinone Methides Strongly Modulate Formation and Stability of Their Nucleophilic Adducts. *J. Am. Chem. Soc.* **2006**, *128* (36), 11940–11947. <https://doi.org/10.1021/ja062948k>.
- (47) Lukeman, M.; Veale, D.; Wan, P.; Munasinghe, V. R. N.; Corrie, J. E. Photogeneration of 1,5-Naphthoquinone Methides via Excited-State (Formal) Intramolecular Proton Transfer (ESIPT) and Photodehydration of 1-Naphthol Derivatives in Aqueous Solution. *Can. J. Chem.* **2004**, *82* (2), 240–253. <https://doi.org/10.1139/v03-184>.
- (48) Shi, Y.; Wan, P. Solvolysis and Ring Closure of Quinone Methides Photogenerated from Biaryl Systems. *Can. J. Chem.* **2005**, *83* (9), 1306–1323. <https://doi.org/10.1139/v05-138>.
- (49) Verga, D.; Richter, S. N.; Palumbo, M.; Gandolfi, R.; Freccero, M. Bipyridyl Ligands as Photoactivatable Mono- and Bis-Alkylating Agents Capable of DNA Cross-Linking. *Org. Biomol. Chem.* **2007**, *5* (2), 233–235. <https://doi.org/10.1039/B616292D>.
- (50) Wang, P.; Liu, R.; Wu, X.; Ma, H.; Cao, X.; Zhou, P.; Zhang, J.; Weng, X.; Zhang, X.-L.; Qi, J.; et al. A Potent, Water-Soluble and Photoinducible DNA Cross-Linking Agent. *J. Am. Chem. Soc.* **2003**, *125* (5), 1116–1117. <https://doi.org/10.1021/ja029040o>.
- (51) Song, Y.; Tian, T.; Wang, P.; He, H.; Liu, W.; Zhou, X.; Cao, X.; Zhang, X.-L.; Zhou, X. Phenol Quaternary Ammonium Derivatives: Charge and Linker Effect on Their DNA Photo-Inducible Cross-Linking Abilities. *Org. Biomol. Chem.* **2006**, *4* (17), 3358–3366. <https://doi.org/10.1039/B604552A>.
- (52) Doria, F.; Richter, S. N.; Nadai, M.; Colloredo-Mels, S.; Mella, M.; Palumbo, M.; Freccero, M. BINOL–Amino Acid Conjugates as Triggerable Carriers of DNA-Targeted Potent Photocytotoxic Agents. *J. Med. Chem.* **2007**, *50* (26), 6570–6579. <https://doi.org/10.1021/jm070828x>.
- (53) Richter, S. N.; Maggi, S.; Mels, S. C.; Palumbo, M.; Freccero, M. Binol Quinone Methides as Bisalkylating and DNA Cross-Linking Agents. *J. Am. Chem. Soc.* **2004**, *126* (43), 13973–13979. <https://doi.org/10.1021/ja047655a>.
- (54) Weng, X.; Ren, L.; Weng, L.; Huang, J.; Zhu, S.; Zhou, X.; Weng, L. Synthesis and Biological Studies of Inducible DNA Cross-Linking Agents. *Angew. Chem. Int. Ed.* **2007**, *46* (42), 8020–8023. <https://doi.org/10.1002/anie.200700844>.
- (55) Modica, E.; Zanaletti, R.; Freccero, M.; Mella, M. Alkylation of Amino Acids and Glutathione in Water by O-Quinone Methide. Reactivity and Selectivity. *J. Org. Chem.* **2001**, *66* (1), 41–52. <https://doi.org/10.1021/jo0006627>.

- (56) Nekongo, E. E.; Popik, V. V. Photoactivatable Fluorescein Derivatives Caged with a (3-Hydroxy-2-Naphthalenyl)Methyl Group. *J. Org. Chem.* **2014**, *16* (79), 7665–7671. <https://doi.org/10.1021/jo501116g>.
- (57) Arumugam, S.; Popik, V. V. Attach, Remove, or Replace: Reversible Surface Functionalization Using Thiol–Quinone Methide Photoclick Chemistry. *J. Am. Chem. Soc.* **2012**, *134* (20), 8408–8411. <https://doi.org/10.1021/ja302970x>.
- (58) Kostikov, A. P.; Popik, V. V. 2,5-Dihydroxybenzyl and (1,4-Dihydroxy-2-Naphthyl)Methyl, Novel Reductively Armed Photocages for the Hydroxyl Moiety. *J. Org. Chem.* **2007**, *72* (24), 9190–9194. <https://doi.org/10.1021/jo701426j>.
- (59) Arumugam, S.; Popik, V. V. Dual Reactivity of Hydroxy- and Methoxy-Substituted o-Quinone Methides in Aqueous Solutions: Hydration versus Tautomerization. *J. Org. Chem.* **2010**, *75* (21), 7338–7346. <https://doi.org/10.1021/jo101613t>.
- (60) Wan, P.; Hennig, D. Photocondensation of O-Hydroxybenzyl Alcohol in an Alkaline Medium: Synthesis of Phenol–Formaldehyde Resins. *J. Chem. Soc. Chem. Commun.* **1987**, No. 12, 939–941. <https://doi.org/10.1039/C39870000939>.
- (61) Wan, P.; Barker, B.; Diao, L.; Fischer, M.; Shi, Y.; Yang, C. 1995 Merck Frosst Award Lecture Quinone Methides: Relevant Intermediates in Organic Chemistry. *Can. J. Chem.* **1996**, *74* (4), 465–475. <https://doi.org/10.1139/v96-051>.
- (62) Basarić, N.; Žabčić, I.; Mlinarić-Majerski, K.; Wan, P. Photochemical Formation and Chemistry of Long-Lived Adamantylidene-Quinone Methides and 2-Adamantyl Cations. *J. Org. Chem.* **2010**, *75* (1), 102–116. <https://doi.org/10.1021/jo902004n>.
- (63) Meier, H.; Eckes, H.-L.; Niedermann, H.-P.; Kolshorn, H. A Non-Stereospecific Diels–Alder Reaction. *Angew. Chem. Int. Ed. Engl.* **1987**, *26* (10), 1046–1048. <https://doi.org/10.1002/anie.198710461>.
- (64) Mayer, A.; Meier, H. 1H-Naphtho[2,1-b]Thiete and 2H-Naphtho[2,3-b]Thiete-Synthesis and Reactivity. *Tetrahedron Lett.* **1994**, *35* (14), 2161–2164. [https://doi.org/10.1016/S0040-4039\(00\)76785-2](https://doi.org/10.1016/S0040-4039(00)76785-2).
- (65) Qiao, G. G.; Lenghaus, K.; Solomon, D. H.; Reisinger, A.; Bytheway, I.; Wentrup, C. 4,6-Dimethyl-o-Quinone Methide and 4,6-Dimethylbenzoxete. *J. Org. Chem.* **1998**, *63* (26), 9806–9811. <https://doi.org/10.1021/jo981445x>.
- (66) Tomioka, H. Matrix Isolation Study of Reactive O-Quinoid Compounds: Generation Detection and Reactions. *Pure Appl. Chem.* **1997**, *69* (4), 837–840. <https://doi.org/10.1351/pac199769040837>.
- (67) Škalamera, Đ.; Mlinarić-Majerski, K.; Martin Kleiner, I.; Kralj, M.; Oake, J.; Wan, P.; Bohne, C.; Basarić, N. Photochemical Formation of Anthracene Quinone Methide Derivatives. *J. Org. Chem.* **2017**, *82* (12), 6006–6021. <https://doi.org/10.1021/acs.joc.6b02735>.
- (68) Škalamera, Đ.; Mlinarić-Majerski, K.; Martin-Kleiner, I.; Kralj, M.; Wan, P.; Basarić, N. Near-Visible Light Generation of a Quinone Methide from 3-Hydroxymethyl-2-Anthrol. *J. Org. Chem.* **2014**, *79* (10), 4390–4397. <https://doi.org/10.1021/jo500290y>.
- (69) Doria, F.; Lena, A.; Bargiggia, R.; Freccero, M. Conjugation, Substituent, and Solvent Effects on the Photogeneration of Quinone Methides. *J. Org. Chem.* **2016**, *81* (9), 3665–3673. <https://doi.org/10.1021/acs.joc.6b00331>.

Chapter 4

PHOTOCHEMISTRY OF QUINOLINE AND QUINOLINIUM *ORTHO*-QUINONE METHIDE PRECURSORS

Abstract

The photochemical dehydration of *ortho*-hydroxybenzyl alcohols, through the formation of quinone methide (QM) intermediates, is an emerging strategy for photoremovable protecting groups for alcohols, amines, and carboxylic acids. Little is known about the tolerance of the reaction to substitution of the aromatic core, a necessary step towards extending the wavelength of reaction. This chapter looks at the photoreactivity of quinoline and quinolinium QM precursors (QMPs) and shows that 2-hydroxymethyl-3-quinolinol (**13a**) and 4-hydroxymethyl-3-quinolinol (**10a**) derivatives both form QMs when irradiated under neutral aqueous conditions. This photochemistry is pH dependent, and it appears that quinolinium QMPs do not undergo photodehydration to the QM intermediate.

4.1 Introduction

The *ortho*-quinone methide precursor (QMP) protecting group for alcohols, amines, and acids¹⁻⁷ is a little used photolabile protecting group that has the potential to work at longer wavelengths and potentially in the NIR (Figure 4.1a,b). The initial photochemical step, ESPT, has a small energy of activation of between 7-14 kcal/mol, and is followed by heterolytic cleavage of the benzylic leaving group bond.^{3,8} The minimum requirements for a QMP are a conjugated hydroxymethyl, -CH₂OH, and a phenol, though there is significant variation in reaction effectiveness depending on the isomer,⁸ substituents,^{9,10} leaving group^{11,12} and overall geometry of the conjugated system.^{8,13-15} Extension of the quinone methide (QM) photochemistry to longer wavelengths should be possible by instillation of the requisite functionality onto a known long wavelength absorbing dye such as a cyanine dye.

In cyanine dyes two heteroaromatic nitrogens are linked by a polymethine chain.^{16,17} Inclusion of a QMP at one or both termini of the cyanine dye could potentially furnish a long wavelength photochemical QMP (Figure 4.1c). Given the synthetic complexity of installing the functionality required for an *ortho*-QMP and the number of

possible long wavelength cyanine frameworks, there is a need for short wavelength model studies to better understand the tolerance of the photochemical QM reaction to substrate modification. This chapter focus on quinoline and quinolinium based QMPs, modest perturbations introducing a heterocyclic aromatic core and a positively charge heterocyclic aromatic core respectively. Quinolinium based cyanine derivatives are known.¹⁶

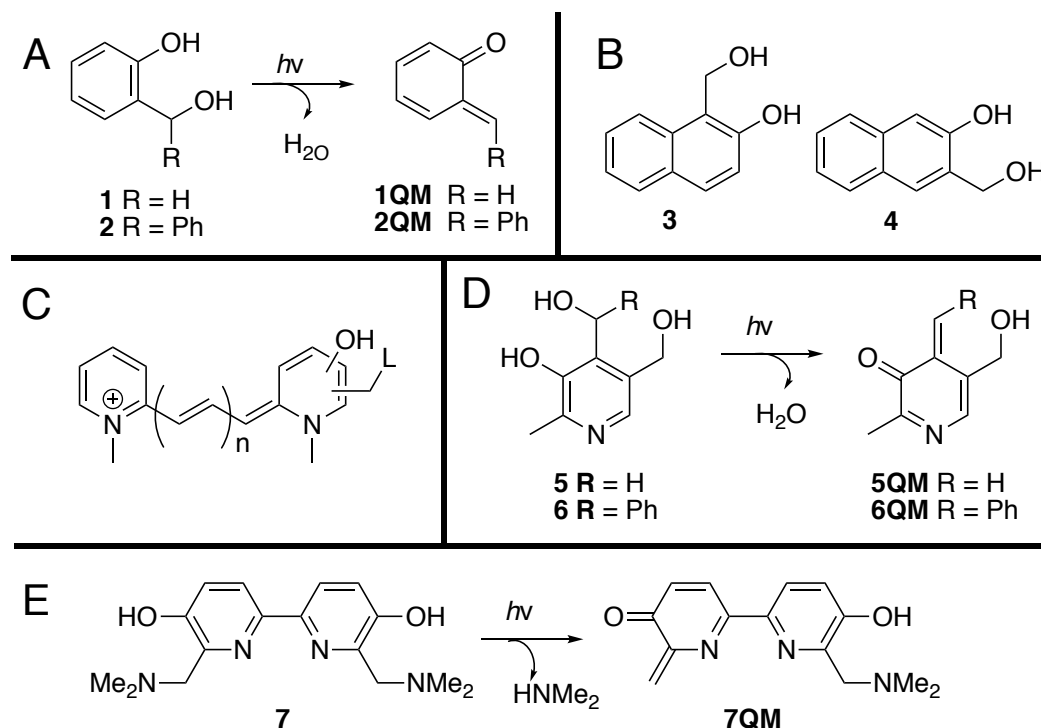


Figure 4.1: *ortho*-Quinone Methide (*ortho*-QM). A) scheme showing the *ortho*-QM photochemical protecting group. B) Naphthol based QM precursors (QMPs) that have been developed as protecting groups. C) Example of a potential cyanine based longer wavelength QMP. D, E) Known pyridine based heterocyclic QMP systems.

There are two previous examples in the literature of shorter wavelength heterocyclic QMPs, including pyridoxine **5** (vitamin B₆)¹⁸ and a Mannich base bipyrindyl QMP **3**¹⁹ (Figure 4.1d,e) but no examples of a QMP with a charged aromatic core. Photolysis of pyridoxine **5** is known to generate a QM group under aqueous conditions. Despite the presence of hydroxymethyl, -CH₂OH, groups, *ortho* and *meta* only the *ortho*-QM has been detected experimentally.¹⁸ Computational studies suggest that for pyridoxine **5** excited state dehydroxylation is favored over ground state for QM formation — a 4 kcal/mol reaction barrier compared to a 20 kcal/mol reaction barrier — and in S₁ the energy barrier for photogeneration of the *ortho*-QM is 8 kcal/mol lower than for the *meta*-QM

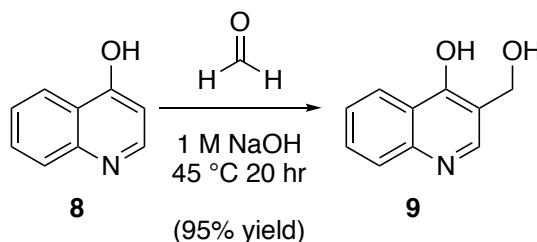
accounting for the selectivity of the photolysis reaction.²⁰ The quantum yield of *ortho*-QM formation is about half that of the comparable benzylic QMP 2-(hydroxy(phenyl)methyl)phenol (**2**) under similar conditions ($\Phi_{\text{rxn}} = 0.2$ for QMP **6**¹⁸ vs $\Phi_{\text{rxn}} = 0.46$ for QMP **2**⁸ in 1:1 MeOH:H₂O at 254 nm). Introduction of an additional pH sensitive functional group may alter the reaction pathway or the nature of the intermediate: transient spectroscopy showed two *ortho*-QM species at pH 7, a protonated QM, the result of ESPT to the nitrogen and a neutral QM, the result of ESPT to either the leaving group or bulk solvent.¹⁸

This chapter explores a series of quinoline QMPs and shows that regional isomers display marked differences in reactivity. This chapter also investigates the photochemistry of quinolinium QMPs for the first time and demonstrates that the positively charged electron withdrawing quinolinium functionality severely inhibits QMP reactivity.

4.2 Quinoline *ortho*-quinone methide:

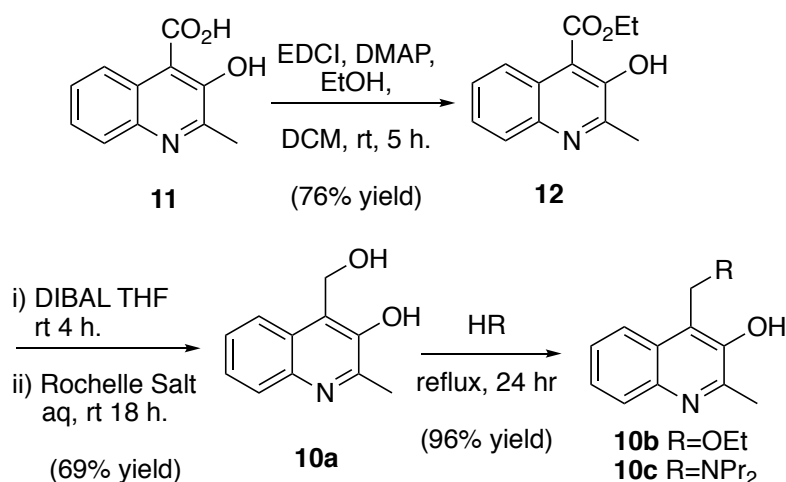
4.2.1 Synthesis of quinoline derivatives:

Three quinoline based *ortho*-QMPs were synthesized and their photochemistry was investigated. *Ortho*-formylation of 4-hydroxyquinoline (**8**) with formic acid produced the desired quinoline **9** in a single step (Scheme 4.1).



Scheme 4.1: Synthesis of 3-(hydroxymethyl)quinoline-4-ol (**9**)

Quinoline **10a** was furnished in two steps from the commercially available quinoline acid **11** (Scheme 4.2); direct reduction of quinoline **11** resulted in low yields and a mixture of products due to the poor solubility of **11** in organic solvents. Instead **11** was esterified using coupling reagent EDCI and then ester **12** was easily reduced to the desired diol **10a** with DIBAL. Heating of diol **10a** in the presence of an alcohol or amine resulted in the derivatives **10b** and **10c** presumable via a thermal *ortho*-QM; interestingly acid catalysis shut down this reaction.



Scheme 4.2: Synthesis of 4-(hydroxymethyl)-2-methylquinolin-3-ol (**10a**)

Initial attempts to synthesize quinoline **13a**, were unsuccessful. As had been reported in the literature²¹ direct synthesis of 2- substituted 3-quinolinol derivatives using the Friedlander condensation was found to be challenging. Similarly a derivatization method starting with the commercially available 3-quinolinamine, adapted from Riego et al.,²² was not reproducible. Specifically, a two-step oxidation by selenium dioxide followed by hydrogen peroxide proved very low yielding (< 15 %) and inconsistent. Instead quinoline **10a** was successfully synthesized by adaption of a protocol from Vippila et al (Scheme 4.3).²³ Selective reduction of 2-nitrobenzaldehyde (**14**) with iron furnished 2-aminobenzaldehyde (**15**) and subsequent condensation with ethyl bromopyruvate provided the amino quinoline **16**. A Sandmeyer reaction converted the amine **16** to hydroxy quinoline **17** and subsequent reduction with DIBAL furnished **13a** reliably in 4 steps. Heating the diol in the presence of alcohol resulted in the derivative **13b**. The amine substituted **13c** was synthesized directly from 3-quinolinol (**18**) by Mannich reaction using Eschenmoser's salt (Scheme 4.3).¹⁹

4.2.2 Photophysics

UV-vis spectra of quinoline **10a** and **13a** are similar and resemble the spectrum of 3-quinolinol (**18**) at pH 7 (Figure 4.2).²⁴ In aqueous solution compounds **10a** and **13a** contain two major UV-vis bands above 300 nm: at $\lambda_{\text{max}} = 320$ nm and 375 nm for **10a** and $\lambda_{\text{max}} = 325$ nm and 370 nm for **13a** but the relative intensities are opposite. The two bands are attributed to a combination of neutral and zwitterionic species being present in solution.²⁴ Both **10a** and **13a** show strong fluorescence (Figure 4.3). Under neutral buffered aqueous conditions both show a broad emission band when excited at 325 or 375 nm ($\lambda_{\text{max}} = 455$ nm for **10a** and $\lambda_{\text{max}} = 475$ nm for **13a**). Quinoline **10a** shows significantly higher fluorescence efficiency ($\Phi_{\text{Fl}} = 0.49$) than **13a** ($\Phi_{\text{Fl}} = 0.26$) at 325 nm excitation. 2-hydroxy-1-naphthalenemethanol (**3**) also has a higher fluorescence efficiency ($\Phi_{\text{Fl}} = 0.30$)³ than 3-hydroxy-2-naphthalenemethanol (**4**) ($\Phi_{\text{Fl}} = 0.23$),³ but it is not as pronounced as in the quinoline isomers.

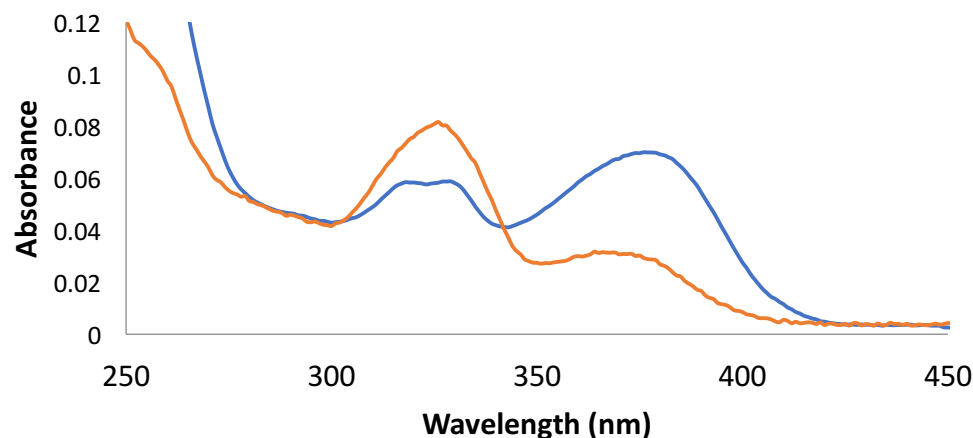


Figure 4.2: UV-Vis spectra of pH neutral phosphate buffered solution of quinoline **10a** (blue) and quinoline **13a** (orange).

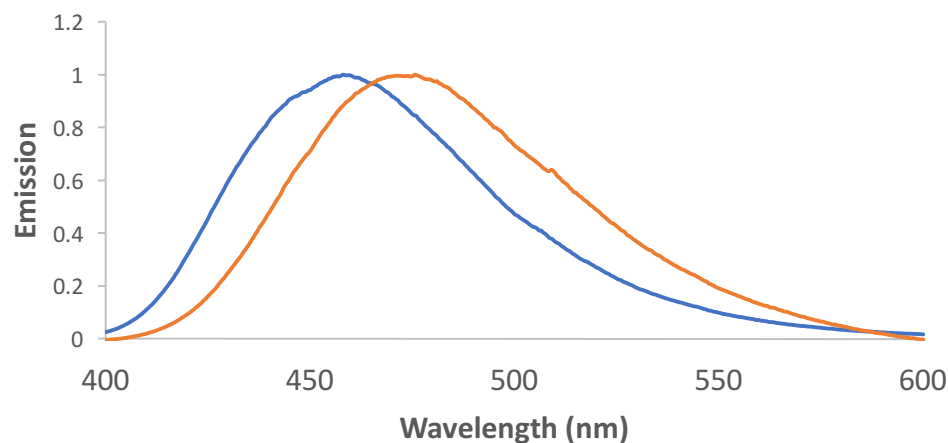


Figure 4.3: Emissions spectra of neutral pH phosphate buffered solution of quinoline **10a** (blue) and quinoline **13a** (orange).

The excited state acidity of quinoline **10a** ($\text{pK}_{\text{a}}^* = 3.5$) was estimated using Förster analysis (Figure 4.4a) and is slightly lower than the known pK_{a}^* of 3-quinolinol (**18**) ($\text{pK}_{\text{a}}^* = 4.0$).²⁵ This is a significant drop in acidity of 4.5 orders of magnitude relative to the ground state pK_{a} of 3-quinolinol ($\text{pK}_{\text{a}} = 8.06$).²⁶ The enhanced acidity of **10a** is most likely due to the intramolecular anion-stabilizing hydrogen bond between the phenolate oxygen and the benzylic hydroxy group as has been observed previously in *ortho*-substituted phenols.³ Quinoline **13a** exhibited a 10 nm bathchromic shift in absorbance between the acid and conjugate base indicative of a photoacid (Figure 4.4b). However, emission at pH 5 occurred from the tautomeric $^-\text{OQN}^+\text{H}$ ($\lambda_{\text{max}} = 450 \text{ nm}$) under neutral conditions which

is red shifted compared to emission from the conjugate base ($\lambda_{\text{max}} = 433 \text{ nm}$). Rapid ESIPT to the nitrogen is known to outcompete fluorescence from the acid for 3-quinolinol²⁴ and can be observed to some extent for quinoline **10a**, which exhibits dual emission at pH 5 from the acid HOQN ($\lambda_{\text{max}} = 370 \text{ nm}$) and zwitterionic $^-\text{OQN}^+\text{H}$ species ($\lambda_{\text{max}} = 454 \text{ nm}$). While it may not be possible to accurately determine the pK_a^* for quinoline **13a** using Förster analysis, quinoline **13a** is certainly still a photoacid.

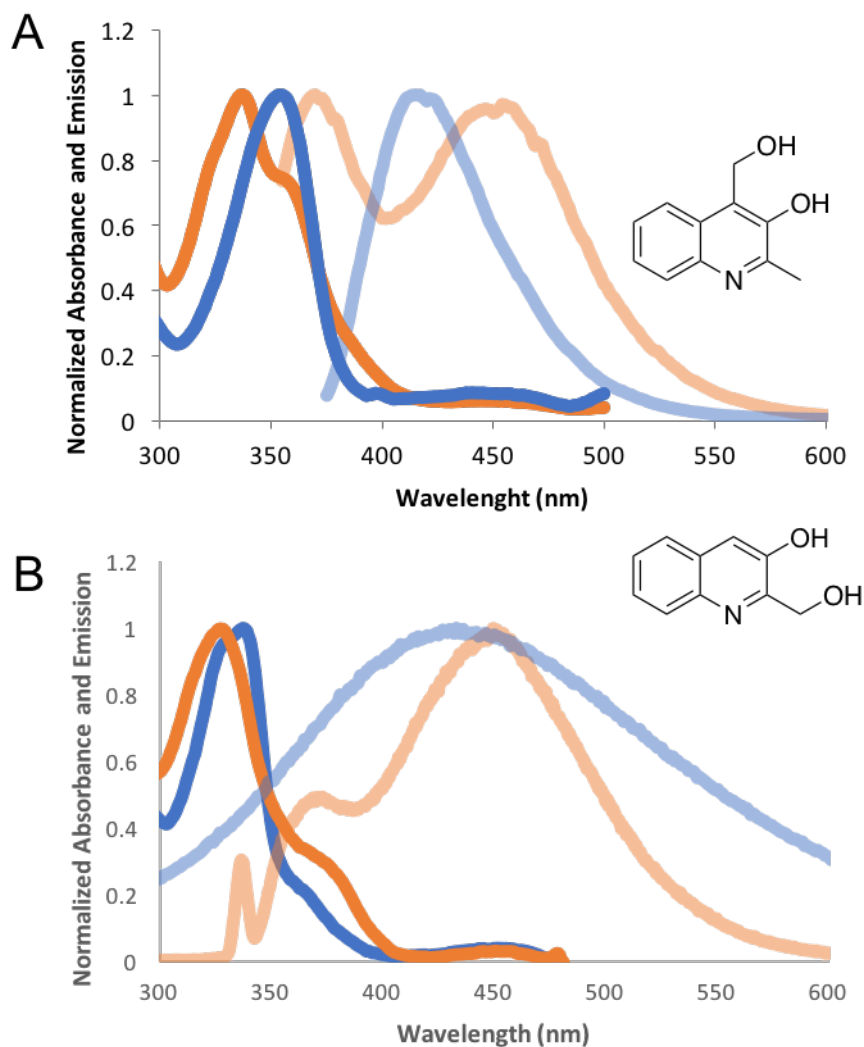


Figure 4.4: Spectra for Förster analysis to determine excited state pK_a (pK_a^*). A) Quinoline **10a** shows a bathochromic shift in absorbance (solid) and emission (faded) between the acid (orange) and the conjugate base (blue). Emission is seen from both the acid HOQN and the zwitterion $^-\text{OQN}^+\text{H}$ at pH 5. B) Quinoline **13a** shows a bathochromic shift in the absorbance (solid) between the acid (orange) and the conjugate base (blue). Emission (faded) is only observed from the zwitterion $^-\text{OQN}^+\text{H}$ at pH 5 (orange) and not the acid resulting in a hypsochromic shift between the acid and conjugate base in the emission. (Absorbance spectra (solid) and emission spectra (faded) pH 5 (orange) and pH > 10 (blue)).

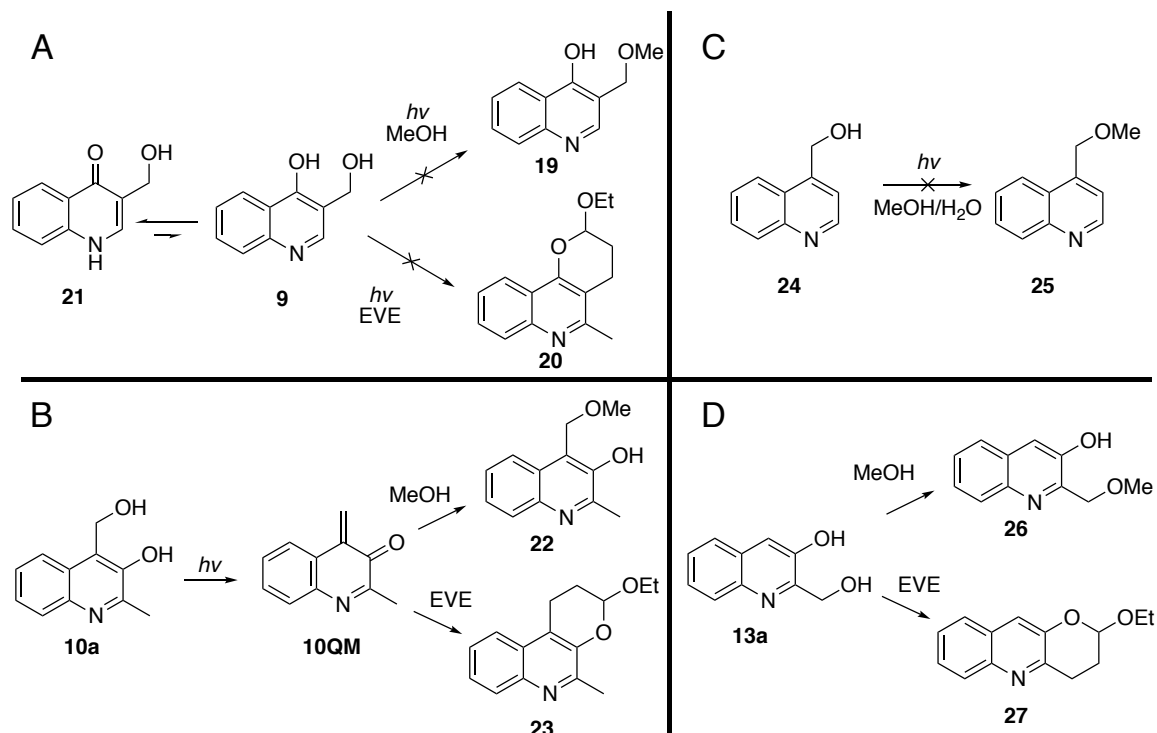
4.2.3 Photochemistry

Quinoline **9** was photostable; irradiation in the presence methanol or ethyl vinyl ether (EVE) did not result in the desired ether **19** or the Diels Alder cycloadduct **20**, respectively (Scheme 4.4a). This is most likely due to tautomerization to the quinolone **21** species at neutral pH;²⁷ 4-hydroxyquinoline has a hydroxyl pKa of 11.74 and a nitrogen pKa of 2.27.²⁸ Lack of a photoacidic proton would explain the photostability of **6** since ESPT is required for the initial step in photo QM formation.⁸

Quinoline isomers **10** and **13** are unable to tautomerize and form a quinolone isomer. Irradiation, at > 320 nm, of quinoline **10a** in a solution of 1:1 H₂O:MeOH resulted in a mixture of the photochemical product ether **22** and the starting material **10a** according to LCMS and NMR (Scheme 4.4b). Water and methanol are both nucleophiles that can quench the *ortho*-QM intermediate resulting in a mixture of products. The reaction proceeded cleanly in the presence of oxygen, as is typical of *ortho*-QM photochemistry, and no difference in reactivity was observed between degassed and non-degassed samples. Photolysis of **10a** with EVE in 1:1 H₂O:MeCN gave the Diels-Alder adduct **23** cleanly at low conversion; the product **23** is prone to secondary photolysis³ and absorbs at similar wavelengths. Formation of EVE product **23** is only possible by reaction of a 1,4-dipolar species with EVE and therefore provides conclusive evidence for the efficient generation of *ortho*-QM **10QM**. Additionally, irradiation of quinolin-4-ylmethanol (**24**) in a 1:1 H₂O:MeOH did not result in any ether product (Scheme 4.4c), ruling out photoinduced homolytic bond cleave as a mechanism and confirming the vital nature of the phenol in the photochemical mechanism. Irradiation of quinoline **10b** or **10c** in 1:1 H₂O:MeOH resulted in ether photoproduct **22** according to LCMS.

The quinoline **13a** exhibited similar photochemistry to **10a**, and when irradiated in the presence of methanol or EVE the expected photoproduct was observed by NMR and LCMS cleanly (Scheme 4.4d). Surprisingly the amine substituted quinoline **13c** appears to be photostable; amines are typically better leaving groups for *ortho*-QM reactions,¹¹ however this doesn't appear to be the case. It is possible that ⁻NMe₂ or HNMe₂ is a better nucleophile and outcompetes quenching by water or methanol: for Mannich base **7**

reactivity was only observed with stronger nucleophiles and no hydration product was observed.¹⁹ However, this does not explain the lack of reactivity with EVE.



Scheme 4.4: Photochemistry of quinoline QMPs. A) Quinoline **9** does not form a QM when irradiated because it tautomerizes to quinolone **21**. B) Photoreactivity of quinoline **10a**. C) Quinoline **24** is photostable. D) Quinoline **13a** forms an *ortho*-QM when irradiated.

Quantum yields are used to compare the efficiency of photochemical reactions. Qualitatively the photodehydration of quinoline **10a** appeared to be less efficient than the equivalent naphthalol QMP when the two reactions were run in parallel. This is not surprising given the quantum yield of benzylic QMP **2** ($\Phi_{\text{rxn}} = 0.46$)⁸ was double that of pyridine QMP **6** ($\Phi_{\text{rxn}} = 0.2$)¹⁸ under similar conditions. Attempts were made using a ferrioxalate actinometer to measure the quantum yield of **10a**. However, issues of phase separation of EVE in MeCN:H₂O solutions made for inconsistency in sample preparation and gave a range of quantum yields between 0.001 and 0.9, a meaninglessly large range.

Without accurate quantum yields it is hard to compare the reactivity of quinoline **10a** and **13a**. Given the high fluorescence efficiency of **10a** it might be expected that quinoline **10a** would have a lower quantum yield of reaction than quinoline **13a** but at least for naphthalol QMPs that logic does not hold. Naphthalol **3** has both a greater quantum yield

or reaction ($\Phi_{\text{rxn}} = 0.2$) and fluorescence ($\Phi_{\text{fl}} = 0.3$) then naphthol **4** ($\Phi_{\text{rxn}} = 0.17$ $\Phi_{\text{fl}} = 0.23$).

Laser flash photolysis (LFP) is an effective method for direct observation of the *ortho*-QM transient which is characterized by a broad, O₂ insensitive, long lived transient that is quenched by the addition of nucleophiles or electron rich dienophiles. Measurements were performed to probe for the *ortho*-QM intermediate of quinoline **10a**. Laser pulsed excitation of quinoline **10a**, by a Nd:YAG laser at 355 nm, resulted in a burst of bright fluorescence covering the region from 400 nm to 475 nm. This intense emission saturated the detector complicating observations in this region. A transient was observed between 405 nm and 475 nm with a lifetime of 1.5 μs in aqueous solution (pH 7 Phosphate Buffer) (Figure 4.5). This lifetime was much shorter than anticipated given the lifetime of pyridoxine **6** ($\tau = 10$ ms)¹⁸ and bipyridyl **7** ($\tau = 50$ μs)¹⁹ and there was no observed change in the lifetime of the transient in the presence of the sodium azide (NaN₃) or EVE, two common *ortho*-QM quenchers.

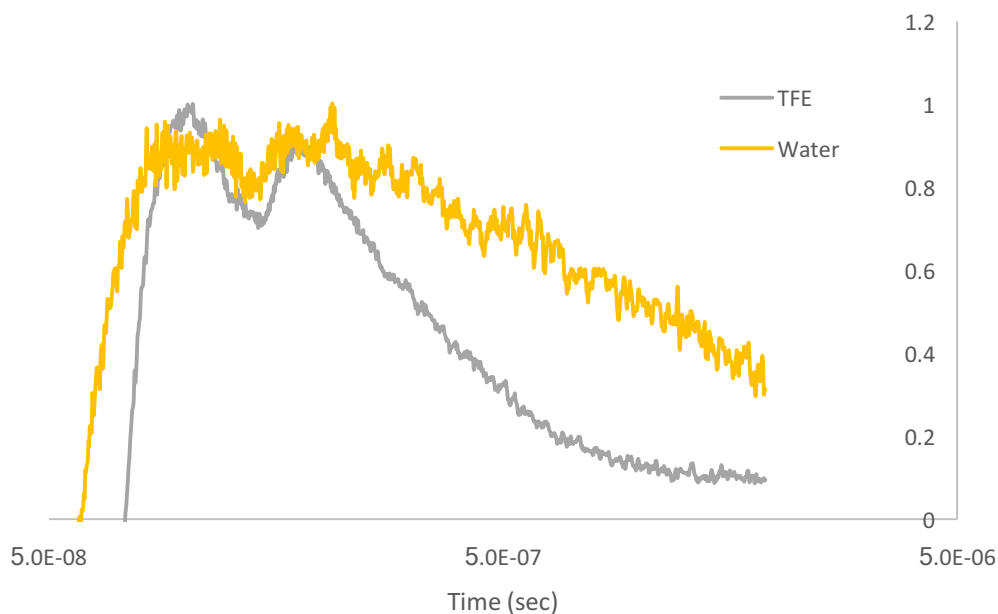


Figure 4.5: Lifetime of the possible transient in pH 7 phosphate buffer (1.5 μs) and trifluoroethanol (200 ns) at 405 nm for **10a**.

Worried that the solvent, water, was quenching the *ortho*-QM intermediate, experiments were carried out in trifluoroethanol (TFE) a polar non-nucleophilic solvent in which electrophilic species such as QMs exhibit longer lifetimes.^{13,29,30} Instead of

increasing the lifetime of the observed transient the lifetime decreased when experiments were conducted in TFE (200 ns) (Figure 4.5). Addition of the nucleophile NaN_3 or EVE did not affect the lifetime of the transient (Figure 4.6). It was concluded that the observed transient was an artifact of the fluorescence event saturating the detector. Others have solved this problem by observing the transient at shorter wave lengths, $< 310 \text{ nm}$, where fluorescence is not a problem;³ however, instrumentation prevented observation at wavelengths shorter than 400 nm. Given the limits in instrumentation it was impossible to determine the lifetimes of the *ortho*-QM intermediates for quinoline **10a** and **13a** and compare them to the known lifetime of the equivalent naphthalol QMPs or other heterocyclic QMPs. The *ortho*-QM intermediate derived from hydroxybenzyl alcohols exhibits a three orders of magnitude longer lifetime than the *ortho*-QM derived from an equivalent heterocyclic pyridine derivative under similar reaction conditions.^{8,18} Similarly, without identification of the transient it is impossible to determine if *ortho*-QM formation occurs via a benzoxetane³ or radical mechanism,³¹ which have been purposed in some instances of photochemical QM generation.

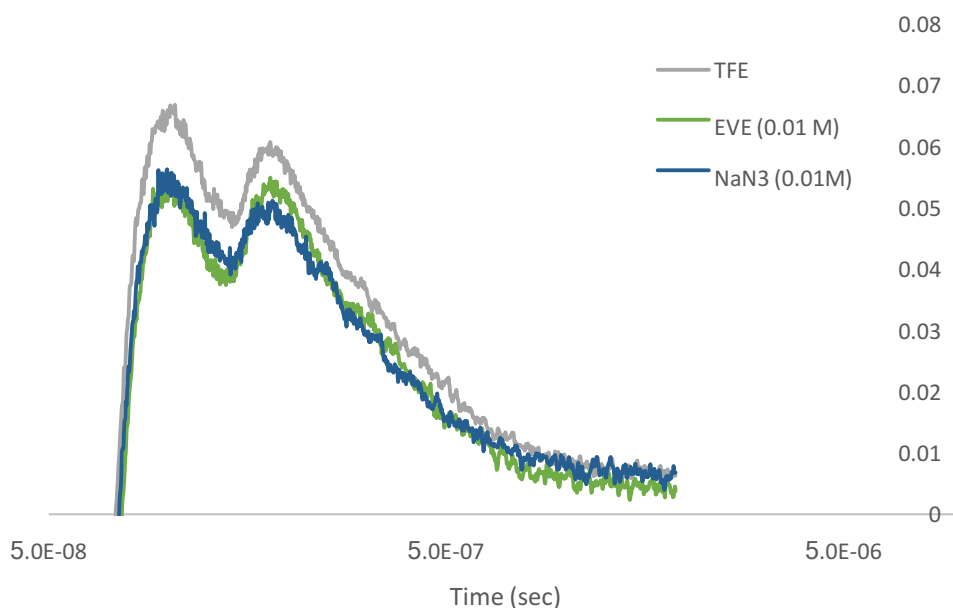
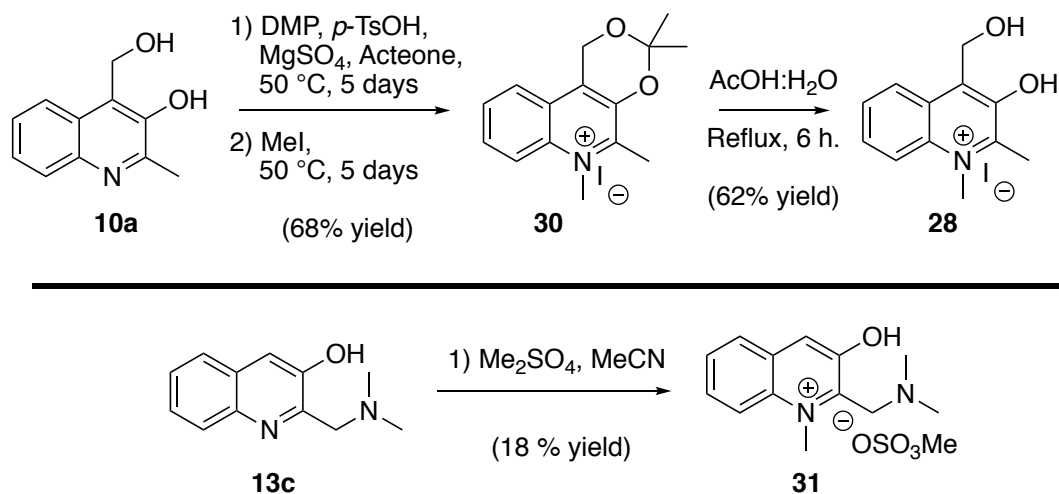


Figure 4.6: Effect of the QM quenchers ethyl vinyl ether (green) and sodium azide (blue) on the lifetime of observed possible transient in trifluoroethanol (gray) at 405 nm for **10a**.

4.3 Quinolinium *ortho*-quinone methide

4.3.1 Synthesis of quinolinium derivatives:

Treatment of quinoline **10a** with methyl iodide resulted in an intractable mixture of the desired quinolinium **28** and the starting material **10a**. Protected quinoline ketal **29** was highly soluble and when treated with methyl iodide the quinolinium **30** crashed out of solution making separation and purification trivial. The ketal protecting group was removed efficiently by refluxing under acidic conditions and the desired quinolinium **28** was purified by HPLC with good separation (Scheme 4.5a).



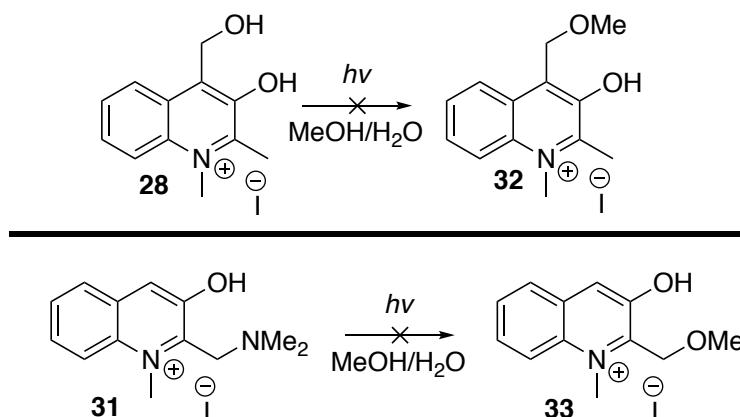
Scheme 4.5: Synthesis of quinolinium derivatives **28** and quinolinium **31**.

Given the initial difficulty in synthesizing quinoline **13a**, efforts focused on the synthesis of Mannich base derived quinolinium **13c** instead. Treatment of quinoline **13c** with methyl iodide did not result in any of the desired quinolinium according to NMR. Instead, the much stronger methylating agent dimethyl sulfate was required to furnish quinolinium **31** in good yield (Scheme 4.5b). Only the single addition product was observed.

4.3.2 Photochemistry

Quinolinium **28** was photostable; irradiation, at > 320 nm, in a 1:1 H₂O:MeOH solution resulted in no observed photochemical product **32** according to LCMS and NMR (Scheme 4.6a). Similarly, photolysis of **28** with EVE in 1:1 H₂O:MeCN gave no Diels-Alder adduct. Under the same conditions, quinolinium **31** was also proved inert (Scheme 4.6b). The photostability of quinoline **13c** complicated analysis of the photostability of

quinolinium **31** and subsequent experiments on counter ion, photoacidity, and charge focused on quinolinium **28**.



Scheme 4.6: Photochemistry of quinolinium derivatives quinolinium **28** and quinolinium **31**.

Iodide, the counter ion in quinolinium **28**, is known to promote intersystem crossing to the triplet and to promote electron transfer to the iodide; both mechanism would inhibit QM formation. Ion exchange to the non-coordinating counterions, CF_3SO_3^- , ClO_4^- , BF_4^- , and PF_6^- did not alter the photostability of quinolinium **28**. Iodide has previously been used as a counter ion for quaternary ammonium salt QM precursors with no observed negative effect on photogeneration of QMs.^{32–34} Similarly, acetate, chloride, and perchlorate ions anions had no effect on QM formation and ionic concentrations of 0.1M didn't negatively impact QM formation or reactivity.³⁵ The counterion is most likely not the source of quinolinium **28** photostability.

Quinolinium **28**, like other known quinoliniums,^{36–38} is a super photoacid with a pK_a^* less than zero. As is typical of photoacids, UV-vis spectra showed a 47 nm bathochromic shift between the acid ($\lambda_{\text{max}} = 342$ nm) and the conjugate base ($\lambda_{\text{max}} = 389$ nm) (Figure 4.7). Indicative of a super photoacid, the emission spectra of the acid and conjugate base are superimposable ($\lambda_{\text{max}} = 477$ nm) (Figure 4.7) because the rate of ESPT eclipses fluorescence from the excited state acid.³⁹ Förster analysis of the UV-vis spectra of the acid and conjugate base indicate an approximate pK_a^* of -2. Using absorbance data alone underestimates the true pK_a^* ⁴⁰ and as the pK_a^* approaches zero Förster analysis becomes less accurate because of increasing entropic factors.⁴¹ There are no examples in the literature of super photoacid QMPs. If QM formation is a concerted process with ESPT

then the ultrafast proton transfer exhibited by super photoacids may be detrimental to QM formation.

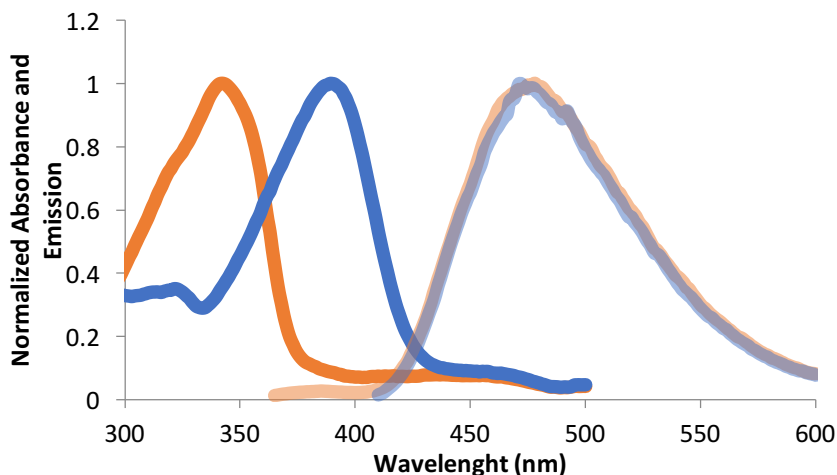


Figure 4.7: Spectra for Förster analysis to determine excited state pK_a (pK_a^*) for quinlonium **28**. A bathochromic shift is observed in absorbance (Solid) between the acid (orange) and the conjugate base (blue). The emissions spectra (faded) for the acid (orange) and conjugate base (blue) are superimposable indicative of a super photoacid.

4.3.3 pH dependence of photochemistry

To understand the effect of a positively charged species on QM formation, the pH dependence of quinoline **10a** was investigated. Under acidic conditions protonation of the nitrogen results in a species isoelectronic with quinolinium **28**. Bulk photolysis of *ortho*-QMPs is typically pH independent over the pH range 2-7.³ The photolysis of quinoline **10a** and **13a** in 1:1 EtOH:citrate-phosphate buffer over the pH range 2.5-6 at low conversion rates showed marked pH dependence on QM formation when controlling for the dark thermal acid catalyzed reaction (Figure 4.8). This was more pronounced for quinoline **10a**, which showed no photoreactivity at pH 3, than for quinoline **13a**. The significant drop in reactivity corresponds to the nitrogen pK_a ($pK_a = 4.3$ for 3-hydroxyquinoline).²⁶ Protonation of the nitrogen reduces or eliminates QM formation.

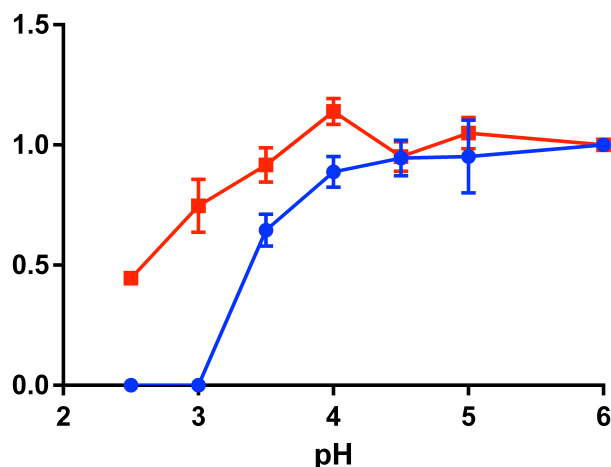


Figure 4.8: pH dependence on the photoreactivity of quinoline **10a** (blue) and quinoline **13a** (red) relative to reactivity at pH 6.0.

pH has not previously been shown to effect bulk quantum yields but it has been shown to affect the lifetime of the QM intermediates in solution. The lifetime of the pyridoxine QMP **6** derived *ortho*-QM was 200 fold shorter at pH 1 than in neutral solution.¹⁸ (Brousmiche and Wan do not report a change in bulk quantum yield of reaction at pH 1 for pyridoxine **6**.) Similarly, the nitrogen protonated QM ($\tau = 50 \mu\text{s}$) was observed to have a much shorter lifetime than the neutral QM ($\tau = 10 \text{ ms}$) at pH 7.¹⁸ The electron withdrawing nature of the quinolinium makes the QM much more reactive because of the electron deficient nature of QMs. Previously this effect was shown to be more pronounced when the EWD was in conjugation with the QM carbonyl⁹ like in the case of quinolinium **28**. QM lifetime doesn't always correlate with the bulk quantum yield,⁸ and without transient spectroscopy it is impossible to determine if quinolinium **28** forms a very short lived QM intermediate. However, given that bulk photolysis resulted in no photoproduct it may be that the quinolinium moiety is so electron withdrawing that it prevents formation of the QM.

4.4 Conclusions

Quinoline derivatives can function as QMPs depending on the isomer. Quinolin-4-ol derivatives do not make good QMPs because under neutral conditions quinoline **9** tautomerizes to quinolone **21**. The same is expected for 2-quinolinol QMPs which similarly tautomerize. Investigation of quinoline **10a** and quinoline **13a** showed that 3-quinolinol

derivatives do form *ortho*-QMs when irradiated as evidenced by their reactivity with EVE and nucleophiles. Quinoline **13** may not be as reactive and or stable given the lack of reactivity of quinoline **13c**.

The electron withdrawing nature of quinoliniums make them ill-suited as QMPs. This is definitely true for 3-hydroxyquinolinium where the QM carbonyl is in conjugation the quinolinium nitrogen. 5- or 7-hydroxyquinolinium based QMPs may display better photochemistry since locations on the distal ring are less effected by the nitrogen and the QM carbonyl would not be in conjugation with the quinolinium.

Acknowledgements:

I would like to thank Dr. Brian Sanders, a Post Doc in the Gray group who trained me on the LFP in BILRIC. This work was funded in part by the NSF GRFP.

4.5 References

- (1) Kostikov, A. P.; Popik, V. V. 2,5-Dihydroxybenzyl and (1,4-Dihydroxy-2-Naphthyl)Methyl, Novel Reductively Armed Photocages for the Hydroxyl Moiety. *J. Org. Chem.* **2007**, *72* (24), 9190–9194. <https://doi.org/10.1021/jo701426j>.
- (2) Kulikov, A.; Arumugam, S.; Popik, V. V. Photolabile Protection of Alcohols, Phenols, and Carboxylic Acids with 3-Hydroxy-2-Naphthalenemethanol. *J. Org. Chem.* **2008**, *73* (19), 7611–7615. <https://doi.org/10.1021/jo801302m>.
- (3) Arumugam, S.; Popik, V. V. Photochemical Generation and the Reactivity of O-Naphthoquinone Methides in Aqueous Solutions. *J. Am. Chem. Soc.* **2009**, *131* (33), 11892–11899. <https://doi.org/10.1021/ja9031924>.
- (4) Arumugam, S.; Popik, V. V. Dual Reactivity of Hydroxy- and Methoxy-Substituted o-Quinone Methides in Aqueous Solutions: Hydration versus Tautomerization. *J. Org. Chem.* **2010**, *75* (21), 7338–7346. <https://doi.org/10.1021/jo101613t>.
- (5) Nekongo, E. E.; Popik, V. V. Photoactivatable Fluorescein Derivatives Caged with a (3-Hydroxy-2-Naphthalenyl)Methyl Group. *J. Org. Chem.* **2014**, *16* (79), 7665–7671. <https://doi.org/10.1021/jo501116g>.
- (6) Arumugam, S.; Popik, V. V. Attach, Remove, or Replace: Reversible Surface Functionalization Using Thiol–Quinone Methide Photoclick Chemistry. *J. Am. Chem. Soc.* **2012**, *134* (20), 8408–8411. <https://doi.org/10.1021/ja302970x>.
- (7) Klán, P.; Šolomek, T.; Bochet, C. G.; Blanc, A.; Givens, R.; Rubina, M.; Popik, V.; Kostikov, A.; Wirz, J. Photoremovable Protecting Groups in Chemistry and Biology: Reaction Mechanisms and Efficacy. *Chem. Rev.* **2013**, *113* (1), 119–191. <https://doi.org/10.1021/cr300177k>.
- (8) Diao, L.; Yang, C.; Wan, P. Quinone Methide Intermediates from the Photolysis of Hydroxybenzyl Alcohols in Aqueous Solution. *J. Am. Chem. Soc.* **1995**, *117* (19), 5369–5370. <https://doi.org/10.1021/ja00124a024>.

- (9) Weinert, E. E.; Dondi, R.; Colloredo-Melz, S.; Frankenfield, K. N.; Mitchell, C. H.; Freccero, M.; Rokita, S. E. Substituents on Quinone Methides Strongly Modulate Formation and Stability of Their Nucleophilic Adducts. *J. Am. Chem. Soc.* **2006**, *128* (36), 11940–11947. <https://doi.org/10.1021/ja062948k>.
- (10) Doria, F.; Lena, A.; Bargiggia, R.; Freccero, M. Conjugation, Substituent, and Solvent Effects on the Photogeneration of Quinone Methides. *J. Org. Chem.* **2016**, *81* (9), 3665–3673. <https://doi.org/10.1021/acs.joc.6b00331>.
- (11) Nakatani, K.; Higashida, N.; Saito, I. Highly Efficient Photochemical Generation of O-Quinone Methide from Mannich Bases of Phenol Derivatives. *Tetrahedron Lett.* **1997**, *38* (28), 5005–5008. [https://doi.org/10.1016/S0040-4039\(97\)01071-X](https://doi.org/10.1016/S0040-4039(97)01071-X).
- (12) Verga, D.; Nadai, M.; Doria, F.; Percivalle, C.; Di Antonio, M.; Palumbo, M.; Richter, S. N.; Freccero, M. Photogeneration and Reactivity of Naphthoquinone Methides as Purine Selective DNA Alkylating Agents. *J. Am. Chem. Soc.* **2010**, *132* (41), 14625–14637. <https://doi.org/10.1021/ja1063857>.
- (13) Lukeman, M.; Veale, D.; Wan, P.; Munasinghe, V. R. N.; Corrie, J. E. Photogeneration of 1,5-Naphthoquinone Methides via Excited-State (Formal) Intramolecular Proton Transfer (ESIPT) and Photodehydration of 1-Naphthol Derivatives in Aqueous Solution. *Can. J. Chem.* **2004**, *82* (2), 240–253. <https://doi.org/10.1139/v03-184>.
- (14) Shi, Y.; Wan, P. Solvolysis and Ring Closure of Quinone Methides Photogenerated from Biaryl Systems. *Can. J. Chem.* **2005**, *83* (9), 1306–1323. <https://doi.org/10.1139/v05-138>.
- (15) Brousmiche, D. W.; Xu, M.; Lukeman, M.; Wan, P. Photohydration and Photosolvolysis of Biphenyl Alkenes and Alcohols via Biphenyl Quinone Methide-Type Intermediates and Diarylmethyl Carbocations. *J. Am. Chem. Soc.* **2003**, *125* (42), 12961–12970. <https://doi.org/10.1021/ja036808b>.
- (16) Doja, M. Q. The Cyanine Dyes. *Chem. Rev.* **1932**, *11* (3), 273–321. <https://doi.org/10.1021/cr60040a001>.
- (17) Shindy, H. A. Fundamentals in the Chemistry of Cyanine Dyes: A Review. *Dyes Pigments* **2017**, *145*, 505–513. <https://doi.org/10.1016/j.dyepig.2017.06.029>.
- (18) Brousmiche, D. Photogeneration of an o -Quinone Methide from Pyridoxine (Vitamin B 6) in Aqueous Solution. *Chem. Commun.* **1998**, *0* (4), 491–492. <https://doi.org/10.1039/A707231G>.
- (19) Verga, D.; Richter, S. N.; Palumbo, M.; Gandolfi, R.; Freccero, M. Bipyridyl Ligands as Photoactivatable Mono- and Bis-Alkylating Agents Capable of DNA Cross-Linking. *Org. Biomol. Chem.* **2007**, *5* (2), 233–235. <https://doi.org/10.1039/B616292D>.
- (20) Wu, M.; Xu, Q.; Strid, Å.; Martell, J. M.; Eriksson, L. A. Theoretical Study of Pyridoxine (Vitamin B6) Photolysis. *J. Phys. Chem. A* **2011**, *115* (46), 13556–13563. <https://doi.org/10.1021/jp205724k>.
- (21) Boger, D. L.; Chen, J.-H. A Modified Friedlander Condensation for the Synthesis of 3-Hydroxyquinoline-2-Carboxylates. *J. Org. Chem.* **1995**, *60* (22), 7369–7371. <https://doi.org/10.1021/jo00127a055>.
- (22) Riego, E.; Bayó, N.; Cuevas, C.; Albericio, F.; Álvarez, M. A New Approach to 3-Hydroxyquinoline-2-Carboxylic Acid. *Tetrahedron* **2005**, *61* (6), 1407–1411. <https://doi.org/10.1016/j.tet.2004.12.011>.

- (23) Vippila, M. R.; Ly, P. K.; Cuny, G. D. Synthesis and Antiproliferative Activity Evaluation of the Disulfide-Containing Cyclic Peptide Thiochondrilline C and Derivatives. *J. Nat. Prod.* **2015**, *78* (10), 2398–2404. <https://doi.org/10.1021/acs.jnatprod.5b00428>.
- (24) Yu, H.; Kwon, O.-H.; Jang, D.-J. Migration of Protons during the Excited-State Tautomerization of Aqueous 3-Hydroxyquinoline. *J. Phys. Chem. A* **2004**, *108* (28), 5932–5937. <https://doi.org/10.1021/jp031293w>.
- (25) Mason, S. F.; Philp, J.; Smith, B. E. Prototropic Equilibria of Electronically Excited Molecules. Part II. 3-, 6-, and 7-Hydroxyquinoline. *J. Chem. Soc. Inorg. Phys. Theor.* **1968**, *0* (0), 3051–3056. <https://doi.org/10.1039/J19680003051>.
- (26) Albert, A.; Phillips, J. N. 264. Ionization Constants of Heterocyclic Substances. Part II. Hydroxy-Derivatives of Nitrogenous Six-Membered Ring-Compounds. *J. Chem. Soc. Resumed* **1956**, *0* (0), 1294–1304. <https://doi.org/10.1039/JR9560001294>.
- (27) Tucker, G. F.; Irvin, J. L. Apparent Ionization Exponents of 4-Hydroxyquinoline, 4-Methoxyquinoline and N-Methyl-4-Quinolone; Evaluation of Lactam—Lactim Tautomerism I. *J. Am. Chem. Soc.* **1951**, *73* (5), 1923–1929. <https://doi.org/10.1021/ja01149a006>.
- (28) Mason, S. F. 131. The Tautomerism of N-Heteroaromatic Hydroxy-Compounds. Part III. Ionisation Constants. *J. Chem. Soc. Resumed* **1958**, *0* (0), 674–685. <https://doi.org/10.1039/JR9580000674>.
- (29) Škalamera, Đ.; Mlinarić-Majerski, K.; Martin-Kleiner, I.; Kralj, M.; Wan, P.; Basarić, N. Near-Visible Light Generation of a Quinone Methide from 3-Hydroxymethyl-2-Anthrol. *J. Org. Chem.* **2014**, *79* (10), 4390–4397. <https://doi.org/10.1021/jo500290y>.
- (30) Xu, M.; Lukeman, M.; Wan, P. Photogeneration and Chemistry of Biphenyl Quinone Methides from Hydroxybiphenyl Methanols†. *Photochem. Photobiol.* **2006**, *82* (1), 50–56. <https://doi.org/10.1562/2005-02-17-RA-444>.
- (31) Škalamera, Đ.; Mlinarić-Majerski, K.; Martin Kleiner, I.; Kralj, M.; Oake, J.; Wan, P.; Bohne, C.; Basarić, N. Photochemical Formation of Anthracene Quinone Methide Derivatives. *J. Org. Chem.* **2017**, *82* (12), 6006–6021. <https://doi.org/10.1021/acs.joc.6b02735>.
- (32) Song, Y.; Tian, T.; Wang, P.; He, H.; Liu, W.; Zhou, X.; Cao, X.; Zhang, X.-L.; Zhou, X. Phenol Quaternary Ammonium Derivatives: Charge and Linker Effect on Their DNA Photo-Inducible Cross-Linking Abilities. *Org. Biomol. Chem.* **2006**, *4* (17), 3358–3366. <https://doi.org/10.1039/B604552A>.
- (33) Doria, F.; Richter, S. N.; Nadai, M.; Colloredo-Mels, S.; Mella, M.; Palumbo, M.; Freccero, M. BINOL–Amino Acid Conjugates as Triggerable Carriers of DNA-Targeted Potent Photocytotoxic Agents. *J. Med. Chem.* **2007**, *50* (26), 6570–6579. <https://doi.org/10.1021/jm070828x>.
- (34) Wang, P.; Liu, R.; Wu, X.; Ma, H.; Cao, X.; Zhou, P.; Zhang, J.; Weng, X.; Zhang, X.-L.; Qi, J.; et al. A Potent, Water-Soluble and Photoinducible DNA Cross-Linking Agent. *J. Am. Chem. Soc.* **2003**, *125* (5), 1116–1117. <https://doi.org/10.1021/ja029040o>.

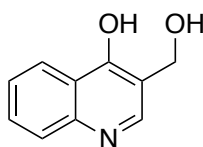
- (35) Modica, E.; Zanaletti, R.; Freccero, M.; Mella, M. Alkylation of Amino Acids and Glutathione in Water by O-Quinone Methide. Reactivity and Selectivity. *J. Org. Chem.* **2001**, *66* (1), 41–52. <https://doi.org/10.1021/jo0006627>.
- (36) Bardez, E.; Chatelain, A.; Larrey, B.; Valeur, B. Photoinduced Coupled Proton and Electron Transfers. 1. 6-Hydroxyquinoline. *J. Phys. Chem.* **1994**, *98* (9), 2357–2366. <https://doi.org/10.1021/j100060a025>.
- (37) Bardez, E.; Fedorov, A.; Berberan-Santos, M. N.; Martinho, J. M. G. Photoinduced Coupled Proton and Electron Transfers. 2. 7-Hydroxyquinolinium Ion. *J. Phys. Chem. A* **1999**, *103* (21), 4131–4136. <https://doi.org/10.1021/jp990097f>.
- (38) Poizat, O.; Bardez, E.; Buntinx, G.; Alain, V. Picosecond Dynamics of the Photoexcited 6-Methoxyquinoline and 6-Hydroxyquinoline Molecules in Solution. *J. Phys. Chem. A* **2004**, *108* (11), 1873–1880. <https://doi.org/10.1021/jp030964n>.
- (39) Kim, T. G.; Topp, M. R. Ultrafast Excited-State Deprotonation and Electron Transfer in Hydroxyquinoline Derivatives. *J. Phys. Chem. A* **2004**, *108* (46), 10060–10065. <https://doi.org/10.1021/jp0471655>.
- (40) Pines, E. UV-Visible Spectra and Photoacidity of Phenols, Naphthols and Pyrenols. In *The Chemistry of Phenols: Part 1*; Rappoport, Z., Ed.; Wiley: Chichester, West Sussex, 2003; pp 491–527.
- (41) Tolbert, L. M.; Haubrich, J. E. Enhanced Photoacidities of Cyanonaphthols. *J. Am. Chem. Soc.* **1990**, *112* (22), 8163–8165. <https://doi.org/10.1021/ja00178a049>.
- (42) Yoon, N. M.; Pak, C. S.; Brown Herbert C.; Krishnamurthy, S.; Stocky, T. P. Selective Reductions. XIX. Rapid Reaction of Carboxylic Acids with Borane-Tetrahydrofuran. Remarkably Convenient Procedure for the Selective Conversion of Carboxylic Acids to the Corresponding Alcohols in the Presence of Other Functional Groups. *J. Org. Chem.* **1973**, *38* (16), 2786–2792. <https://doi.org/10.1021/jo00956a011>.
- (43) Velapoldi, R. A.; Mielenz, K. D. A Fluorescence Standard Reference Material: Quinine Sulfate Dihydrate. *Appl. Opt.* **1981**, *20* (9), 1718–1718. <https://doi.org/10.1364/AO.20.001718>.
- (44) Brouwer, A. M. Standards for Photoluminescence Quantum Yield Measurements in Solution (IUPAC Technical Report). *Pure Appl. Chem.* **2011**, *83* (12), 2213–2228. <https://doi.org/10.1351/PAC-REP-10-09-31>.
- (45) Williams, A. T. R.; Winfield, S. A.; Miller, J. N. Relative Fluorescence Quantum Yields Using a Computer-Controlled Luminescence Spectrometer. *Analyst* **1983**, *108* (1290), 1067–1071. <https://doi.org/10.1039/AN9830801067>.
- (46) Dempsey, J. L.; Winkler, J. R.; Gray, H. B. Mechanism of H₂ Evolution from a Photogenerated Hydridocobaloxime. *J. Am. Chem. Soc.* **2010**, *132* (47), 16774–16776. <https://doi.org/10.1021/ja109351h>.
- (47) McIlvaine, T. C. A Buffer Solution for Colorimetric Comparison. *J. Biol. Chem.* **1921**, *49* (1), 183–186.

4.6 Experimental

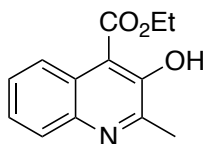
4.6.1 General Procedures

Unless otherwise stated reactions were carried out at ambient temperatures under argon. Any potentially light sensitive compounds were protected from light using aluminum foil and were carried out under low ambient light conditions. Commercially available reagents were obtained from Sigma Aldrich, AK scientific, Alfa Aesar, Acros Organics, or Strem Chemicals. Solvents used in photolysis and UV-vis experiments were EMD Millipore (OmniSolve®) grade. Other solvents were used as received unless otherwise noted. Reactions were monitored with thin layer chromatography using EMD/Merck silica gel 60 F254 pre coated glass plates (0.25 mm). Flash column chromatography was conducted using 60 Å, 230-400 mesh silica gel purchased from Alfa Aesar. NMR spectra were recorded on Varian (300, 500, or 600 MHz) or Bruker (400 MHz) spectrometers. UV-vis spectra were obtained using a Cary 60 spectrometer in 1 cm pathlength quartz cuvettes. Photolysis experiments were conducted in quartz cuvettes or custom quartz test tubes using either a 300 W Hg arc lamp (66011, Oriel) with glass filters or a M365LP1 365 nm 1150 mW LED lamp (Thor Labs).

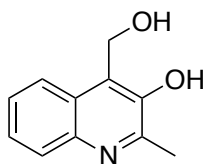
4.6.2 Synthesis



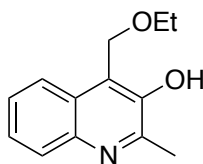
3-(hydroxymethyl)quinolin-4-ol (9): Formaldehyde 37% (0.3 mL, 3.4 mmol, 2 eq) was added to a solution of 4-hydroxyquinoline (**8**) (0.25 g, 1.7 mmol, 1 eq) in 1 M NaOH aq (3 mL). The reaction was stirred at 45 °C for 18 hours, cooled to room temperature, acidified with 2 M HCl (2 mL) and cooled in an ice bath. White crystals were isolated and washed with EtOAc (2 X 5 mL). Recrystallized from hot methanol to yield give 0.29 g (1.6 mmol) of **9** in 95% yield as a white solid. ¹H NMR (300 MHz, DMSO-*d*₆) δ 11.75 (s, 1H), 8.10 (dd, *J* = 8.2, 1.5 Hz, 1H), 7.86 (dt, *J* = 6.0, 1.0 Hz, 1H), 7.62 (ddd, *J* = 8.4, 6.8, 1.5 Hz, 1H), 7.57 – 7.48 (m, 1H), 7.29 (ddd, *J* = 8.1, 6.8, 1.2 Hz, 1H), 4.90 (t, 1H), 4.41 (d, *J* = 4.6 Hz, 2H).



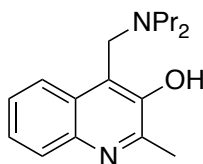
ethyl 3-hydroxy-2-methylquinoline-4-carboxylate (12): 200 proof ethanol (15 mL, 257 mmol, 10 eq), and DMAP (0.50 g, 4.1 mmol, 0.16 eq) were added to a suspension of 2-methyl-3-hydroxy-4-quinolinecarboxylic acid (**11**) (5.0 g, 24.6 mmol, 1 eq) in DCM (100 mL), in a 500 mL RBF. The reaction was cooled to 0 °C and EDCI (5.73 g, 30.0 mmol, 1.2 eq) was added in 5 portions over the course of 10 minutes. Reaction was stirred for 5 hours at room temperature, diluted with water (100 mL), extracted with DCM (3 x 50 mL), washed with brine (50 mL), dried over MgSO₄, and concentrated. Purified by flash column chromatography on silica (EtOAc:Hexane, 15:85) to give 4.32 g (18.7 mmol) of **12** in 76% yield as a white solid. ¹H NMR (500 MHz, Chloroform-*d*) δ 12.04 (s, 1H), 8.63 – 8.57 (m, 1H), 8.02 – 7.96 (m, 1H), 7.57 – 7.51 (m, 2H), 4.16 (s, 3H), 2.73 (q, *J* = 1.7 Hz, 2H), 1.59 (t, *J* = 1.7 Hz, 3H). ¹³C NMR (126 MHz, Chloroform-*d*) δ 172.19, 155.52, 153.86, 142.27, 129.70, 127.79, 126.25, 124.72, 123.84, 108.66, 53.04, 29.74, 20.60.



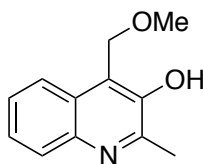
4-(hydroxymethyl)-2-methylquinolin-3-ol (10a): A solution of quinoline ester **12** (1.00 g, 4.34 mmol, 1 eq) in THF (20 mL) was added dropwise to DIBAL 1 M in THF (15 mL, 15 mmol, 3.2 eq) at -78 °C. Reaction was stirred at room temperature for 4 hours and quenched by dropwise addition of EtOAc (20 mL) at 0 °C, followed by slow addition of 1/2 saturated Rochelle salt aq (60 mL) at room temperature. Solution was stirred for 48 hours at room temperature, extracted with EtOAc (6 x 50 mL), washed with brine (1 x 50 mL), dried over MgSO₄, and concentrated. Purified by flash column chromatography (Methanol:DCM, 5:95) to give 570 mg (3.0 mmol) of **10a** in 69% yield as a white solid. ¹H NMR (400 MHz, DMSO-*d*₆) δ 9.71 (s, 1H), 7.99 – 7.91 (m, 1H), 7.85 – 7.78 (m, 1H), 7.53 – 7.43 (m, 2H), 5.80 (t, *J* = 4.7 Hz, 1H), 5.07 (d, *J* = 4.6 Hz, 2H), 3.34 (s, 1H), 2.55 (s, 3H). ¹³C NMR (101 MHz, DMSO-*d*₆) δ 152.76, 147.50, 142.34, 128.82, 127.18, 126.12, 126.07, 124.61, 123.54, 56.21, 21.32.



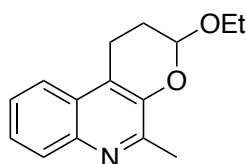
4-(ethoxymethyl)-2-methylquinolin-3-ol (10b): Quinoline **10a** (90 mg, 0.48 mmol, 1 eq) was dissolved in absolute EtOH (10 mL) and heated to reflux for 24 hours. Reaction was cooled to room temperature, concentrated, and purified by flash column chromatography (EtOAc:Hexane, 20:80) to give 100 mg (0.46 mmol) of **10b** in 96% yield as white solid. ^1H NMR (400 MHz, Chloroform-*d*) δ 9.25 (s, 1H), 7.96 (dd, $J = 8.3, 1.4$ Hz, 1H), 7.57 (dd, $J = 8.2, 1.5$ Hz, 1H), 7.54 – 7.39 (m, 2H), 5.23 (s, 2H), 3.77 (q, $J = 7.0$ Hz, 2H), 2.66 (s, 3H), 1.37 (t, $J = 7.0$ Hz, 3H). ^{13}C NMR (101 MHz, Chloroform-*d*) δ 152.85, 148.46, 142.03, 129.27, 126.09, 125.99, 125.53, 120.40, 118.01, 69.34, 67.82, 29.73, 20.43, 15.06



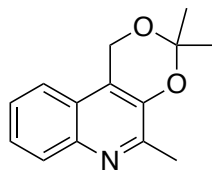
4-((N, N-dipropylamino)methyl)-2-methylquinolin-3-ol (10c): Dipropylamine (2.5 mL) was added to quinoline **10a** (105 mg, 0.55 mmol, 1 eq) dissolved in MeCN (12 mL). The reaction was heated to reflux for 3 days before being cooled and concentrated. The reaction was purified by flash column chromatography (Methanol:DCM, 2:98) to give 136 mg (0.50 mmol) of **10c** in 91% yield as a white solid. ^1H NMR (500 MHz, Chloroform-*d*) δ 8.07 – 8.03 (m, 1H), 7.74 (ddd, $J = 8.2, 1.5, 0.6$ Hz, 1H), 7.53 – 7.40 (m, 2H), 4.21 (s, 2H), 3.49 (s, 3H), 2.62 – 2.54 (m, 4H), 1.68 – 1.59 (m, 4H), 0.92 (t, $J = 7.4$ Hz, 6H). ^{13}C NMR (126 MHz, Chloroform-*d*) δ 152.54, 151.13, 141.86, 129.36, 127.02, 125.88, 125.47, 120.57, 118.27, 56.37, 53.21, 20.36, 19.68, 11.87.



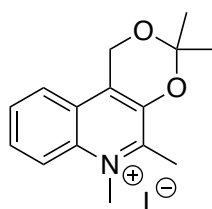
4-(methoxymethyl)-2-methylquinolin-3-ol (22): Quinoline diol **10a** (50 mg, 0.26 mmol, 1 eq) in H₂O:MeOH (1:1, 220 mL) was irradiated with a 300 W Hg arc lamp (Oriel Instruments) using a 320 nm long pass filter and UG-II filter for 6 hours in a 300 mL Quartz RBF. Methanol was removed under reduced pressure and the photolysis product was extracted with DCM (3 x 100 mL), dried over MgSO₄, and concentrated. Purified by flash column chromatography (Methanol:DCM, 1:99) to give 13 mg (0.062 mmol) of **22** in 24% yield as yellow oil. ¹H NMR (300 MHz, Chloroform-*d*) δ 7.97 (dd, *J* = 8.2, 1.5 Hz, 1H), 7.65 – 7.40 (m, 3H), 5.22 (s, 2H), 3.63 (s, 3H) 2.67 (s, 3H). ¹³C NMR (101 MHz, CDCl₃) δ 152.98, 148.57, 142.15, 129.38, 126.29, 126.19, 125.67, 120.51, 117.93, 71.42, 59.67, 20.50.



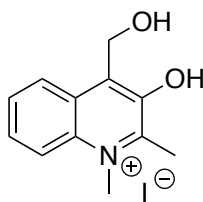
3-ethoxy-5-methyl-2,3-dihydro-1H-pyrano[2,3-c]quinoline (23): Quinoline diol **10a** (36 mg, 0.20 mmol, 1 eq) and ethyl vinyl ether (1.9 mL, 20 mmol, 100 eq) in H₂O:MeCN (1:1, 200 mL) was irradiated with a 300 W Hg arc lamp (Oriel Instruments) using a 320 nm long pass filter and UG-II filter for 7 hours in a 300 mL quartz RBF. Acetonitrile was removed under reduced pressure and product was extracted with EtOAc (3 x 100 mL), washed with water (1 x 50 mL) and brine (1 x 50 mL), dried over MgSO₄, and concentrated. Purified by flash column chromatography (EtOAc:Hexane, 20:80) to give 0.014 g (0.058 mmol) of **23** in 30% yield as yellow oil. ¹H NMR (500 MHz, Chloroform-*d*) δ 8.02 – 7.92 (m, 1H), 7.82 – 7.75 (m, 1H), 7.50 (dddd, *J* = 27.5, 8.2, 6.8, 1.4 Hz, 2H), 5.42 (t, *J* = 2.8 Hz, 1H), 3.87 (dq, *J* = 9.7, 7.1 Hz, 1H), 3.71 (dq, *J* = 9.7, 7.1 Hz, 1H), 3.19 – 3.01 (m, 2H), 2.64 (s, 3H), 2.25 (ddt, *J* = 13.2, 6.5, 3.3 Hz, 1H), 2.17 – 1.98 (m, 1H), 1.18 (dt, *J* = 15.6, 7.0 Hz, 3H).



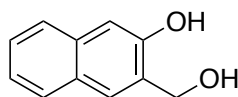
3,3,5-trimethyl-1H-[1,3]dioxino[4,5-c]quinoline (29): Quinoline diol **10a** (110 mg, 0.59 mmol, 1 eq) was combined with *p*-TsOH•H₂O (10 mg, 0.053 mmol, 0.11 eq), 2,2-dimethoxypropane (2.5 mL, 20 mmol, 30 eq), and anhydrous MgSO₄ (90 mg, 0.75 mmol, 1.3 eq) in 10 mL acetone and stirred at 50 °C for 5 days. Reaction was concentrated and the residue was dissolved in EtOAc (50 mL) and water (50 mL), extracted with EtOAc (2 x 30 mL) washed with 1 M NaOH aq. (2 x 25 mL), dried over MgSO₄, and concentrated. Purified by flash column chromatography (EtOAc:Hexane, 5:95) to give 110 mg (0.50 mmol) of **29** in 84% yield as a white solid. ¹H NMR (300 MHz, Chloroform-*d*) δ 7.97 (dt, *J* = 8.2, 1.0 Hz, 1H), 7.60 – 7.43 (m, 3H), 5.17 (s, 2H), 2.61 (s, 3H), 1.62 (s, 6H). ¹³C NMR (101 MHz, CDCl₃) δ 152.08, 143.61, 141.82, 129.21, 126.58, 126.23, 124.06, 120.55, 118.11, 100.03, 58.80, 24.57, 19.84.



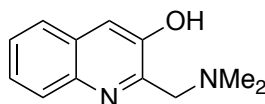
3,3,5,6-tetramethyl-1H-[1,3]dioxino[4,5-c]quinolin-6-ium (30): Solid quinoline ketal **29** (93 mg, 0.41 mmol, 1 eq) was dissolved in methyl iodide (5 mL) in a Schlenk flask. Flask was sealed and stirred at 50 °C for 3 days. Yellow powder was isolated and washed with hexane to give 120 mg (0.34 mmol) of **30** in 81% yield. ¹H NMR (300 MHz, DMSO-*d*₆) δ 8.53 (d, *J* = 8.9 Hz, 1H), 8.14 – 7.99 (m, 2H), 7.99 – 7.88 (m, 1H), 5.54 (s, 2H), 4.46 (s, 3H), 2.89 (s, 3H), 1.63 (s, 6H). ¹³C NMR (101 MHz, DMSO) δ 154.07, 143.65, 133.93, 131.75, 129.77, 129.27, 124.00, 123.82, 119.36, 102.29, 58.67, 24.17, 15.33.



3-hydroxy-4-(hydroxymethyl)-1,2-dimethylquinolin-1-ium (28): Quinolinium ketal **30** (52 mg, 0.14 mmols, 1 eq) was dissolved in water (1 mL) and acetic acid (4 mL) and refluxed for 6 hours. Reaction was concentrated and purified by HPLC (Water:Acetonitrile, 95:5) to give 29 mg (0.087 mmol) of **28** in 62% yield as a white solid. ^1H NMR (500 MHz, Methanol- d_4) δ 8.42 (dt, $J = 9.0, 0.8$ Hz, 1H), 8.22 (ddd, $J = 8.6, 1.5, 0.9$ Hz, 1H), 7.97 (ddd, $J = 9.0, 7.0, 1.3$ Hz, 1H), 7.90 – 7.83 (m, 1H), 5.55 (s, 1H), 4.53 (s, 2H), 3.02 (s, 3H).

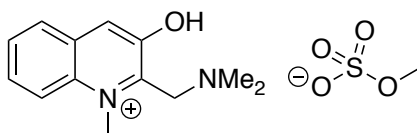


3-(hydroxymethyl)naphthalen-2-ol (4):⁴² 3-hydroxy-2-naphthoic acid (0.98 g, 5.3 mmol, 1 eq) dissolved in THF (10 mL) was added dropwise to a solution of sodium borohydride (0.240 g, 6.4 mmol, 1.2 eq) dissolved in THF (10 mL). The reaction was cooled to 0 °C and iodine (0.67 g, 2.7 mmol, 0.5 eq) dissolved in THF (10 mL) was added dropwise. The reaction was stirred at room temperature overnight, quenched with 3 M HCl (4 mL), diluted with water (20 mL) and extracted with ethyl ether (3 x 10 mL). The combined organic layers were extracted with 3 M NaOH (3 x 10 mL), neutralized with 3 M HCl, and the white precipitate was isolated with suction filtration and washed with water (15 mL) to yield 0.20 g (1.15 mmol) of **3** in 22% yield as a white solid. ^1H NMR (300 MHz, DMSO- d_6) δ 9.82 (s, 1H), 7.80 (s, 1H), 7.76 (d, $J = 8.0$ Hz, 1H), 7.64 (d, $J = 8.2$ Hz, 1H), 7.37 – 7.28 (m, 1H), 7.28 – 7.20 (m, 1H), 7.09 (s, 1H), 5.16 (t, $J = 5.6$ Hz, 1H), 4.62 (d, $J = 5.6$ Hz, 2H).

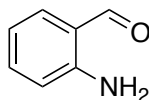


2-((dimethylamino)methyl)quinolin-3-ol (13c): dimethylmethylenediammonium iodide (410 mg, 2.2 mmol, 1.5 eq) and K_2CO_3 (100 mg, 0.71 mmol, 0.5 eq) were added to a solution of 3-hydroxyquinoline (**18**) (210 mg, 1.4 mmol, 1 eq) dissolved in DCM (10 mL).

The reaction was refluxed for 16 hours. After cooling to room temperature, the solid was isolated with vacuum filtration. The solid was dissolved in MeOH (50 mL) and the filtrate was isolated and concentrated to yield 280 mg (2.2 mmol) of **13c** in > 95% crude yield as a yellow solid, which was used without further purification. ^1H NMR (500 MHz, DMSO- d_6) δ 8.73 (s, 1H), 8.19 – 8.13 (m, 1H), 8.01 – 7.95 (m, 1H), 7.68 – 7.56 (m, 3H), 4.59 (s, 2H), 2.74 (s, 6H). ^{13}C NMR (126 MHz, DMSO- d_6) δ 150.50, 143.12, 142.55, 129.66, 127.79, 127.67, 126.29, 123.01, 115.26, 49.77, 43.00.

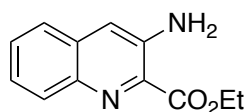


2-((dimethylamino)methyl)-3-hydroxy-1-methylquinolin-1-ium (31): Dimethyl sulfate (12.5 mL, 132 mmol, 100 eq) was added to a solution of quinoline **13c** (270 mg, 1.32 mmol, 1 eq) dissolved in acetonitrile (100 mL). Reaction was stirred overnight at room temperature, quenched with water (15 mL), concentrated, and resuspended in a minimal amount of acetonitrile and Et₂O was added slowly until a yellow precipitate formed. Solid was collected and washed with Et₂O (3 x 10 mL) to yield 72 mg (0.24 mmol) of **31** in 18% crude yield as a yellow solid, which was used without further purification. ^1H NMR (500 MHz, Methanol- d_4) δ 9.08 (s, 1H), 8.58 – 8.52 (m, 1H), 8.49 (d, J = 8.9 Hz, 1H), 8.15 – 8.05 (m, 2H), 5.06 (s, 2H), 4.74 (s, 3H), 3.67 (s, 3H, H₃COSO₃[−]), 3.04 (s, 6H).

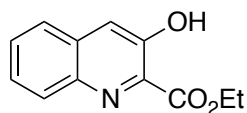


2-aminobenzaldehyde (15): Iron powder (5.54g, 99.2 mmol, 10 eq) and concentrated HCl (0.1 ml) were added to a solution of 2-nitrobenzaldehyde (**14**) (1.54 g, 10.2 mmol, 1 eq) in 37.5 ml ethanol/water (4:1). The reaction was heated to reflux for 2 h., cooled to room temperature, diluted with 100 ml EtOAc, dried over anhydrous MgSO₄, and filtered. The filtrate was concentrated and purified by column chromatography on silica (EtOAc:Hexane, 10:90) to give 740 mg (6.1 mmol) of 2-aminobenzaldehyde (**15**) in 61% yield as a yellow solid: ^1H NMR (500 MHz, Chloroform- d) δ 9.87 (s, 1H), 7.52 – 7.45 (m,

1H), 7.35 – 7.26 (m, 1H), 6.79 – 6.70 (m, 1H), 6.68 – 6.62 (m, 1H), 6.11 (s, 2H); ¹³C NMR (126 MHz, Chloroform-*d*) δ 194.24, 150.00, 135.87, 135.34, 118.99, 116.54, 116.15, 77.41, 77.16, 76.91.

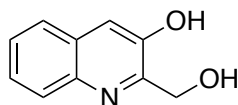


ethyl 3-aminoquinoline-2-carboxylate (16): Ethyl bromopyruvate (0.8 mL, 6.6 mmol, 1.05 eq) dissolved in EtOH (11 mL) was added dropwise to a solution of pyridine (0.5 mL, 6.4 mmol, 1.05 eq) dissolved in EtOH (16 mL). The reaction was heated to 60 °C for 1.5 hr and then cooled to room temperature before **15** in EtOH (2 mL) and pyridine (1.2 mL) were added. The reaction was heated to 90 °C for 5 hr and then cooled to room temperature before pyrrolidine (1.2 mL, 14.6 mmol, 2.4 eq) was added and the reaction was heated to 70 °C for 2 hr. Reaction was purified with flash column chromatography (EtOAc:Hexane, 30:70) to give 760 mg (3.5 mmol) of quinoline **16** in 58% yield as yellow solid. ¹H NMR (500 MHz, Chloroform-*d*) δ 8.08 – 8.02 (m, 1H), 7.60 – 7.54 (m, 1H), 7.49 – 7.41 (m, 2H), 7.26 (s, 1H), 4.55 (q, *J* = 7.1 Hz, 2H), 1.52 (t, *J* = 7.1 Hz, 3H). ¹³C NMR (101 MHz, Chloroform-*d*) δ 167.25, 142.86, 141.59, 134.35, 131.40, 130.61, 129.08, 126.16, 125.31, 118.79, 77.48, 77.16, 76.84, 62.24, 14.51.

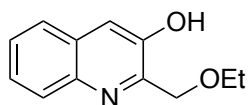


ethyl 3-hydroxyquinoline-2-carboxylate (17): Aminoquinoline **16** (480 mg, 2.2 mmol, 1 eq) was dissolved in 40% sulfuric acid solution (3 mL) at room temperature. To this was added ice (3 g) and the mixture was stirred for 5 min to form an orange paste and then cooled to 0 °C. NaNO₂ (190 mg, 2.4 mmol, 1.1 eq) in water (1 mL) was added dropwise to the reaction. the reaction was stirred for 15 min at 0 °C before being transferred to a refluxing solution of 50% sulfuric acid (20 mL). The reaction was refluxed for 10 min before being poured over ice water (100 mL). Reaction was neutralized with NaHCO₃, extracted with EtOAc (3 x 150 mL), washed with brine (50 mL), dried over MgSO₄, and concentrated. Reaction was purified with flash column chromatography (EtOAc:Hexane,

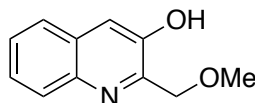
12:88) to give 153 mg (0.7 mmol) of quinoline **17** in 32% yield as yellow solid. ^1H NMR (500 MHz, Chloroform-*d*) δ 10.51 (s, 1H), 8.12 (dd, $J = 8.5, 1.7$ Hz, 1H), 7.72 – 7.66 (m, 2H), 7.58 – 7.51 (m, 2H), 4.61 (q, $J = 7.1$ Hz, 2H), 1.53 (t, $J = 7.1$ Hz, 4H). ^{13}C NMR (101 MHz, Chloroform-*d*) δ 169.73, 154.39, 143.04, 133.05, 132.50, 130.99, 129.85, 127.99, 126.73, 121.17, 77.79, 77.48, 77.16, 63.60, 14.73.



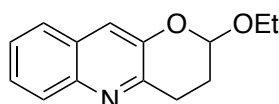
2-(hydroxymethyl)quinolin-3-ol (13a): A solution of quinoline ester **17** (230 mg, 1.1 mmol, 1 eq) in THF (20 mL) was added dropwise to DIBAL 1 M in THF (5.3 mL, 5.3 mmol, 5 eq) at 0 °C and stirred at room temperature for 4.5 hr. Reaction was quenched by the slow dropwise addition of saturated Rochelle salt aq (20 mL) at 0 °C. The solution was stirred overnight at room temperature, extracted with EtOAc (3 x 25 mL), washed with brine (1 x 25 mL), dried over MgSO_4 , and concentrated. Reaction was purified with flash column chromatography (Methanol:DCM, 5:95) to give 170 mg (0.96 mmol) of quinoline **13a** in 91% yield as white solid. ^1H NMR (500 MHz, DMSO-*d*₆) δ 10.41 (s, 1H), 7.89 (dt, $J = 8.6, 1.0$ Hz, 1H), 7.78 (dd, $J = 8.0, 1.6$ Hz, 1H), 7.53 – 7.41 (m, 3H), 5.03 (s, 1H), 4.72 (s, 2H). ^{13}C NMR (126 MHz, DMSO-*d*₆) δ 153.29, 149.12, 141.53, 129.17, 128.37, 126.58, 126.49, 126.25, 115.38, 61.08.



2-(ethoxymethyl)quinolin-3-ol (13b): Quinoline **13a** (55 mg, 0.27 mmol, 1 eq) was dissolved in absolute EtOH (10 mL) and heated to reflux for 3 days. Reaction was cooled to room temperature, concentrated, and purified by column chromatography on silica (Methanol:DCM, 1:99) to give 31 mg (0.15 mmol) of quinoline **13b** in 55% yield as a white solid. ^1H NMR (500 MHz, Methanol-*d*₄) δ 8.56 (s, 1H), 8.13 – 8.07 (m, 1H), 7.96 – 7.90 (m, 1H), 7.60 – 7.53 (m, 2H), 5.04 (s, 2H), 3.65 (q, $J = 7.1$ Hz, 2H), 2.70 (s, 1H), 1.22 (t, $J = 7.0$ Hz, 3H).



2-(methoxymethyl)quinolin-3-ol (26): Quinoline diol **13a** (59 mg, 0.34 mmol, 1 eq) in H₂O:MeOH (1:1, 200 mL) was irradiated with a 300 W Hg arc lamp (Oriel Instruments) using a 320 nm long pass filter and UG-II filter for 6 hours in a 300 mL Quartz RBF. Methanol was removed under reduced pressure and the photolysis product was extracted with EtOAc (3 x 25 mL), dried over MgSO₄, and concentrated. Purified by flash column chromatography (EtOAc:Hexane, 20:80) to give 15 mg (0.079 mmol) of **26** in 23% yield as white powder. ¹H NMR (500 MHz, Chloroform-*d*) δ 8.46 (s, 1H), 8.04 (dd, *J* = 8.2, 1.2 Hz, 1H), 7.77 (dd, *J* = 8.2, 1.5 Hz, 1H), 7.64 – 7.57 (m, 2H), 7.54 (ddd, *J* = 8.1, 6.8, 1.3 Hz, 1H), 5.11 (s, 2H), 3.66 (s, 3H). ¹³C NMR (126 MHz, Chloroform-*d*) δ 150.32, 147.49, 142.60, 129.45, 128.67, 127.01, 126.95, 126.50, 118.49, 76.84, 59.32.



2-ethoxy-3,4-dihydro-2H-pyrano[3,2-*b*]quinoline (27): Quinoline **13a** (48 mg, 0.23 mmol, 1 eq) and ethyl vinyl ether (1 ml, 10 mmol, 50 eq) in H₂O:MeCN (1:1, 200 mL) was irradiated with a 300 W Hg arc lamp (Oriel Instruments) using a 320 nm long pass filter and UG-II filter for 5 hours in a 300 mL quartz RBF. Acetonitrile was removed under reduced pressure and product was extracted with EtOAc (3 x 25 mL) dried over MgSO₄ and concentrated. Purified by flash column chromatography (EtOAc:Hexane, 15:85 to 20:80) to give 15 mg (0.066 mmol) of **27** in 28% yield as clear oil. ¹H NMR (500 MHz, Chloroform-*d*) δ 7.96 (dq, *J* = 8.5, 0.9 Hz, 1H), 7.67 (ddd, *J* = 8.2, 1.5, 0.7 Hz, 1H), 7.53 (ddd, *J* = 8.4, 6.9, 1.5 Hz, 1H), 7.48 (s, 1H), 7.42 (ddd, *J* = 8.1, 6.8, 1.2 Hz, 1H), 5.35 (t, *J* = 2.7 Hz, 1H), 3.89 (dq, *J* = 9.6, 7.1 Hz, 1H), 3.68 (dq, *J* = 9.6, 7.1 Hz, 1H), 3.38 (ddd, *J* = 17.2, 12.5, 6.3 Hz, 1H), 3.07 (ddd, *J* = 17.2, 6.0, 3.2 Hz, 1H), 2.28 (ddt, *J* = 13.6, 6.2, 3.0 Hz, 1H), 2.18 (dddd, *J* = 13.5, 12.4, 6.0, 2.6 Hz, 1H), 1.18 (t, *J* = 7.1 Hz, 3H). ¹³C NMR (126 MHz, Chloroform-*d*) δ 148.87, 146.95, 143.52, 128.88, 128.40, 127.09, 126.50, 126.17, 119.24, 97.12, 64.05, 26.84, 25.09, 15.19.

4.6.3 Quantum Yield of Fluorescence

Sample preparation and data collection. All UV-vis and fluorescence experiments were performed using EMD Millipore (OmniSolve®) grade solvents in 1 cm pathlength quartz cuvettes open to air. All UV-Vis absorbance measurements were on a Cary 60 spectrometer. Emission spectra were recorded on a Jobi Yvon Spec Fluorolog-3-11. Samples were excited with a Xe arc lamp with a monochromator providing wavelength selection. Right angle emission was filtered using a monochromator and detected with a Hamamatsu R928P photomultiplier tube with photon counting. All emission and excitation spectra were subtracted from blank spectra recorded at the same wavelength on the same day.

Quantum yield of fluorescence measurements were determined by comparison to the established standard quinine sulfate in 0.5 M sulfuric acid.^{43,44} Five samples of each compound to be tested, in 0.1 M phosphate buffer, and the standard were prepared with absorbance at 325 nm between 0.015 and 0.1 to minimize the effect of self-quenching and nonlinear effects. Emission spectra, with excitation at 325 nm, were collected for all samples and the maximum fluorescence intensity was recorded.

Analysis. The quantum yield of fluorescence Φ for the compound (x) is related to the known quantum yield of fluoresce for a standard (st) by the formula:

$$\phi_x = \phi_{st} \left(\frac{Grad_x}{Grad_{st}} \right) \left(\frac{\eta_x^2}{\eta_{st}^2} \right) \quad (4.1)$$

where *Grad* is the gradient generated from plotting the fluorescence intensity against absorbance and η refers to the refractive index of the respective solvent. The refractive index of 0.1 M phosphate buffer and 0.5 M sulfuric acid were assumed to be the same.⁴⁵

4.6.4 Transient Absorption Spectroscopy

Samples were dissolved in water or trifluoroethanol (TFE) and the concentration was diluted to an $A_{350} < 0.3$ and placed in a four-sided quartz cuvette with a small stir bar and sealed with a Teflon cap. For quenching experiments stock solution of NaN_3 (1 M and 10 mM) and MeOH (1 M), were serial diluted to the desired concentration. For EVE 3 μL was added to 3 mL solution of quinoline dissolved water of TFE.

Single wavelength transient absorption measurements were performed at the Beckman Institute Laser Resource Center (California Institute of Technology). Samples were excited using a 355 nm laser pulse, 8 ns, at 10 Hz provided by the third harmonic from a Q-switched Nd:YAG laser (Spectra-Physics Quanta-Ray Pro-Series). Probe light provided by a 75-W Xe arc lamp (PTI Model A 1010) was passed through the sample collinearly and was operated in continuous wave or pulsed modes depending timescale of observation. Short-pass and long-pass filters were used to remove scattered excitation light and a neutral density filter was used to regulate light intensity before the probe wavelength was selected by a double monochromator (Instruments SA DH-10) with a 1 mm slit. Light was detected with a photomultiplier tube (PMT, Hamamatsu R928) and amplified using a 200 MHz wideband voltage amplifier (FEMTO, DHPVA-200). All instruments and electronics were controlled by software written in LabView (National Instruments). Data were recorded in units of ΔOD . ($\Delta OD = -\log_{10}(I/I_0)$, where I is the time resolved probe light intensity with laser excitation, and I_0 is the intensity without excitation.) At each wavelength of observation around 100 shots were averaged, the data were log-compressed and then fit in MATLAB (Mathworks, Inc.).⁴⁶

4.6.5 pH Dependent Relative Quantum Yield of Reaction

Sample Preparation for Photolysis: Stock solutions of citrate-phosphate buffer, pH 2.5, 3.0, 3.5, 4.0, 4.5, 5.0, and 6.0, were prepared as described previously.⁴³ Buffer, 0.5 mL, was added to a solution of quinoline **10a** or **13a** in absolute ethanol (0.5 mL, 0.001 M) in a custom 10 mL quartz test tube. The mixture was shaken thoroughly and 0.35 mL were transferred to an amber HPLC vial and capped as a dark control. The remaining 0.65 mL was sealed for photolysis experiments.

Photolysis: The prepared samples were irradiated using a 150 W Hg arc lamp (Oriel Instruments) with a UG-II filter on a custom-made merry-go-round apparatus rotating at 20 rpm mounted on an optical rail to minimize variation in light exposure. Upon completion the test tubes were uncapped and the solution was transferred to an amber HPLC vial and capped for analysis. Paired samples (dark and irradiated) were randomized before running on an Agilent 1100 LCMS equipped with a diode array detector.

Data collection and analysis: Quantitative analysis for the photolysis of **10a** and **13a** was performed by on a LCMS using a 5% to 95% acetonitrile in water gradient and integrating the peak corresponding to the ether product **10b** or **13b** in the 254 nm absorbance trace. Dark control samples were subtracted to control for thermal QM reaction. Samples were normalized to a concurrently run pH 6 sample. All experiments were run in triplicate and plotted using prism (GraphPad).

4.6.6 Quantum Yield of Reaction

General: All chemicals and solvents were purchased at the highest grade available (Spectral grade). Samples were prepared in custom 10 mL quartz test tubes, sealed with a Teflon cap. Samples were photolyzed using a 300 W Hg arc lamp (Oriel Instruments) with a 320 nm long pass filter and UG-II filter on a custom-made merry-go-round apparatus rotating at 20 rpm. All procedures were carried out in darkness with a dim red filtered safety light. Data were collected on an Agilent 1260 HPLC equipped with a diode array detector. Absorbance spectra were recorded on a Cary 60 using 10 mm quartz cuvettes.

Synthesis of potassium ferrioxalate: In the dark 1.5 M potassium oxalate monohydrate (300 mL) was mixed with 1.5 M ferric chloride hexahydrate (100 mL) and stirred in the dark for 30 min at room temperature. The solid was collected, recrystallized three times from warm water, and dried over warm air overnight to produce lime green potassium ferrioxalate trihydrate crystals, which were allocated into 60 mg amounts and stored in the dark at room temperature.

Ferrioxalate actimometry: Immediately before use and in the dark, potassium ferrioxalate (60 mg) was dissolved in 0.05 M H₂SO₄ (20 mL) and shaken to ensure a homogeneous solution. In addition, a solution of 1,10-phenanthroline (40 mg) in 1 M sodium acetate buffer (20 mL; made by adding 82 g of NaOAc•3H₂O and 10 mL H₂SO₄ to 1 L of H₂O) was prepared.

Using a 1 mL gas-tight syringe fitted with a four inch needle, 0.5 mL of potassium ferrioxalate solution was transferred to a quartz test tube, capped and irradiated. Upon completion, 0.1 mL was transferred to a vial containing 0.8 mL of the 1,10-phenanthroline solution and 1.1 mL of water measured using a volumetric pipet. The solution was developed in the dark for 45 min before being transferred to a cuvette and UV-Vis

absorbance spectrum taken. The average absorbance of three samples irradiated for five minutes was used to determine a photon flux per minute for the lamp.

Sample Preparation for Photolysis: A solution of **10a** (0.95 mL) in 0.01 M phosphate buffer/acetonitrile (1:1) with an absorbance between 0.05 and 0.1 at 330 nm was transferred to an amber HPLC vial and 0.05 mL of ethyl vinyl ether. The mixture was shaken thoroughly and 0.5 mL was transferred to a quartz test tube, sealed, and irradiated. The remaining 0.5 mL was capped for HPLC analysis and stored in the dark.

Photolysis: The prepared samples were irradiated using a Hg arc lamp and a merry-go-round apparatus mounted on an optical rail to minimize variation in light exposure. Upon completion the test tubes were uncapped and the solution was transferred to an amber HPLC vial and capped for analysis. Paired samples (dark and irradiated) were randomized before running on HPLC.

Data collection: In general, quantitative analysis for the photolysis of **10a** was performed by HPLC using an isocratic elution of 5% acetonitrile in water and integrating the peak corresponding to **23** in the 254 nm absorbance trace. Quantitative analysis for the photolysis of potassium ferrioxalate was performed by UV/Vis spectroscopy, and measuring the absorbance at 510 nm corresponding to the Fe^{2+} -phenanthroline complex.

Calculations of the quantum yield: The quantum yield for the disappearance of **10a** (Φ_s) due to photolysis is given by equation 4.2,

$$\phi_s = \frac{n_s}{p_s} \quad (4.2)$$

where n_s is the number of moles of the sample consumed, and p_s is the number of moles of photons absorbed by the sample. The amount of the sample consumed can be represented by the difference in the number of mole pre- and post-photolysis (Equation 4.3), which can be calculated from integrations of HPLC traces (I_s) with the use of a calibration function (f), and the volume of the photolysis sample (V).

$$n_s = f(I_s^{\text{dark}} - I_s^{h\nu})V \quad (4.3)$$

The moles of photons absorbed p_s is measured using the ferrioxalate actinometer (Equation 4.4) where C is an absorbance correction factor typically measured as the transmittance of the sample divided by the transmittance of the potassium ferrioxalate (Fe^{3+}) solution before irradiation at the wave length of irradiation. However, given that the

sample was irradiated over a range of wavelengths the transmittance between 330 and 365 nm was integrated for both the potassium ferrioxalate (Fe^{3+}) solution and the sample (Equation 4.5) The range of 330 to 365 nm was determined by region the UG II and 320 nm long pass filters allowed at least 50% transmittance.

$$p_{\text{Sample}} = C \cdot \frac{n_{\text{Fe}^{2+}}}{\phi_{\text{Fe}^{2+}}} \quad (4.4)$$

$$C = \frac{\int_{330}^{365} T_s \cdot T_{S \text{ at } 330}}{\int_{330}^{365} T_{\text{Fe}^{3+}} \cdot T_{\text{Fe}^{2+} \text{ at } 330}} \quad (4.5)$$

$\phi_{\text{Fe}^{2+}}$ is the known quantum yield for Fe^{2+} generation (1.23 at 350 nm) and $n_{\text{Fe}^{2+}}$ the moles of Fe^{2+} produced. The latter can be determined by the absorbance of the Fe^{2+} -phenanthroline complex at 510 nm ($\text{Abs}_{\text{Fe}^{2+}}$), the known extinction coefficient ε of the complex ($11100 \text{ M}^{-1} \text{ cm}^{-1}$) and the photolysis volume as given in equation 4.6:

$$n_{\text{Fe}^{2+}} = \frac{\text{Abs}_{\text{Fe}^{2+}} \cdot V_1 \cdot V_3}{\varepsilon \cdot V_2} \quad (4.6)$$

where V_1 is the total irradiation volume, V_2 is the volume developed, and V_3 is the volume of developed solution.

Chapter 5

ATTEMPTS AT IMPROVING THE EFFICIENCY OF QUINONE TRIMETHYL LOCK PROTECTIVE GROUP USING A RADICAL DECARBOXYLATION STRATEGY

Abstract

The quinone trimethyl lock system has proved to be an efficient photoremovable protecting group for amine and alcohols. Efforts to extend the quinone chromophore to longer wavelengths and to improve the efficiency of the photochemical reduction have proved challenging. A radical decarboxylation strategy was tested to improve quantum efficiency and increase reactivity at longer wavelengths by trapping the charge transfer state. A glycine was installed on both a benzoquinone and a phenoxazine substrate and the photochemistry of both was evaluated. Both derivatives proved stable to irradiation.

5.1 Introduction

Our lab recently published a series of visible light triggered photoremovable protecting groups for alcohols and amines based on a quinone trimethyl lock (TML)^{1,2} (Figure 5.1) and more recently based on a quinone cis-alkenyl lock.³ The TML is a highly versatile decaging system; the unmasking of a phenol results in rapid cyclization of either an ester or amide and the releases of an alcohol or amine respectively in seconds to minutes. The increased rate of lactonization is due to the three interlocking methyl groups prepositioning the substrate into a conformer similar to the transition state and the relief of strain achieved upon cyclization.^{4,5} Previously, unmasking of a phenol for TML chemistry has been achieved using chemical or enzymatic means to remove a protecting group or reduction of a quinone to a hydroquinone. This was the first time TML release was achieved by photoreducing a quinone with visible light.

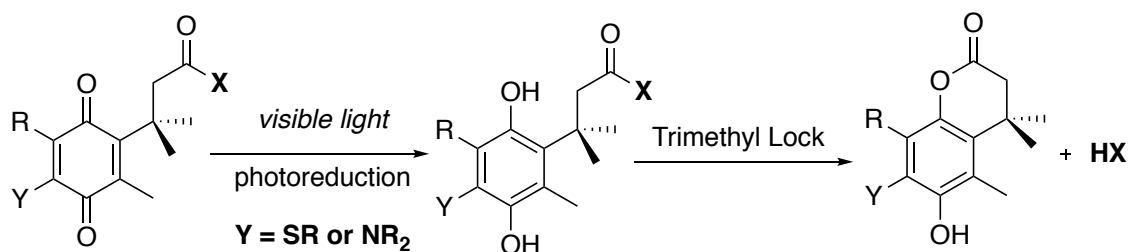


Figure 5.1: Visible light triggered photoremovable quinone trimethyl lock (TML) protecting group.

Amine substituted quinones and naphthoquinones are known to be photoreactive: on exposure to visible light, 2,5-diamino-1,4-benzoquinone (**1**), undergoes a formal hydrogen shift from the amine substituent to the quinone core, oxidizing the amine and reducing the quinone. The final product in most cases is a cyclized benzoxazoline **2** (Figure 5.2a).^{6–17} A correctly positioned alkyl substituent is required: primary amine substituted quinones are photostable because hydrogen bonding orients the alkyl substituent away from the quinone carbonyl¹³ and aziridino and azetidino amine substituents are inert to photolysis because of a too long O---H distance (Figure 5.2b).¹²

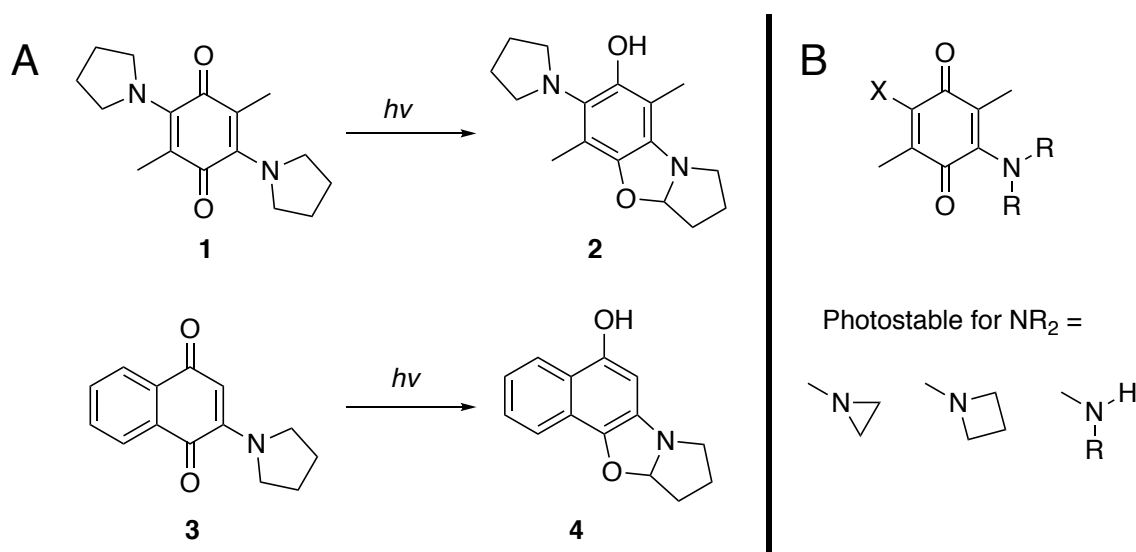
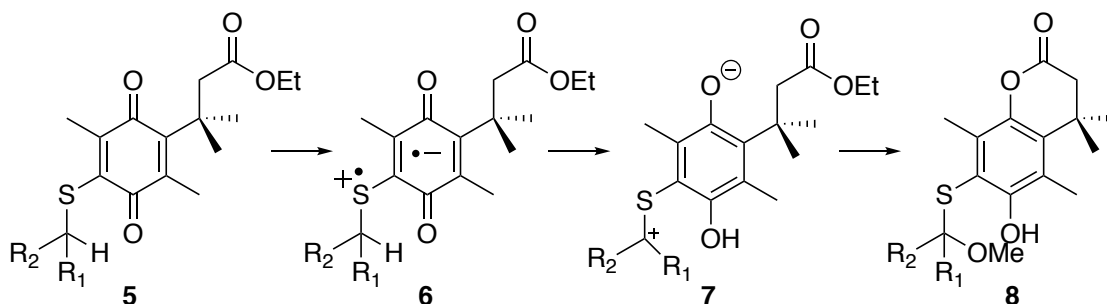


Figure 5.2: Aminoquinone and aminonaphthoquinone photochemistry. a) Photoreduction of amine substituted quinones and naphthoquinones primarily result in cyclized benzoxazoline products. b) photostability of aziridino and azetidino and primary amines.

Addition of an electron donating amine to the quinone results in a broad visible light charge transfer band. Excitation of this long wavelength band results in considerable charge transfer from the amine to the quinone carbonyl oxygen. It is understood that it is

this polar state that undergoes a proton transfer in the primary photochemical step of the mechanism. With increasing solvent polarity, the quantum yield of reaction decreases most likely due to influences of the dielectric constant and hydrogen bonding on the charge transfer excited state.^{9,17} Detailed mechanistic studies on dialkylamino-1,4-naphthoquinones showed no radical species after photolysis at 77 K but did identify two intermediates that when warmed formed the photolysis product.^{8,9} Work in our lab by Regan et al. showed that for sulfide substituted TML quinone **5** reaction occurred from both the singlet and triplet charge transfer state supporting a sequential ionic mechanism (Scheme 5.1).²

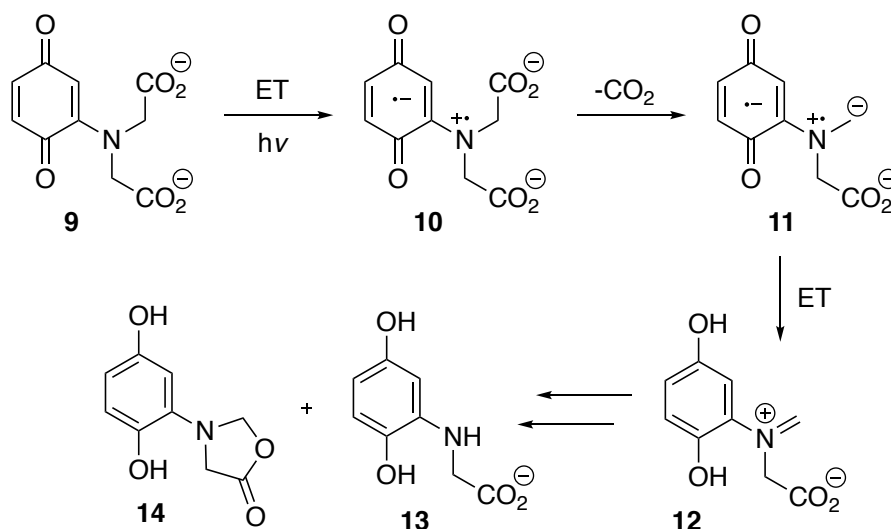


Scheme 5.1: Mechanism for the photoreduction of alkyl sulfide substituted quinones.

Alternatively, direct conjugation of the amine and quinone allows for hydrogen atom transfer (HAT) to an n,π^* carbonyl in a standard radical mechanism through a conventional Norrish II reaction. However, Norrish type II reactions experience opposite solvation effects; increasing solvent polarity increases the quantum yield of the reaction.¹⁸ Additionally, when radical clocks 5-hexenyl, cyclopropylmethyl and 2-phenylcyclopropylmethyl were included in sulfide substituted TML quinone derivatives no discernable radical products were detected.² Compared to the HAT mechanism, the proposed mechanism of sequential electron transfer followed by proton transfer should be energetically favorable at longer wavelengths.

Efforts in our lab to extend the wavelength of reaction for quinone derivatives have suffered from lower quantum yields of reaction and in some cases, did not react at all. Regan et al. showed that for sulfide substituted quinones the majority of molecules excited to the charge transfer state, between 92-98%, relaxed nonradiatively back to the ground state without undergoing proton transfer.² It was hypothesized that if the quinone could be trapped in the charge transfer state with radical decarboxylation, then the quantum yield of the reaction could be improved.

In the presence of either an inter- or intramolecular electron donor, carboxylic acids and their respective anions can be photochemically decarboxylated resulting in a carbon radical.¹⁹ Photochemical radical decarboxylation has been used in organic synthesis,^{20–22} and for protecting groups.^{23,24} It was envisioned that a quinone with a correctly positioned glycine carboxylic acid derivative could be photoreduced (Scheme 5.2). Upon excitation electron transfer from the amine to the quinone would result in charge transfer state **10** which could undergo radical decarboxylation trapping the charge transfer state **11**. The radical decarboxylation of glycine derivatives is fast, on the order of 100 ns²⁵ and could provide a generalizable alternative to proton abstraction for quinone photoreduction. Subsequent electron transfer and proton transfer from bulk solvent would result in imine hydroquinone **12** which could react with water to form hydroquinone **13** or cyclize to form hydroquinone **14**. This would be the first example of an intramolecular radical decarboxylation quinone photocage. Two quinones were synthesized and their photochemistry explored in this chapter.



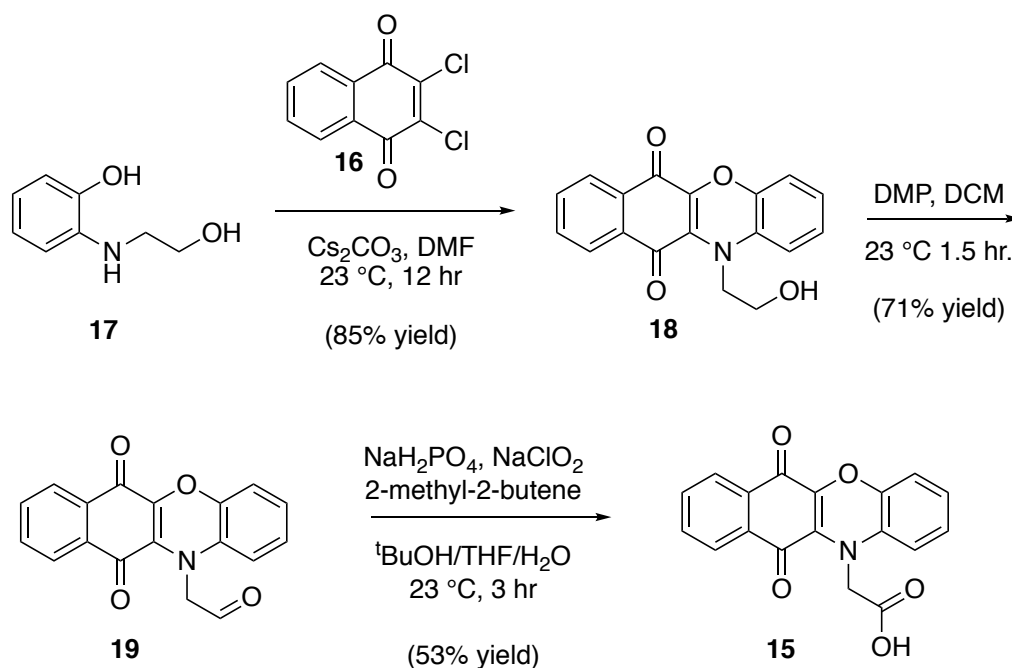
Scheme 5.2: Proposed quinone radical decarboxylation photoreduction.

5.2 Results

5.2.1 Synthesis of Phenoxazine 15

Since the photoreduction of the quinone and the trimethyl lock reaction are distinct events, quinone derivatives lacking the TML moiety can be screened for photoreactivity greatly simplifying the synthesis. Initial designs for a radical decarboxylation assisted quinone photoreduction focused on the red shifted phenoxazine quinone derivative **15**

(Scheme 5.3).²⁶ Dichloro-naphthoquinone **16** was reacted with the phenol **17** to yield the dark blue solid phenoxazine quinone **18**.²⁶ Attempts at direct oxidation of alcohol **18** to the carboxylic acid **15** proved impossible as the quinone was not stable under all standard oxidation conditions tested. Instead a two-step oxidation strategy was employed. Reaction of phenoxazine quinone **18** with Dess-Martin periodinane (DMP) afforded aldehyde **19** in good yield, and subsequent oxidation with buffered NaClO₂ in the presence of radical scavenger 2-methyl-2-butene resulted in the desired carboxylic acid **15**.²⁷



Scheme 5.3: Synthesis of phenoxazine **15**

5.2.2 Phenoxazine Photochemistry

UV-vis of phenoxazine **15** showed a broad charge transfer band centered around 665 nm in aqueous buffer. **15** was stable to irradiation at > 600 nm in pH 7 buffered water (Figure 5.3a,b). The reaction was monitored by UV-Vis and LCMS, and no appearance of photoproduct or disappearance of starting material was observed. Freeze pump thawing to remove oxygen had no effect nor did changing solvent to acetonitrile or acetonitrile/buffer 50:50. Irradiation at shorter wavelengths (> 335 nm) did not result in any appreciable photochemistry. Addition of EDTA, a sacrificial reductant, had no effect. It should be noted that samples were only irradiated for a total of 30 minutes. At the time, all quinone derivatives tested in our lab showed significant photo bleaching in a couple of minutes.

However, since then members of the lab have characterized quinones that exhibit slower photobleaching.²⁸ Longer irradiation periods may reveal phenoxazine **15** does undergo radical decarboxylation and photoreduction of the quinone but this is unlikely. Concurrent work by David Walton in the lab showed that other cyclic quinones did not undergo the desired photochemistry²⁸ (Figure 5.3c) and it was proposed that a twisted charged transfer state^{29,30} was required for the desired photochemistry to occur. Phenoxazine **15** is cyclic and cannot twist in the excited state, and therefore the photostability of **15** does not conclusively eliminate radical decarboxylation as a strategy for improving photoreduction efficiency because under the proposed mechanism radical decarboxylation occurs from the charger transfer state (Scheme 5.2).

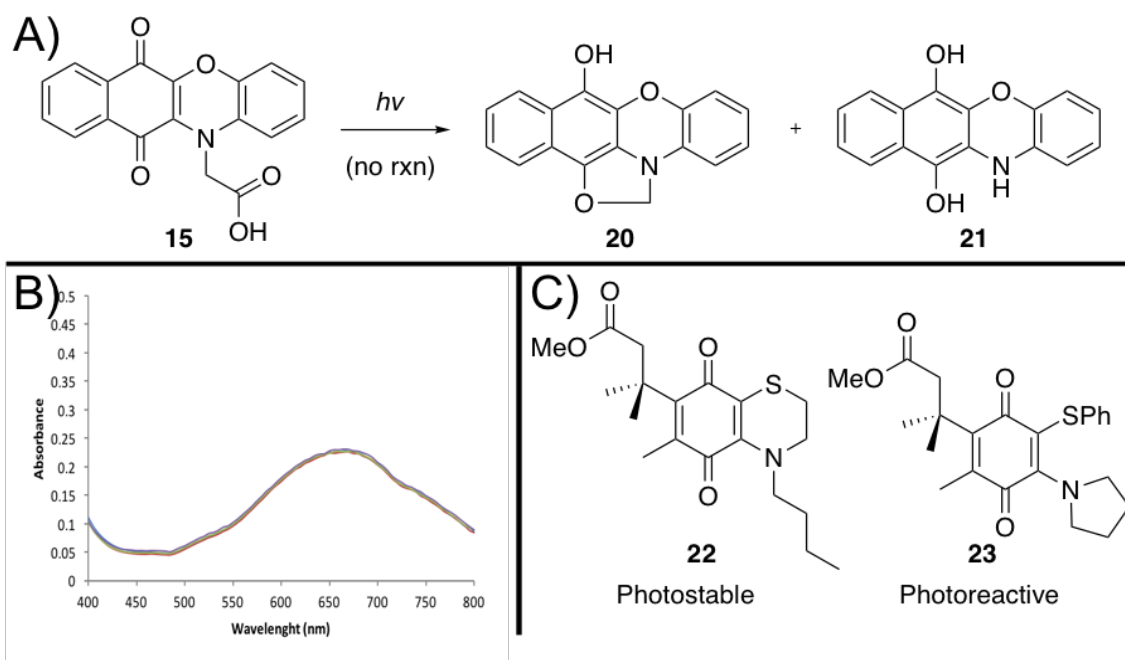
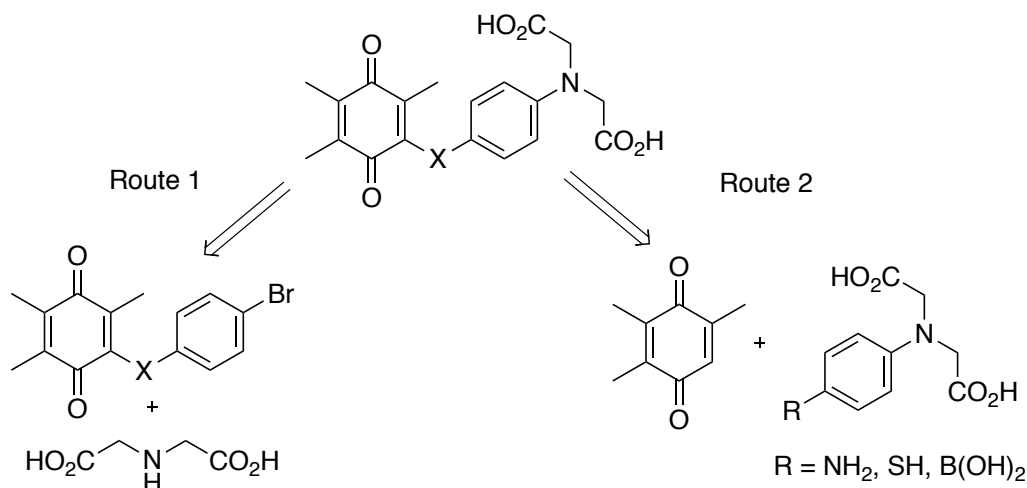


Figure 5.3: Photochemistry of phenoxazine **15**. A) Predicted photochemical products. B) Change in UV-Vis over 30 minutes when phenoxazine **15** was irradiated at > 600 nm in aqueous phosphate buffer. C) Cyclic thiol quinone TML **22** is photostable compared with equivalent acyclic Quinone TML **23**.

5.2.3 Synthesis of an acyclic quinone

Focus then shifted towards the synthesis of a non-cyclic quinone that could adopt a twisted confirmation in the excited state and contained a glycine substituent for radical decarboxylation (Scheme 5.4). For proof of concept it was determined that far red absorption was not necessary and instead efforts focused on a shorter wavelength absorbing benzoquinone derivative.



Scheme 5.4: Retrosynthesis for a glycine substituted benzoquinone.

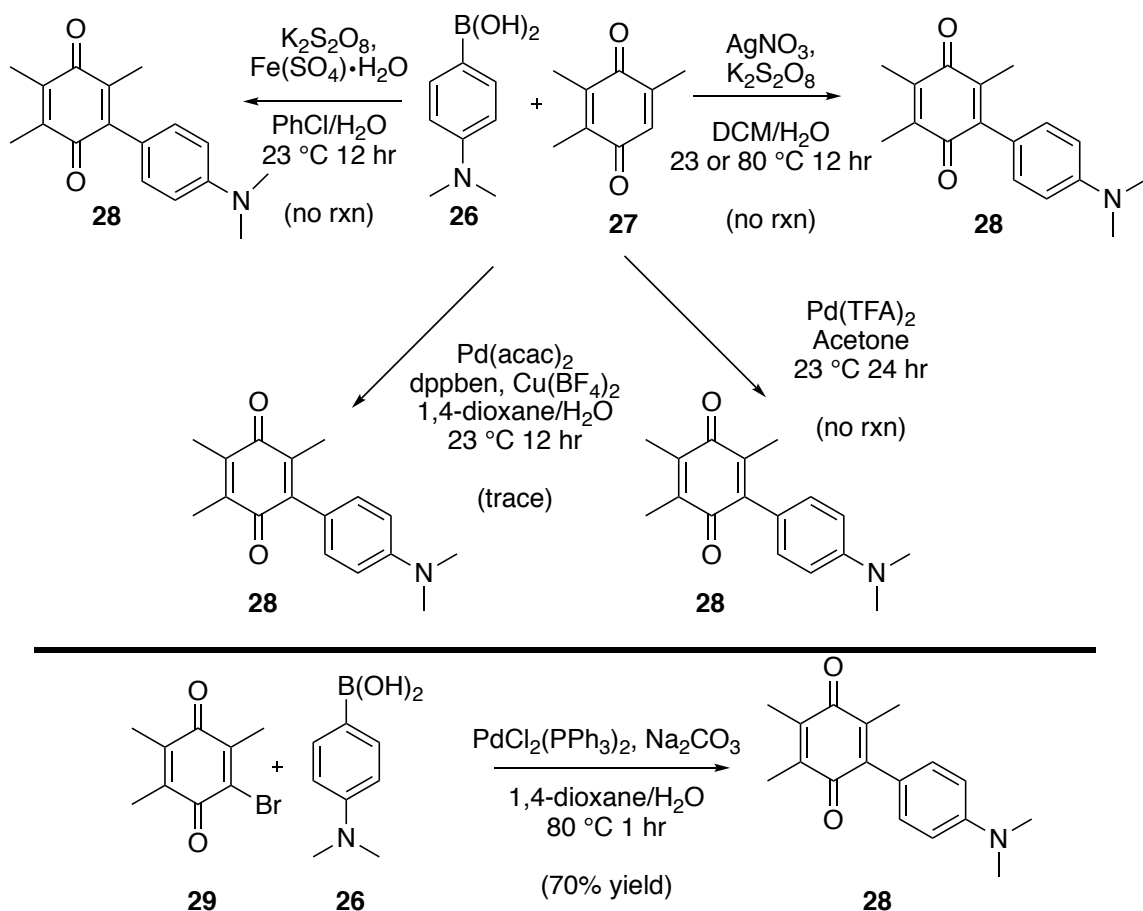
Initial synthetic efforts focused on using Buchwald-Hartwig cross-coupling to attach the desired amine, iminodiacetic acid (IDA) to quinone **24**, which had previously been synthesized in our lab (Scheme 5.4, Route 1). This proved challenging. Despite screening common Buchwald-Hartwig reaction conditions, decomposition of the quinone starting material was observed every time (Table 5.1).^{31,32} Subsequent screening using morpholine as the amine showed that the problem was stability of the quinone, and not the atypical amine used in the cross coupling.

Table 5.1: Buchwald-Hartwig reaction conditions screened in an attempt to synthesize quinone **25**.

Entry	Amine	Base	Solvent	Temp	Time (hr)	Outcome
1	R=CH ₂ CO ₂ H	Cs ₂ CO ₃	THF	80	20	Decomposed
2	R=CH ₂ CO ₂ H	Cs ₂ CO ₃	Toluene	80	20	Decomposed
3	R=CH ₂ CO ₂ H	Cs ₂ CO ₃	^t BuOH	90	20	Decomposed
4	R=CH ₂ CO ₂ H	LiHMDS	THF	90	6	Decomposed
5	R=CH ₂ CH ₂ OH	LiHMDS	THF	90	20	Decomposed
6	Morpholine	Cs ₂ CO ₃	^t BuOH	90	40	Decomposed
7	Morpholine	LiHMDS	THF	90	20	Decomposed

Given the issues of appending the glycine moiety to the quinone the decision was made to assemble the glycine moiety and then attach it to the quinone core via a linker

(Scheme 5.4, Route 2). In the presence of strong base aryl amines react with alkyl halides to form tertiary alkylamines. Thiol aryl amines were eliminated from consideration because of their propensity to oxidize and form disulfides and diaminobenzenes were also eliminated because of the need for protecting groups. Instead we envisioned synthesis of a boronic acid, containing the requisite glycine functionality, which could then be coupled to the quinone via C-C bond formation. Remember, in the proposed photochemistry mechanism electron donation occurs from the glycine nitrogen; a sulfur or nitrogen linker is not required.

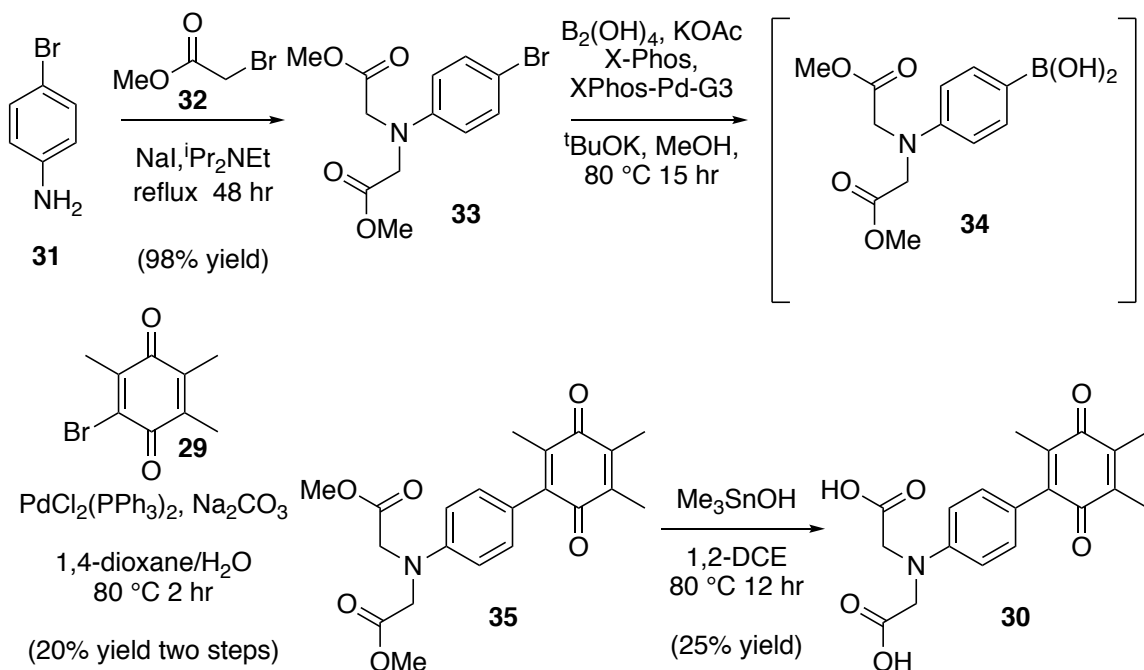


Scheme 5.5: Quinone cross coupling reactions conditions.

Direct coupling of boronic acids to unfunctionalized quinones and naphthoquinones is known in the literature.^{33–36} However, all literature examples had limited substrate scopes and none included examples of amines despite examples with other electron donating groups. Reaction conditions were screened using the commercially available boronic acid **26** as a model substrate (Scheme 5.5). No direct C-H coupling

conditions were found to work with boronic acid **26** and instead Suzuki-Miyaura conditions were identified to couple bromo quinone **29** to boronic acid **26** (Scheme 5.5). With coupling conditions in hand attention turned to synthesizing the desired photoreductive quinone **30**.

To synthesize quinone **30**, 4-Bromoaniline (**31**) was reacted with bromoacetate **32** in the presence of base to furnish dialkyl **33** in good yield.^{37,38} (Scheme 5.6) Halogen-containing **33** was not suited to direct coupling because under Heck coupling conditions quinones complex with palladium and can reoxidize Pd(0) species.³⁹ Conversion of the halide to the boronic acid⁴⁰ proceeded smoothly with only a small amount of hydration side product. However, boronic acid **34** was unstable to purification and the isolated crude mixture was reacted directly with quinone **29** in a Suzuki coupling⁴¹ to form quinone **35**. Finally, all that remained was hydrolysis of the diester **35** to furnish the desired quinone **30**. Quinone **35** was sensitive to both base catalyzed hydrolysis and acid catalyzed hydrolysis: treatment with either LiOH or formic resulted in degradation of starting material. Instead the very mild and selective methyl ester hydrolysis reagent trimethyltin hydroxide was employed.⁴² This resulted in the smooth generation of the diacid **30**, the low yield was a result of problems with the work up.



Scheme 5.6: Synthesis of acyclic quinone **30**.

5.2.4 Quinone Photochemistry

UV-Vis spectra of acid **30** showed a broad charge transfer band centered around 475 nm in methanol (Figure 5.4); there was a marked redshift of 35 nm in water. Acid **30** was stable to irradiation at 470 nm in methanol for 24 hours. The reaction was monitored by UV-Vis, LCMS and NMR and no appearance of photoproduct or disappearance of starting material was observed. Freeze pump thawing to remove oxygen had no effect on the photostability of **30**. Acid **30** also proved photostable in water and phosphate buffer (0.01 M, pH 7.6) when irradiated at 565 nm or 470 nm. Finally, addition of the external electron donor EDTA had no effect on quinone **30**. Given the photostability of quinone **30** under all conditions tested, it was unclear if glycine based radical decarboxylation could trap the charge transfer state or if quinone **30** could be reduced at all.

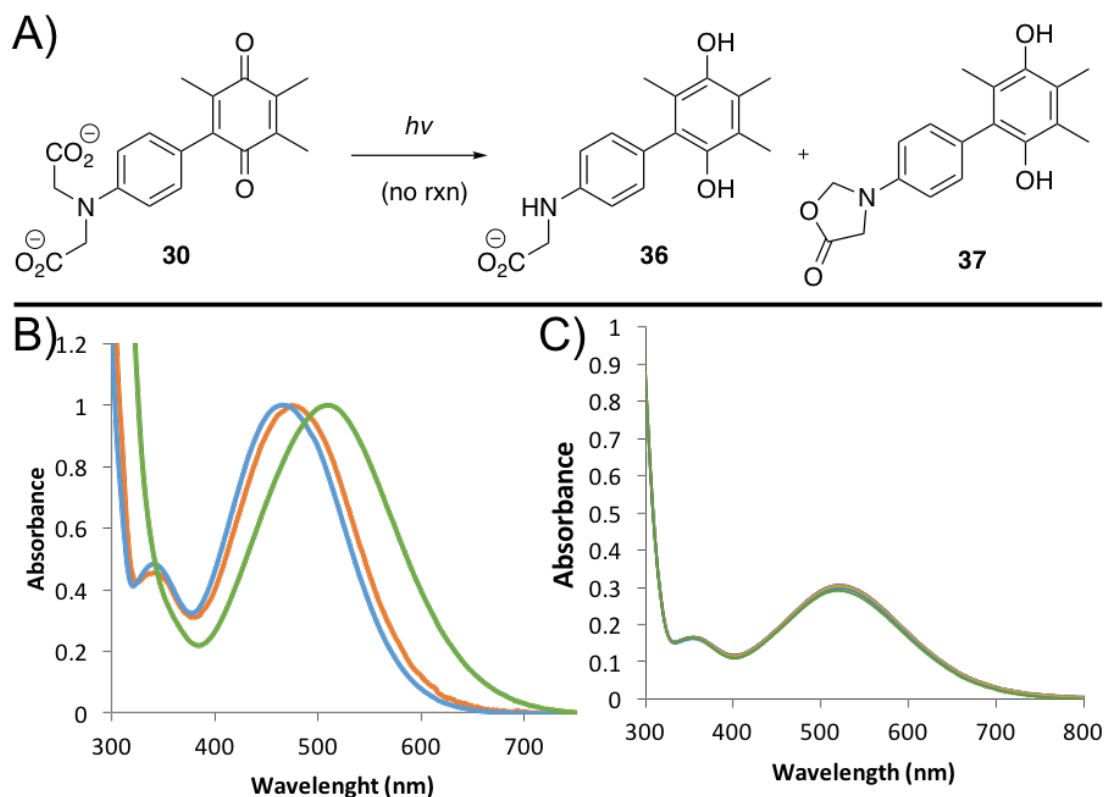


Figure 5.4: Photochemistry of quinone acid **30**. A) predicted products of photochemical reductive radical decarboxylation of acid **30**. B) UV-Vis spectra of acid **30** (orange), ester **35** (blue) and alkyl amine **28** (green) in methanol. C) Change in UV-Vis over 24 hours for acid **30** when irradiated at 470 nm in water after freeze pump thawing.

5.2.5 Quinone Electrochemistry

The electrochemistry of alkyl quinone **28**, ester quinone **35**, and acid quinone **30**, were investigated to determine their one electron reduction potentials. For alkyl quinone **28** two reversible single electron reductive peaks were observed as expected for a quinone in acetonitrile (-1.2 and -1.8 V respectively) (Figure 5.5a). Alkyl quinone **28** exhibited a large non-reversible oxidation event (0.5 V) that suppresses subsequent reduction cycling events. This is the result of amine oxidation and subsequent reaction of the radical amine cation with the electrode surface as has been observed previously for tertiary amine.⁴³ Ester **35** exhibited two much weaker and broader single electron reduction events than quinone **28** (-1.1 V and -1.8 V respectively) (Figure 5.5b). It is not clear why a significant decrease in current is observed for both reduction events for quinone **35** compared to quinone **28** but this may explain the lack of reactivity for quinone **30**. No similar reduction in current is observed for the oxidation of quinone **35**, which is shifted 36 mV towards higher voltage. The first of the two smaller oxidation peaks is an artifact of reductive cycling and is most likely not the result of radical decarboxylation as it is present for both ester **35** and amine **28** neither of which are expected to undergo decarboxylation. The second small oxidation peak is not an artifact of reductive cycling but it is unclear what it represents and may be the result of a small impurity in the sample. Acid **30** did not dissolve in acetonitrile and cyclic voltammetry experiments in DMF resulted in significantly broadened and weak end peaks for all three compounds, **30**, **35**, and **28**, making analysis difficult.

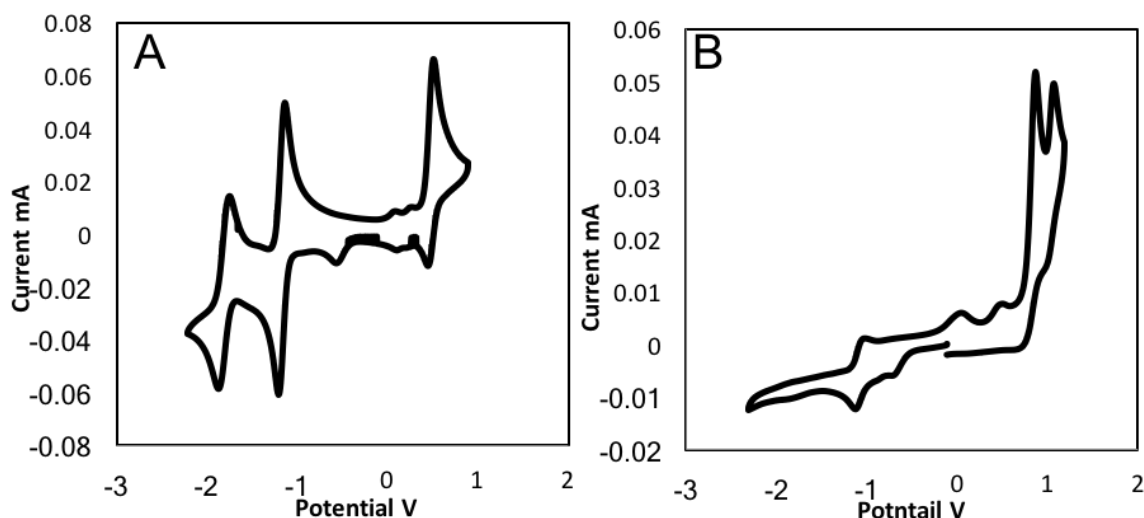


Figure 5.5: Cyclic voltammetry of alkyl amine **28** (A) and ester **35** (B) performed under an inert atmosphere in MeCN with 0.1 M TBAPF₆ at 100 mV/s. A) Quinone **28** shows two reversible reduction events. Scanning to positive potentials reveals one irreversible oxidation event. B) Quinone **35** shows much weaker reductive events relative to oxidative events when compared to quinone **28**.

5.3 Discussion

It is apparent that both quinone **30** and phenoxazine **15** are photostable. No radical decarboxylation hydroquinone product was detected when either compound was irradiated. Since neither quinone **30** nor phenoxazine **15** showed any photochemical reactivity it is difficult to determine what is the cause of this photostability and if radical decarboxylation could ever work in the context of quinone photoreduction. The cyclic nature of phenoxazine **15** most likely explains the photostability of **15** given the theorized twisted nature of the charge transfer state. The photostability of quinone **30** could be the result of the large delocalized aromatic system of **30** which would result in a delocalized charge transfer state that may be less likely to undergo radical decarboxylation and subsequent proton transfer. Alternatively, the charge transfer state of **30** may not be long lived enough for radical decarboxylation to compete with other non-productive relaxation pathways. (The rate of glycine radical decarboxylation is on the order of 100 ns.)²⁵ A less likely possibility is that the charge transfer state of reactive quinones could energetically mix or thermally populate the nearby $n-\pi^*$ state and undergo HAT. The radical decarboxylation quinone **30** has no extractable hydrogen making a HAT mechanism impossible. Future

work should focus on the direct substitution of a glycine to a quinone, as in quinone **9**, to address concerns over the delocalized nature of an aromatic system and the possibility that an extractable hydrogen for HAT may be required. However, this work suggests that radical decarboxylation is unlikely to work as a general method for photoreducing quinones.

Acknowledgements:

Paul Walton for starting this project and for supplying some of the intermediates need for the synthesis as well as providing invaluable feedback and discussion. I would also like to thank Wesley Kramer a Post Doc in the Gray group who helped me collect all the cyclic voltammetry data. This work was funded in part by WM Keck.

5.4 Reference

- (1) Walton, D. P.; Dougherty, D. A. A General Strategy for Visible-Light Decaging Based on the Quinone Trimethyl Lock. *J. Am. Chem. Soc.* **2017**, *139* (13), 4655–4658. <https://doi.org/10.1021/jacs.7b01548>.
- (2) Regan, C. J.; Walton, D. P.; Shafaat, O. S.; Dougherty, D. A. Mechanistic Studies of the Photoinduced Quinone Trimethyl Lock Decaging Process. *J. Am. Chem. Soc.* **2017**, *139* (13), 4729–4736. <https://doi.org/10.1021/jacs.6b12007>.
- (3) Walton, D. P.; Dougherty, D. A. A General Strategy for Visible-Light Decaging Based on the Quinone Cis-Alkenyl Lock. *Chem. Commun.* **2019**. <https://doi.org/10.1039/C9CC01073D>.
- (4) Okoh, O. A.; Klahn, P. Trimethyl Lock: A Multifunctional Molecular Tool for Drug Delivery, Cellular Imaging, and Stimuli-Responsive Materials. *ChemBioChem* **2018**, *19* (16), 1668–1694. <https://doi.org/10.1002/cbic.201800269>.
- (5) Levine, M. N.; Raines, R. T. Trimethyl Lock: A Trigger for Molecular Release in Chemistry, Biology, and Pharmacology. *Chem. Sci.* **2012**, *3* (8), 2412–2420. <https://doi.org/10.1039/C2SC20536J>.
- (6) Falci, K. J.; Franck, R. W.; Smith, G. P. Approaches to the Mitomycins. Photochemistry of Aminoquinones. *J. Org. Chem.* **1977**, *42* (20), 3317–3319. <https://doi.org/10.1021/jo00440a033>.
- (7) Berezhnaya, V. N.; Shishkina, R. P.; Pavlova, N. V.; Trofimov, A. S.; Eroshkin, V. I. Synthesis, Photolysis, and Redox Properties of 2-Dialkylamino-3-Methoxy-1,4-Naphthoquinones. *Bull. Acad. Sci. USSR Div. Chem. Sci.* **1990**, *39* (3), 578–583. <https://doi.org/10.1007/BF00959587>.
- (8) Gritsan, N. P.; Bazhin, N. M. Nature and Properties of the Reaction State in the Photolysis of 2-Amino-1,4-Naphthoquinone Derivatives. *Bull. Acad. Sci. USSR Div. Chem. Sci.* **1980**, *29* (6), 897–902. <https://doi.org/10.1007/BF00958803>.

- (9) Gritsan, N. P.; Bazhin, N. M. The Mechanism of Photolysis of 2-Amino-1,4-Naphthoquinone Derivatives. *Bull. Acad. Sci. USSR Div. Chem. Sci.* **1981**, 30 (2), 210–214. <https://doi.org/10.1007/BF00953566>.
- (10) Shishkina, R. P.; Berezhnaya, V. N. Photochemistry of 2-Dialkylamino-1,4-Naphthoquinones. *Russ. Chem. Rev.* **1994**, 63 (2), 139–146. <https://doi.org/10.1070/RC1994v063n02ABEH000076>.
- (11) Cameron, D. W.; Giles, R. G. F. A Photochemical Rearrangement Involving Aminated Quinones. *Chem. Commun. Lond.* **1965**, No. 22, 573–574. <https://doi.org/10.1039/C19650000573>.
- (12) Cameron, D. W.; Giles, R. G. F. Photochemical Formation of Benzoxazoline Derivatives from Aminated Quinones. *J. Chem. Soc. C Org.* **1968**, 0 (0), 1461–1464. <https://doi.org/10.1039/J39680001461>.
- (13) Giles, R. G. F. The Photochemistry of an Aminated 1,4-Benzoquinone. *Tetrahedron Lett.* **1972**, 13 (22), 2253–2254. [https://doi.org/10.1016/S0040-4039\(01\)84819-X](https://doi.org/10.1016/S0040-4039(01)84819-X).
- (14) Maruyama, K.; Kozuka, T.; Otsuki, T. The Intramolecular Hydrogen Abstraction Reaction in the Photolysis of Aminated 1,4-Naphthoquinones. *Bull. Chem. Soc. Jpn.* **1977**, 50 (8), 2170–2173. <https://doi.org/10.1246/bcsj.50.2170>.
- (15) Jones; Qian, X. Photochemistry of Quinone-Bridged Amino Acids. Intramolecular Trapping of an Excited Charge-Transfer State. *J. Phys. Chem. A* **1998**, 102 (15), 2555–2560. <https://doi.org/10.1021/jp972325g>.
- (16) Chen, Y.; Steinmetz, M. G. Photochemical Cyclization with Release of Carboxylic Acids and Phenol from Pyrrolidino-Substituted 1,4-Benzoquinones Using Visible Light. *Org. Lett.* **2005**, 7 (17), 3729–3732. <https://doi.org/10.1021/ol051362k>.
- (17) Chen, Y.; Steinmetz, M. G. Photoactivation of Amino-Substituted 1,4-Benzoquinones for Release of Carboxylate and Phenolate Leaving Groups Using Visible Light. *J. Org. Chem.* **2006**, 71 (16), 6053–6060. <https://doi.org/10.1021/jo060790g>.
- (18) Wagner, P. J.; Kemppainen, A. E.; Jellinek, T. Type II Photoreactions of Phenyl Ketones. Competitive Charge Transfer in .Alpha.-, .Gamma.-, and .Delta.-Dialkylamino Ketones. *J. Am. Chem. Soc.* **1972**, 94 (21), 7512–7519. <https://doi.org/10.1021/ja00776a038>.
- (19) Griesbeck, A. G.; Hoffmann, N.; Warzecha, K. Photoinduced-Electron-Transfer Chemistry: From Studies on PET Processes to Applications in Natural Product Synthesis. *Acc. Chem. Res.* **2007**, 40 (2), 128–140. <https://doi.org/10.1021/ar068148w>.
- (20) Griesbeck, A. G.; Henz, A.; Peters, K.; Peters, E.-M.; Schnering, H. G. von. Photo Electron Transfer Induced Macrocyclization of N-Phthaloyl- ω -Aminocarboxylic Acids. *Angew. Chem. Int. Ed. Engl.* **1995**, 34 (4), 474–476. <https://doi.org/10.1002/anie.199504741>.
- (21) Gallagher, S.; Hatoum, F.; Zientek, N.; Oelgemöller, M. Photodecarboxylative Additions of N-Protected α -Amino Acids to N-Methylphthalimide. *Tetrahedron Lett.* **2010**, 51 (28), 3639–3641. <https://doi.org/10.1016/j.tetlet.2010.05.020>.
- (22) Yoon, U. C.; Jin, Y. X.; Oh, S. W.; Park, C. H.; Park, J. H.; Campana, C. F.; Cai, X.; Duesler, E. N.; Mariano, P. S. A Synthetic Strategy for the Preparation of

- Cyclic Peptide Mimetics Based on SET-Promoted Photocyclization Processes. *J. Am. Chem. Soc.* **2003**, *125* (35), 10664–10671. <https://doi.org/10.1021/ja030297b>.
- (23) E. Falvey, D.; Sundararajan, C. Photoremovable Protecting Groups Based on Electron Transfer Chemistry. *Photochem. Photobiol. Sci.* **2004**, *3* (9), 831–838. <https://doi.org/10.1039/B406866A>.
- (24) Borak, J. B.; Falvey, D. E. A New Photolabile Protecting Group for Release of Carboxylic Acids by Visible-Light-Induced Direct and Mediated Electron Transfer. *J. Org. Chem.* **2009**, *74* (10), 3894–3899. <https://doi.org/10.1021/jo900182x>.
- (25) Bonifačić, M.; Štefanić, I.; Hug, G. L.; Armstrong, D. A.; Asmus, K.-D. Glycine Decarboxylation: The Free Radical Mechanism. *J. Am. Chem. Soc.* **1998**, *120* (38), 9930–9940. <https://doi.org/10.1021/ja9815428>.
- (26) Illescas, B.; Martin, N.; Segura, J. L.; Seoane, C.; Orti, E.; Viruela, P. M.; Viruela, R. Synthesis and Characterization of Novel Donor-Acceptor Naphthoquinone Derivatives with Photoinduced Charge-Transfer Properties. A Joint Experimental and Theoretical Study. *J. Org. Chem.* **1995**, *60* (17), 5643–5650. <https://doi.org/10.1021/jo00122a054>.
- (27) Overman, L. E.; Paone, D. V. Enantioselective Total Syntheses of Ditryptophenaline and Ent-WIN 64821. *J. Am. Chem. Soc.* **2001**, *123* (38), 9465–9467. <https://doi.org/10.1021/ja0166141>.
- (28) Walton, D. P. General Strategies for Visible-Light Decaging Based on Quinone Photochemistry. phd, California Institute of Technology, 2019. [https://doi.org/Walton, David P. \(2019\) General Strategies for Visible-Light Decaging Based on Quinone Photochemistry. Dissertation \(Ph.D.\), California Institute of Technology. doi:10.7907/0793-KJ34](https://doi.org/Walton, David P. (2019) General Strategies for Visible-Light Decaging Based on Quinone Photochemistry. Dissertation (Ph.D.), California Institute of Technology. doi:10.7907/0793-KJ34). <http://resolver.caltech.edu/CaltechTHESIS:02012019-134839099> <<http://resolver.caltech.edu/CaltechTHESIS:02012019-134839099>>.
- (29) Grabowski, Z. R.; Rotkiewicz, K.; Rettig, W. Structural Changes Accompanying Intramolecular Electron Transfer: Focus on Twisted Intramolecular Charge-Transfer States and Structures. *Chem. Rev.* **2003**, *103* (10), 3899–4032. <https://doi.org/10.1021/cr940745l>.
- (30) Sasaki, S.; Drummen, G. P. C.; Konishi, G. Recent Advances in Twisted Intramolecular Charge Transfer (TICT) Fluorescence and Related Phenomena in Materials Chemistry. *J. Mater. Chem. C* **2016**, *4* (14), 2731–2743. <https://doi.org/10.1039/C5TC03933A>.
- (31) Maiti, D.; Fors, B. P.; Henderson, J. L.; Nakamura, Y.; Buchwald, S. L. Palladium-Catalyzed Coupling of Functionalized Primary and Secondary Amines with Aryl and Heteroaryl Halides: Two Ligands Suffice in Most Cases. *Chem. Sci.* **2010**, *2* (1), 57–68. <https://doi.org/10.1039/C0SC00330A>.
- (32) Surry, D. S.; Buchwald, S. L. Dialkylbiaryl Phosphines in Pd-Catalyzed Amination: A User's Guide. *Chem. Sci.* **2010**, *2* (1), 27–50. <https://doi.org/10.1039/C0SC00331J>.
- (33) Fujiwara, Y.; Domingo, V.; Seiple, I. B.; Gianatassio, R.; Del Bel, M.; Baran, P. S. Practical C–H Functionalization of Quinones with Boronic Acids. *J. Am. Chem. Soc.* **2011**, *133* (10), 3292–3295. <https://doi.org/10.1021/ja111152z>.

- (34) Komeyama, K.; Kashihara, T.; Takaki, K. FeSO₄-Promoted Direct Arylation of Benzoquinones with ArB(OH)₂ or ArBF₃K. *Tetrahedron Lett.* **2013**, *54* (9), 1084–1086. <https://doi.org/10.1016/j.tetlet.2012.12.031>.
- (35) Molina, M. T.; Navarro, C.; Moreno, A.; Csáky, A. G. Arylation of Benzo-Fused 1,4-Quinones by the Addition of Boronic Acids under Dicationic Pd(II)-Catalysis. *Org. Lett.* **2009**, *11* (21), 4938–4941. <https://doi.org/10.1021/ol902084g>.
- (36) Ilangovan, A.; Polu, A.; Satish, G. K₂S₂O₈-Mediated Metal-Free Direct C–H Functionalization of Quinones Using Arylboronic Acids. *Org. Chem. Front.* **2015**, *2* (12), 1616–1620. <https://doi.org/10.1039/C5QO00246J>.
- (37) Lin, S.-T.; Huang, R.-J. One-Pot Synthesis of Substituted Aniline-N,N-Diacetic Acids. *Synthesis* **1989**, *1989* (07), 548–549. <https://doi.org/10.1055/s-1989-27314>.
- (38) Canales, Á.; Mallagaray, Á.; Berbís, M. Á.; Navarro-Vázquez, A.; Domínguez, G.; Cañada, F. J.; André, S.; Gabius, H.-J.; Pérez-Castells, J.; Jiménez-Barbero, J. Lanthanide-Chelating Carbohydrate Conjugates Are Useful Tools To Characterize Carbohydrate Conformation in Solution and Sensitive Sensors to Detect Carbohydrate–Protein Interactions. *J. Am. Chem. Soc.* **2014**, *136* (22), 8011–8017. <https://doi.org/10.1021/ja502406x>.
- (39) Walker, S. E.; Jordan-Hore, J. A.; Johnson, D. G.; Macgregor, S. A.; Lee, A.-L. Palladium-Catalyzed Direct C–H Functionalization of Benzoquinone. *Angew. Chem. Int. Ed.* **2014**, *53* (50), 13876–13879. <https://doi.org/10.1002/anie.201408054>.
- (40) Molander, G. A.; Trice, S. L. J.; Dreher, S. D. Palladium-Catalyzed, Direct Boronic Acid Synthesis from Aryl Chlorides: A Simplified Route to Diverse Boronate Ester Derivatives. *J. Am. Chem. Soc.* **2010**, *132* (50), 17701–17703. <https://doi.org/10.1021/ja1089759>.
- (41) Viault, G.; Grée, D.; Das, S.; Yadav, J. S.; Grée, R. Synthesis of a Focused Chemical Library Based on Derivatives of Embelin, a Natural Product with Proapoptotic and Anticancer Properties. *Eur. J. Org. Chem.* **2011**, *2011* (7), 1233–1241. <https://doi.org/10.1002/ejoc.201001627>.
- (42) Nicolaou, K. C.; Estrada, A. A.; Zak, M.; Lee, S. H.; Safina, B. S. A Mild and Selective Method for the Hydrolysis of Esters with Trimethyltin Hydroxide. *Angew. Chem. Int. Ed.* **2005**, *44* (9), 1378–1382. <https://doi.org/10.1002/anie.200462207>.
- (43) Adenier, A.; Chehimi, M. M.; Gallardo, I.; Pinson, J.; Vilà, N. Electrochemical Oxidation of Aliphatic Amines and Their Attachment to Carbon and Metal Surfaces. *Langmuir* **2004**, *20* (19), 8243–8253. <https://doi.org/10.1021/la049194c>.

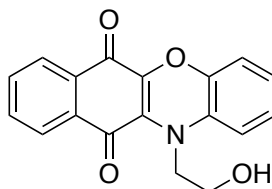
5.5 Experimental

5.5.1 General Procedure

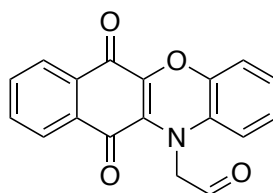
Unless otherwise stated reactions were carried out at ambient temperatures under argon. Any potentially light sensitive compounds were protected from light using aluminum foil and carried out under low ambient light conditions. Commercially available reagents were obtained from Sigma Aldrich, AK scientific, Alfa Aesar, Acros Organics, or

Strem Chemicals. Solvents used in photolysis and UV-vis experiments were EMD Millipore (OmniSolve®) grade. Other solvents were used as received unless otherwise noted. Reactions were monitored with thin layer chromatography using EMD/Merck silica gel 60 F254 precoated class plates (0.25 mm). Flash column chromatography was conducted using 60 Å, 230-400 mesh silica gel purchased from Alfa Aesar. NMR spectra were recorded on Varian (300 or 500 MHz) or Bruker (400 MHz) spectrometers. UV-vis spectra were obtained using a Cary 60 spectrometer. Photolysis experiments were conducted in a quartz cuvette using either a 300 W Hg arc lamp (66011, Oriel) with glass filters or a 650 mW, 470 nm LED (M4703) or a 880 mW 565 nm LED (M565L3) from ThorLabs.

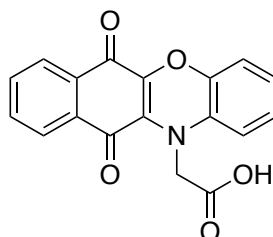
5.5.2 Synthesis



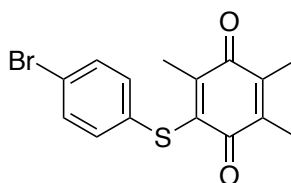
12-(2-hydroxyethyl)-11H-benzo[*b*]phenoxazine-6,11(12H)-dione (18): Phenol (**17**) (110 mg, 0.65 mmol 1 eq) and Cs₂CO₃ (420 mg, 1.3 mmol, 2 eq) were dissolved in anhydrous DMF (15 mL) resulting in a dark green solution. 2,3-dichloronaphthalene-1,4-dione (**16**) (150 mg, 0.68 mmol, 1.05 eq) was added and the reaction was stirred overnight under argon. Reaction was quenched by the addition of 200 mL of water and the dark blue solid was isolated with suction filtration. Purified by flash column chromatography on silica (EtOAc/Hexanes: 1/1) to give 170 mg (0.55 mmol) of **18** in 85% yield as a dark blue solid. ¹H NMR (300 MHz, DMSO-*d*₆) δ 7.96 – 7.86 (m, 2H), 7.84 – 7.74 (m, 2H), 7.05 – 6.72 (m, 4H), 4.96 (s, 1H), 3.95 (t, *J* = 5.4 Hz, 2H), 3.66 (t, *J* = 5.4 Hz, 2H).



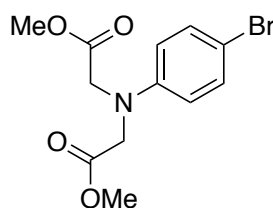
2-(6,11-dioxo-6,11-dihydro-12H-benzo[b]phenoxazin-12-yl)acetaldehyde (19): Dess Martin Periodinane, DMP, (112 mg, 0.26 mmol, 1.5 eq) was added to alcohol **18** (53 mg, 0.17 mmol, 1 eq) dissolved in dry DCM (5 mL) and stirred under argon for 1.5 hours. Reaction was diluted with Et₂O (20 mL) and an aq solution (20 mL) of sodium thiosulfate (100 g/L Na₂S₂O₃) and NaHCO₃ (100 g/L) was added and the reaction was vigorously stirred for 15 min. The organic layer was separated, washed with brine, and dried with MgSO₄. Purified by flash column chromatography on silica (EtOAc/Hexanes: 1/3) to give 37 mg (0.12 mmol) of aldehyde **19** in 71% yield as a dark blue solid. ¹H NMR (500 MHz, Chloroform-*d*) δ 8.09 – 8.04 (m, 1H), 7.97 – 7.92 (m, 1H), 7.69 (dtd, *J* = 22.0, 7.4, 1.4 Hz, 2H), 6.90 – 6.83 (m, 3H), 6.40 (dt, *J* = 7.2, 1.4 Hz, 1H), 4.43 (s, 2H).



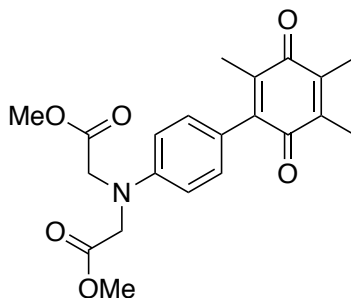
2-(6,11-dioxo-6,11-dihydro-12H-benzo[b]phenoxazin-12-yl)acetic acid (15): Aldehyde **19** (20 mg, 0.07 mmol, 1 eq) was added to a solution of H₂O (16 mL), THF (16 mL), *t*-BuOH (4 mL) and 2-methyl-1-butene (4 mL). To this was added NaH₂PO₄ (73 mg, 0.52 mmol, 8 eq) and sodium chlorite (39 mg, 0.26 mmol, 4 eq) and stirred in the dark for 3 hr. Diluted with aq. NH₄Cl (50 mL), extracted with EtOAc (3 x 50 mL). The combined organic layers were washed with brine (25 mL), dried over MgSO₄, and concentrated. The residue was purified by flash chromatography (DCM/MeOH/AcOH: 99/0.5/0.5) to give 11 mg (0.034 mmol) of acid **15** in 53% yield as a dark blue solid. ¹H NMR (500 MHz, Methanol-*d*₄) δ 8.01 – 7.94 (m, 2H), 7.78 – 7.68 (m, 2H), 6.89 (td, *J* = 7.7, 1.6 Hz, 1H), 6.84 (td, *J* = 7.7, 1.4 Hz, 1H), 6.75 (dd, *J* = 7.8, 1.5 Hz, 1H), 6.67 (dd, *J* = 7.8, 1.5 Hz, 1H), 4.55 (s, 2H).



2-((4-bromophenyl)thio)-3,5,6-trimethylcyclohexa-2,5-diene-1,4-dione (24): Quinone **29** (340 mg, 1.5 mmol, 1 eq) and NaOAc (140 mg, 1.65 mmol, 1 eq) were dissolved in MeOH (40 mL) and stirred open to air. To this was added 4-bromothiophenol (0.23 mL, 1.65 mmol, 1.1 eq) in MeOH (10 mL) dropwise. Reaction turned bright red and was stirred for 20 minutes. Reaction was concentrated and the residue purified by flash column chromatography (EtOAc/Hexanes: 5/95) to give 463 mg (1.4 mmol) of quinone **24** in 93% yield as a dark red oil. ^1H NMR (500 MHz, Chloroform-*d*) δ 7.47 – 7.39 (m, 2H), 7.25 – 7.18 (m, 2H), 2.28 (s, 3H), 2.07 (dq, $J = 24.8, 1.2$ Hz, 6H).



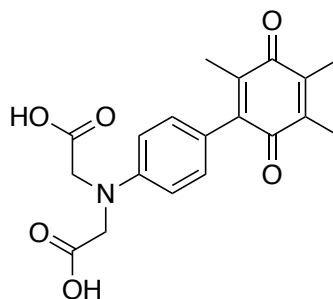
dimethyl 2,2'-((4-bromophenyl)azanediyl)diacetate (33): 4-Bromoaniline (**31**) (210 mg, 1.16 mmol, 1 eq), methyl 2-bromoacetate (**33**) (1.3 mL, 13 mmol, 12 eq), NaI (360 mg, 2.1 mmol, 1.8 eq) and *i*-Pr₂NEt (1.2 mL, 7.0 mmol, 6 eq) were added to MeCN (20 mL). Reaction was refluxed for 48 hr. Diluted with water (20 mL) and DCM (20 mL), and extracted with DCM (3 x 20 mL). The organic layers were combined, washed with brine (15 mL), dried over MgSO₄, and concentrated. The residue was purified with flash column chromatography (EtOAc/Hexanes: gradient 10/90 to 25/75) to give 420 mg (1.14 mmol) of bromophenyl diacetate **33** in 98 % yield as a yellow oil. ^1H NMR (500 MHz, Chloroform-*d*) δ 7.33 – 7.26 (m, 2H), 6.52 – 6.44 (m, 2H), 4.12 (s, 4H), 3.76 (s, 6H).



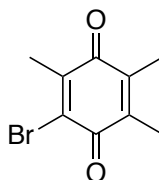
dimethyl 2,2'-((3',4',6'-trimethyl-2',5'-dioxo-2',5'-dihydro-[1,1'-biphenyl]-4-

yl)azanediyl)diacetate (25): A dry Schlenk flask was charged with (X-Phos) palladium(II) phenethylamine chloride (18 mg, 0.023 mmol, 0.01 eq), X-Phos (24 mg, 0.043 mmol, 0.02 eq), tetrahydroxydiboron (305 mg, 3.4 mmol, 1.5 eq), KOAc (670 mg, 6.8 mmol, 3 eq) and KO*t*-Bu (4.8 mg, 0.023 mmol, 0.01 eq). The flask was sealed, evacuated and back filled with argon (9x). Bromophenyl diacetate **33** (700 mg, 2.27 mmol, 1 eq) was dissolved in dry MeOH (10 mL) and added to the flask. The reaction was heated to 80 °C for 14.5 hours. The reaction was cooled to rt then filtered through a pad of celite (eluting with 150 mL EtOAc) and concentrated. To the crude white solid was added 1 M aq HCl (50 mL) and EtOAc (50 mL) and this solution was stirred for 120 min. The aq layer was extracted with EtOAc (3 x 30 mL) and the combined organic layers were washed with brine (30 mL) dried over MgSO₄, concentrated to yield crude boronic acid **34**. ¹H NMR (500 MHz, Chloroform-*d*) δ 8.17 – 7.93 (m, 2H), 6.81 – 6.62 (m, 2H), 4.22 (s, 4H), 3.78 (s, 6H). ¹³C NMR (126 MHz, Chloroform-*d*) δ 171.15, 150.94, 137.41, 135.00, 111.60, 53.30, 52.42.

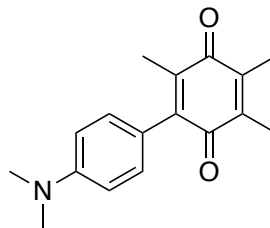
Bromotrimethylquinone **29** (260 mg, 1.1 mmol, 0.5 eq), Palladium(II)bis(triphenylphosphine) dichloride (21 mg, 0.03 mmol, 0.1 eq) and Na₂CO₃ (260 mg, 2.3 mmol, 1 eq) were added to crude boronic acid **34** in 1,4-dioxane (20 mL) and H₂O (6 mL). Reaction was heated open to air to 80 °C for 2 hr, and cooled to rt. Reaction was diluted with DCM (25 mL) and H₂O (25 mL) and separated. The aq layer was extracted with DCM (3 x 25 mL). Combined organic layers were washed with brine and dried over MgSO₄, concentrated, and purified with flash column chromatography (EtOAc/Hexanes: 20/80) to give 160 mg (0.43 mmol) of quinone diester **35** in 20 % yield as a red oil. ¹H NMR (500 MHz, Chloroform-*d*) δ 7.07 – 7.00 (m, 2H), 6.66 – 6.60 (m, 2H), 4.18 (s, 4H), 3.77 (s, 6H), 2.05 (dt, *J* = 11.6, 1.2 Hz, 6H), 1.98 (s, 3H).



2,2'-((3',4',6'-trimethyl-2',5'-dioxo-2',5'-dihydro-[1,1'-biphenyl]-4-yl)azanediyl)diacetic acid (30): Ester quinone **35** (42 mg, 0.11 mmol, 1 eq) and trimethyltin hydroxide (100 mg, 0.55 mmol, 5 eq) were dissolved in DCE (10 mL) and refluxed overnight in the dark. The reaction was cooled to rt, concentrated, and dissolved in EtOAc (25 mL). Solution was washed with aq 0.01 M NaHSO₄ (3 x 25 mL), Brine (25 mL) dried over MgSO₄, concentrated, and purified with flash column chromatography (MeOH/AcOH/DCM: 10/1/90) to give 10 mg (0.03 mmol) of quinone **30** in 25 % yield as a red oil. ¹H NMR (400 MHz, Methanol-*d*₄) δ 7.15 – 6.99 (m, 2H), 6.77 – 6.56 (m, 2H), 4.21 (s, 4H), 2.07 (s, 3H), 2.05 (s, 3H), 1.96 (s, 3H).



2-bromo-3,5,6-trimethylcyclohexa-2,5-diene-1,4-dione (29): Bromine (0.7 mL, 13.2 mmol, 2.2 eq) dissolved in AcOH (6mL) was added dropwise to 2,3,5-trimethylhydroquinone (1.07 g, 6.6 mmol, 1 eq) dissolved in AcOH (45 mL). Reaction was stirred at rt for 21 hr before diluting with H₂O (500 mL). Product was extracted with EtOAc (3 x 200 mL). The combined organic layers were washed with brine (200 mL), dried with MgSO₄, concentrated, and purified with flash column chromatography (EtOAc/Hexanes: 1/99) to give 0.91 g (3.95 mmol) of bromo quinone **29** in 60 % yield as a yellow solid. ¹H NMR (300 MHz, Chloroform-*d*) δ 2.23 (s, 3H), 2.13 – 2.05 (m, 6H).



4'-(dimethylamino)-3,4,6-trimethyl-[1,1'-biphenyl]-2,5-dione (28):

Bromotrimethylquinone **29** (61 mg, 0.26 mmol, 1 eq), boronic acid **26** (85 mg, 0.52 mmol, 2 eq), Na₂CO₃ (55 mg, 0.52 mmol, 2 eq) and palladium(II)bis(triphenylphosphine) dichloride (21 mg, 0.03 mmol, 0.1 eq) were added to 1,4-dioxane (4 mL) and H₂O (1 mL). Reaction was heated to 80 °C for 1 hr, turned deep red in color, and was cooled to rt. Reaction was diluted with DCM (30 mL), dried over MgSO₄, filtered over a pad of celite, and concentrated. Reaction was purified with flash column chromatography (EtOAc/Hexanes: 5/95) to give 49 mg (0.18 mmol) of alkyl amine quinone **28** in 70% yield as a purple oil. ¹H NMR (500 MHz, Chloroform-*d*) δ 7.09 – 7.03 (m, 2H), 6.77 – 6.71 (m, 2H), 3.00 (s, 6H), 2.07 (s, 3H), 2.05 (s, 3H), 2.02 (s, 3H). ¹³C NMR (126 MHz, cdcl₃) δ 188.52, 187.24, 150.39, 143.45, 140.63, 140.48, 139.65, 131.15, 120.86, 111.47, 77.41, 77.16, 76.91, 40.40, 14.34, 12.61, 12.53.

5.5.3 Cyclic Voltammetry

Cyclic voltammetry experiments were performed using a glassy carbon working electrode, Ag/AgCl reference electrode, and a platinum wire counter electrode using a Bio-Logic potentiostat. Experiments were performed in MeCN, DMF and 0.1 M phosphate buffered water with 0.1 M TBAPF₆ supporting electrolyte under a N₂ atmosphere. Concentrations of compounds used were approximately 10⁻³ M. Bulk electrolysis measurements were made using a glassy graphite plate working electrode, a platinum counter wire electrode, and silver wire reference electrode separated by a glass frit. Ferrocenium/ferrocene was used as an external reference.

5.5.4 Additional Data

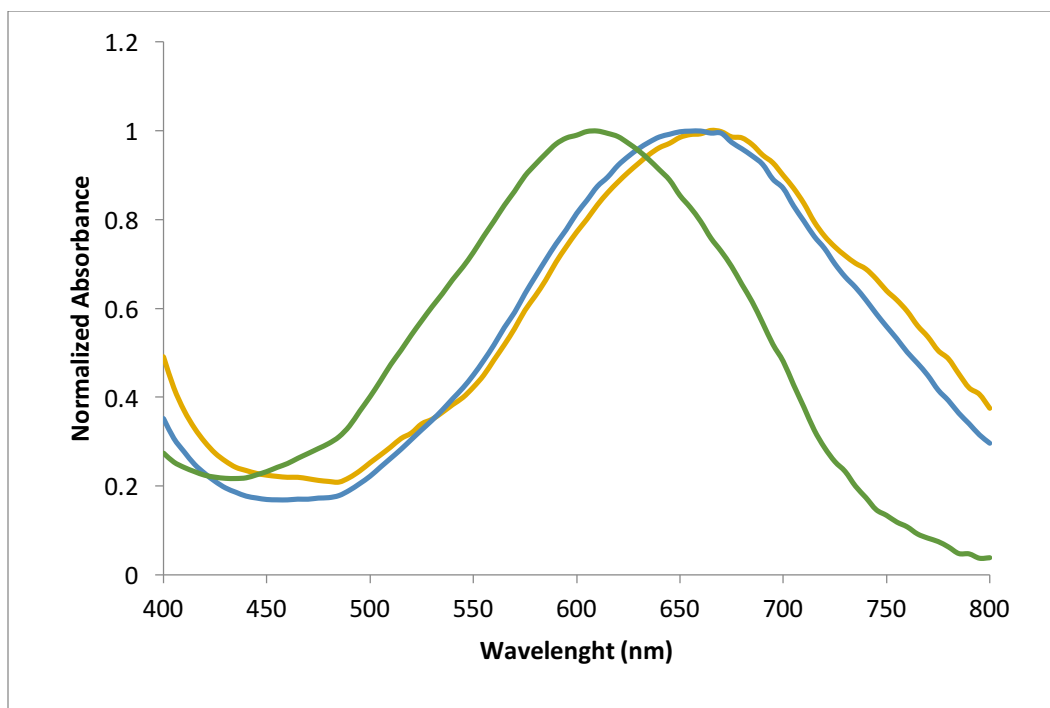


Figure 5.6: UV-Vis of phenoxazine quinone **15** in MeCN (λ_{max} 610 nm, green), 0.01 M pH 7 phosphate buffer (λ_{max} 665 nm, yellow) and a 1:1 MeCN:Buffer (λ_{max} 660 nm, blue).

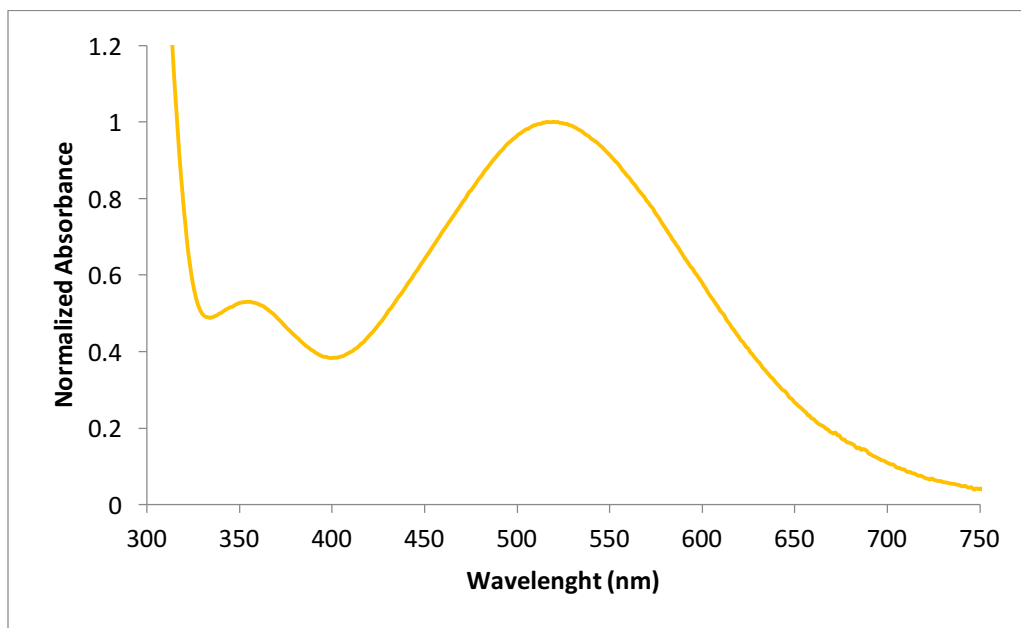


Figure 5.7: UV-vis spectra of **30** in 0.01 M pH 7 phosphate buffer.

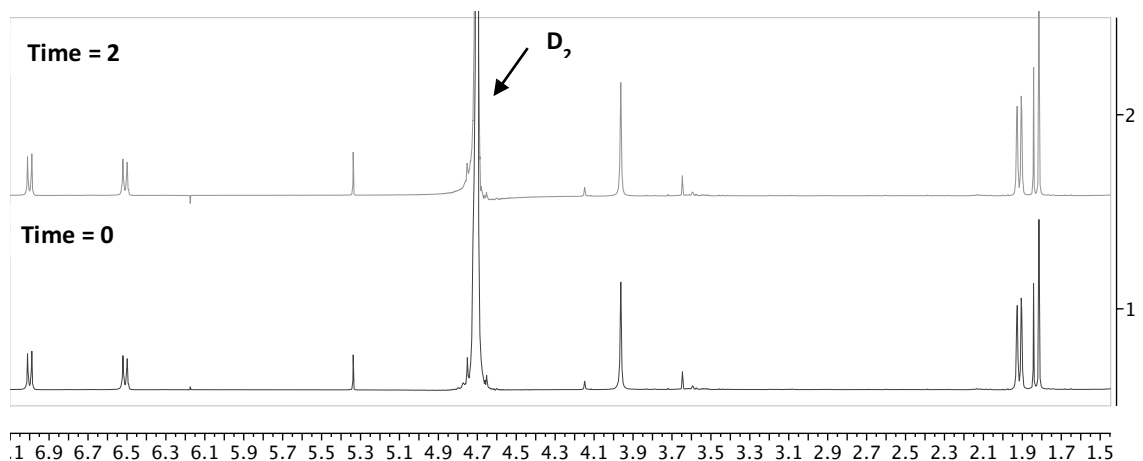


Figure 5.8: NMR spectra of acid **30** before and after 2 hours of irradiation at 470 nm showing no change in spectra.

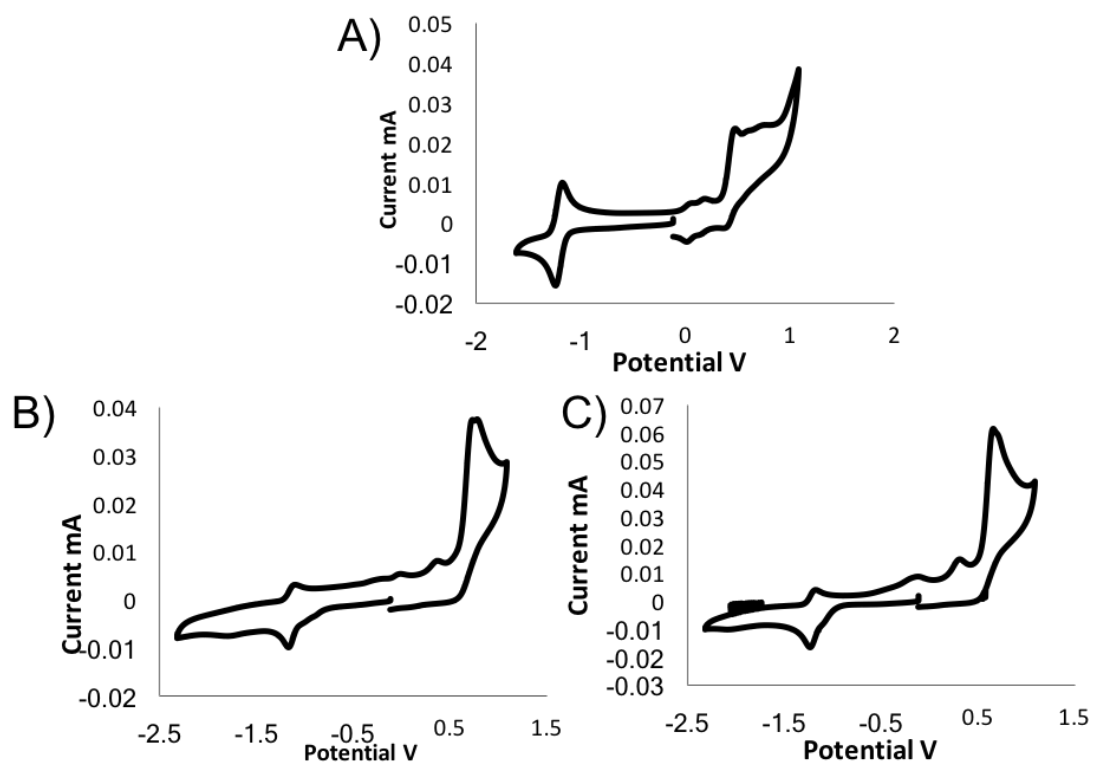


Figure 5.9: Cyclic voltammetry of alkyl amine **28** (A), ester **35** (B) and acid **30** (C) performed under an inert atmosphere in DMF with 0.1 M TBAPF₆ at 100 mV/s.